Available online at www.sciencedirect.com
SCIENCE DIRECT®
Earth-Science Reviews 65 (2004) 141–194
EARTH-SCIENCE REVIEWS
www.elsevier.com/locate/earscirev

Radiogenic isotopes: systematics and applications to earth surface processes and chemical stratigraphy

Jay L. Banner*

Department of Geological Sciences, University of Texas, Austin, TX 78712, USA

Accepted 23 June 2003

Abstract

Radiogenic isotopes have wide application to chemical stratigraphy, geochronology, provenance studies, and studies of temporal changes in Earth surface processes. This paper briefly reviews the principles of radiogenic isotope geochemistry and the distribution of a number of elements of interest in the environment, and then uses this information to explore the range of applications to chemical stratigraphy and other fundamental subjects of sedimentary geology. Many of these applications center on the reconstruction of secular variations in paleoseawater isotope signals. These "seawater isotope curves" can be used for stratigraphic correlation and to assess changes through Earth history in processes such as tectonic uplift, climate change, biogeochemical cycling, ocean circulation, crustal growth, and surface water evolution. Understanding the modern biogeochemical cycle of the element/isotope system of interest is essential for gaining the maximum information regarding the operation of ancient cycles. The main sources of uncertainty for reconstructing seawater isotope curves involve diagenetic alteration, sample impurities, and errors in age assignments. Rigorous sample selection criteria and pretreatment methods are keys to reconstructing the most accurate seawater isotope curves. Applications are discussed for the Rb–Sr, Sm–Nd, La–Ce, Lu–Hf, Re–Os, U–Th–Pb, K–Ar, and cosmogenic isotope systems.

Keywords: Isotopes; Chemostratigraphy; Seawater; Strontium; Rare earth elements; Geochronology; Provenance

1. Introduction

Different isotopes of an element have the same atomic number and different atomic mass by virtue of having different numbers of neutrons. For example, the oxygen atoms within a sample of rock or water or animal will be comprised of some mixture of the isotopes oxygen-16, oxygen-17, and oxygen-18 (i.e., ^{16}O, ^{17}O, and ^{18}O). The isotopes of oxygen have negligible radioactivity and are termed stable. In contrast, a radiogenic isotope is a daughter isotope produced from the decay of a radioactive parent isotope. Variations in radiogenic isotopes can provide independent and complementary information to stable isotope variations in sedimentary environments. In sedimentary geology and environmental science, radiogenic isotopes are useful for the following:

(1) tracing the sources and transport of dissolved and detrital constituents in the sedimentary, hydrologic, and biogeochemical cycles, and in ecosystems;
(2) reconstructing temporal changes in ocean water chemistry and applying these changes to studies

* Tel.: +1-512-471-5016; fax: +1-512-471-9425.
E-mail address: banner@mail.utexas.edu (J.L. Banner).

0012-8252/$ - see front matter © 2003 Elsevier B.V. All rights reserved.
doi:10.1016/S0012-8252(03)00086-2

of stratigraphic correlation and temporal changes in the hydrologic, sedimentary, and biogeochemical cycles; and
(3) dating the time of formation of rocks and minerals.

Radiogenic isotope ratios are measured in ancient marine authigenic sediments, including carbonates, phosphates, sulfates, oxides, and hydroxides, as a means to reconstruct the chemistry of ancient oceans. This endeavor involves using measurements on well-preserved biogenic and inorganic chemical precipitates to determine the isotopic composition of seawater at a given time. Data for samples from different age strata are combined to construct records of secular (i.e., temporal) change and thereby provide a baseline of marine values for stratigraphic correlation. A major issue to be addressed in this pursuit is determining the extent to which a given rock or mineral sample preserves an original marine signal.

The classic example of a radiogenic isotope record of temporal change in ocean chemistry is the secular Sr isotope curve of Burke et al. (1982). The "Burke curve" (Fig. 1) covers the Phanerozoic eon, and is constructed from analyses of marine carbonates and evaporites. Following earlier efforts by Peterman et al. (1970), Dasch and Biscaye (1971), and Veizer and Compston (1974), publication of the Burke curve intrigued the Earth science community with its potential applications to stratigraphic correlation, diagenesis and fluid flow, paleotectonics, and paleoenvironmental change. In this paper, I discuss the systematics of radiogenic isotope systems as a means to understand the processes that govern the variations exhibited in secular curves, such as that of Burke et al. (1982), and explore how such curves are constructed and their utility in sedimentary geology. The seawater Sr isotope curve of Fig. 1 will be used as a framework for posing questions such as:

(1) How are such curves constructed?
(2) How well are the curves known, and what criteria can be applied to evaluating and refining them?
(3) What Earth system processes control the radiogenic isotope chemistry of the oceans?

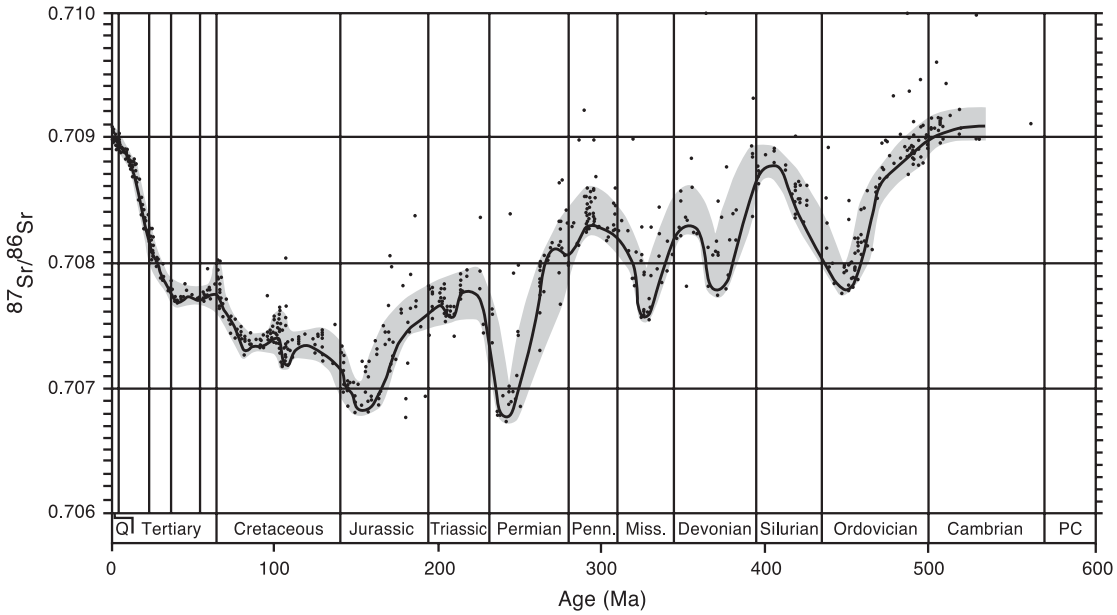

Fig. 1. The Burke et al. (1982) secular curve for seawater $^{87}Sr/^{86}Sr$ variations during the Phanerozoic based on analyses of marine carbonate and evaporite rocks and fossils. Increasing scatter with age is due to greater diagenetic alteration of original marine phases and increased effects of high Rl/Sr phases such as silicates in older samples and greater uncertainties in age assignments for older samples. The shaded area around the curve is the error envelope of best estimate seawater value by Burke et al. (1982). Results are plotted here relative to a $^{87}Sr/^{86}Sr$ value of 0.71014 for NIST $SrCO_3$ Standard Reference Material 987 (SRM 987).

(4) How can radiogenic isotopes be used as a stratigraphic correlation tool, as a tracer of groundwater and surface water evolution, and as a means of determining the relative and absolute ages of rocks and minerals?

This paper will first summarize the principles of radioactive decay, the isotope evolution of the Earth, and the geochemical behavior of the elements that comprise these isotope systems. This will provide background to an analysis of how these geochemical systems are used in the study of items 1 through 4 above. This treatment is intended to provide the reader with the basic knowledge needed to gain insight into the unique applicability of radiogenic isotope systems to problems in sedimentary geology.

We will use the Rb–Sr isotope system in carbonates as a template to present the basic principles of how radiogenic isotope systems work and to describe the distribution of an element in modern surface water and the oceans. This information will be used to present applications to stratigraphic and biogeochemical cycle analysis. The Rb–Sr isotope system in carbonates is a useful example because: (1) there is an extensive Sr isotope database on nearly all types of rocks, minerals, and natural waters; (2) the geochemical behaviors of the elements Rb and Sr are well understood; (3) the low-temperature geochemical behavior of these elements has special application to chemostratigraphy, as will be discussed; and (4) carbonates are widespread in the rock record and their diagenesis has been extensively studied. We will focus on this system and integrate examples of applications of other radiogenic isotope systems and other rock types. In addition, we will illustrate the biogeochemical cycle of Sr, as well as help define criteria for well-preserved ancient marine samples.

2. Radioactivity, radioactive decay, and decay mechanisms

Radioactive decay is the spontaneous disintegration of a radioactive parent isotope to produce a radiogenic daughter isotope and a nuclear particle. The driving force of the decay process is the instability of the radioactive parent isotope. The instability is a function of an individual nucleus' configuration of protons and neutrons, and its binding energy (per atomic particle), which generally decreases with increasing atomic weight above mass 56. Hence, many of the radioactive elements that we will consider have relatively large atomic masses, whereas many of the stable isotope systems of interest (e.g., C, H, O, N, S, and B) have relatively low atomic mass. Much of the treatment given here of the principles of radioactive decay is based on a more comprehensive coverage

Table 1
Some radioactive decay schemes of interest in sedimentary geology

Radioactive parent isotope	Radiogenic daughter isotope	Decay mechanism	Decay constant (λ)	Half-life[a] ($T_{1/2}$), billion years
^{87}Rb	^{87}Sr	Beta	1.42×10^{-11}	48.8
^{147}Sm	^{143}Nd	Alpha	6.54×10^{-12}	106
^{238}U[b]	^{234}U**, ^{230}Th**, ^{206}Pb	Alpha and beta	1.551×10^{-10}	4.468
^{235}U[b]	^{231}Pa**, ^{207}Pb	Alpha and beta	9.8485×10^{-10}	0.704
^{232}Th[b]	^{208}Pb	Alpha and beta	4.9475×10^{-11}	14.010
^{40}K	^{40}Ar	Electron capture	0.581×10^{-10}	11.93[c]
^{40}K	^{40}Ca	Beta	4.962×10^{-10}	1.397[c]
^{187}Re	^{187}Os	Beta	1.64×10^{-11}	42.3
^{138}La	^{138}Ce	Beta branched decay	2.24×10^{-12}	310
^{176}Lu	^{176}Hf	Beta	1.94×10^{-11}	35.7
^{14}C	^{14}N	Beta	1.75×10^{-4}	5730 years
^{137}Cs	^{137}Ba	Beta	2.29×10^{-2}	30.3 years

Data from compilations by Faure (1986), Blum (1995), Dickin (1995), and Brownlow (1997).

[a] See Appendix A for derivation of the relationship between decay constant and half-life.

[b] Unlike the other radioactive parent isotopes listed that produce a stable daughter isotope, ^{238}U, ^{235}U, and ^{232}Th each decay to produce a series of intermediate daughter isotopes that are themselves radioactive (these are denoted by **). A stable isotope of lead (^{206}Pb, ^{207}Pb, ^{208}Pb, respectively) is produced at the end of these three decay chains. The application of the U and Th decay series to sedimentary geology is discussed in the Geochronology section. The relationship between decay constant and half life is given in Appendix 1.

[c] ^{40}K undergoes branched decay to ^{40}Ar and ^{40}Ca, the sum of which yields a decay constant of 5.543×10^{-10} years and a half-life of 1.25×10^{9} years.

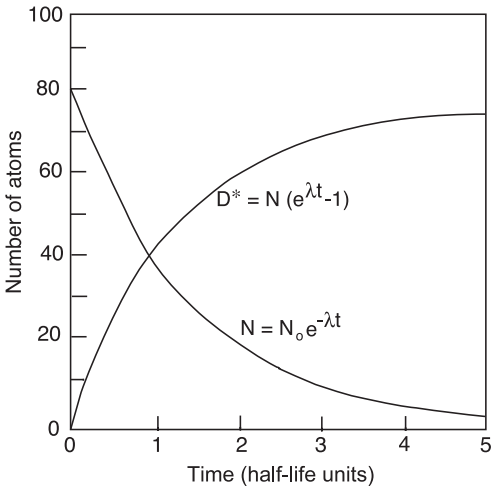

Fig. 2. Illustration of rate of decay of radioactive parent isotope N and growth of radiogenic daughter isotope D^* using Eqs. (1) and (2). Time axis is in terms of half-life units of the parent isotope. These curves apply to any radioactive parent–radiogenic daughter isotope pair. See Faure (1986).

that can be found in Faure (1986, chapters 2–4), Dickin (1995, chapter 1), and White (1996).

Most radioactive isotopes are extinct, having been produced by nucleosynthetic (i.e., element-building) processes during stellar evolution, and subsequently having decayed to extinction over geologic time. The radioactive isotopes that still exist in measurable concentrations in geologic materials do so because of one of several reasons:

(1) they have a long half-life relative to the age of the Earth (e.g., ^{238}U, ^{87}Rb),
(2) they are radioactive daughter isotopes that result from the decay of radioactive parent isotopes that have a long half-life (e.g., ^{234}U produced from decay of ^{238}U),
(3) they are produced cosmogenically; that is, by the bombardment of stable isotopes by cosmic rays (e.g., ^{14}C), or
(4) they are produced by human activities and released to the environment (e.g., ^{90}Sr).

Radioactive decay occurs by one of several mechanisms, depending on the nuclear configuration of a particular isotope. The principal mechanisms are identified by the process (e.g., fission) or by the nuclear particle that is emitted during decay, including alpha, beta, and positron particles. For the Rb–Sr isotope system, the mechanism of interest is the decay of a ^{87}Rb atom to produce a ^{87}Sr atom, decay energy, and two nuclear particles—an anti-neutrino and a beta particle (β^-). A beta particle is a negatively charged particle with no mass, and an anti-neutrino is an atomic particle with negligible charge and mass. This decay event is represented as $^{87}Rb \rightarrow {}^{87}Sr + \beta^-$. The decay mechanisms, decay constants, and half-lives for the major radiogenic isotope systems used in sedimentary geology are given in Table 1.

2.1. Equations for radioactive decay

The rate of radioactive decay of a given isotope is proportional to the number of radioactive parent atoms (N) present at a given time. This rate of decay,

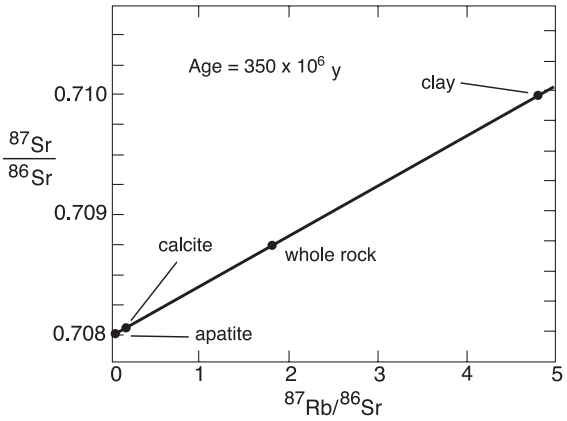

Fig. 3. $^{87}Sr/^{86}Sr$–$^{87}Rb/^{86}Sr$ isotope systematics in a hypothetical 350-million-year-old sedimentary rock composed of biogenic calcite and apatite and authigenic clay minerals. These minerals all formed from seawater with an $^{87}Sr/^{86}Sr$ value of 0.7080. The range of the mineral's present-day $^{87}Sr/^{86}Sr$ values is a function of higher $^{87}Rb/^{86}Sr$ values in K- and Rb-rich clay minerals. The slope of a given line on this diagram defines a unique age (i.e., isochron), as discussed for Eq. (5). The isochron method is used to determine a rock sample's age by (1) measuring the present-day $^{87}Sr/^{86}Sr$ and $^{87}Rb/^{86}Sr$ ratios in a suite of cogenetic minerals from the sample, (2) constructing a best-fit line to the data, and (3) determining the slope of the line. This is the basis for application of Rb–Sr isotope system as a geochronometer. The accuracy of isochron ages is dependent upon several assumptions discussed in text, including that of closed system behavior. In sedimentary systems such as the one portrayed, evaluating the closed system assumption requires assessment of the amount of detrital vs. authigenic clay components, and knowledge of the timing and extent of diagenesis.

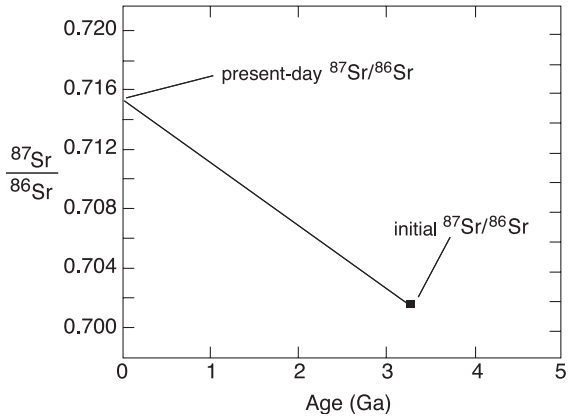

Fig. 4. $^{87}Sr/^{86}Sr$ evolution of a 3.2 b.y. rock or mineral sample as a function of time. The line portrays the growth with time of radiogenic ^{87}Sr in a rock, mineral, or other reservoir. Such lines are termed "evolution lines", and have slopes with magnitudes proportional to $^{87}Rb/^{86}Sr$ (and to Rb/Sr), per discussion after Eq. (5). Given closed-system behavior, the present-day Sr isotope composition of a sample is thus a function of its starting, or initial, Sr isotope composition, its Rb/Sr ratio, and its age.

or loss of atoms with time, is expressed mathematically as $-dN/dt \propto N$, or $-dN/dt = \lambda N$, where λ is the proportionality constant (termed the decay constant) that has a unique value for each radioactive decay scheme. Algebraic derivation, given in Appendix A, leads to the following expressions that represent the decay of a radioactive parent and growth of a radiogenic daughter isotope:

$$N = N_o e^{-\lambda t} \quad (1)$$

and

$$D^* = N(e^{\lambda t} - 1) \quad (2)$$

where N_o = the number of original parent atoms in the system (or rock sample) before decay began; N = the number of parent atoms remaining at a given time; t = the amount of time since decay began; D^* = the amount of daughter isotope accumulated during time t.

Fig. 2 illustrates the exponential nature of decay and growth in radiogenic isotope systems. Using Eq. (2), the total number of atoms of the daughter isotope present today in a sample (D) is the sum of those that were initially present in the system (D_o) and those daughter atoms produced by radiogenic growth (D^*), so that

$$D = D_o + N(e^{\lambda t} - 1). \quad (3)$$

Eq. (3) is useful when considering the applicability of various radioactive systems to geochronology and the evolution of various reservoirs such as the Earth's mantle and crust.

The analogous expression for the Sr isotope system is

$$^{87}Sr = {}^{87}Sr_o + {}^{87}Rb(e^{\lambda t} - 1). \quad (4)$$

Since isotope measurements are most easily made as isotope ratios, we use the more common expression obtained by dividing by a stable, non-radiogenic isotope, in this case ^{86}Sr.

$$^{87}Sr/^{86}Sr = {}^{87}Sr/^{86}Sr_o + {}^{87}Rb/^{86}Sr(e^{\lambda t} - 1). \quad (5)$$

Eq. (5) is in the form of a straight line $y = b + mx$, whereby on a diagram of $^{87}Sr/^{86}Sr$ vs. $^{87}Rb/^{86}Sr$, $^{87}Sr/^{86}Sr_o$ (the initial $^{87}Sr/^{86}Sr$ value) is the y-intercept and the slope of any straight line is proportional to

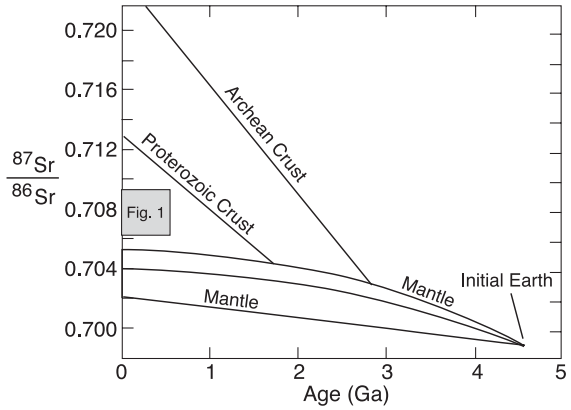

Fig. 5. Sr isotope evolution of the Earth (after Faure, 1986). Crust and mantle evolution lines constructed as in Fig. 4. The crust evolution lines shown represent only a small part of the spectrum of evolution lines that would correspond to the wide range of Rb–Sr ratios and ages found in different parts of the continental crust. The mantle evolution lines encompass most of the variability found in the Earth's mantle. The low slope of the mantle evolution lines is due to its low Rb–Sr. Mantle evolution lines are curvilinear because the mantle's average Rb–Sr decreases with time as the crust with relatively high Rb/Sr is progressively extracted from the mantle. Inset is space occupied by Fig. 1, which contains the Phanerozoic seawater Sr isotope curve. Note that seawater $^{87}Sr/^{86}Sr$ today and throughout the Phanerozoic has never attained values as high as the average continental crust values, nor as low as oceanic crust values. The estimated initial $^{87}Sr/^{86}Sr$ value of the Earth is based on analyses of well-preserved, old basaltic achondrite meteorites (Papanastassiou and Wasserburg, 1969).

time (i.e., $m = e^{\lambda t} - 1$; Fig. 3). Lines with shallower slopes correspond to younger ages, and steeper slopes correspond to older ages. This is the basis for the use of the $^{87}Rb/^{86}Sr$ – $^{87}Sr/^{86}Sr$ diagram for geochronology. On a plot of $^{87}Sr/^{86}Sr$ vs. time, the slope of any straight line is proportional to a system's (or sample's) Rb/Sr ratio (Fig. 4). This type of diagram is useful for portraying the Sr isotope evolution of geochemical reservoirs of different origin and age, such as those within the Earth's mantle and crust. Tracking Sr isotope evolution in this manner is in turn useful for interpreting the mechanisms that drive secular changes in ocean chemistry, as will be illustrated in the discussion accompanying Fig. 5.

3. Sample selection and analytical methods for radiogenic isotope analysis

Chemical stratigraphy, or ''chemostratigraphy'', involves the correlation of geographically separated strata using a geochemical signature. Applied to marine sedimentary rocks, chemostratigraphy requires that a well-preserved marine geochemical signature can be obtained from the strata. Several steps are involved in conducting radiogenic isotope analyses of sedimentary rocks for the purpose of chemostratigraphy. The use of appropriate sample selection and analytical methods is the key to assuring that reliable geologic information is obtained from the isotope data that result. A complete sequence of sample analysis includes: (1) selection of samples using stratigraphic, petrographic, and geochemical criteria; (2) physical extraction from the host sample; (3) chemical pretreatment to remove ions from exchangeable or leachable sites within or on surfaces of minerals; (4) dissolution of the sample; (5) chemical separation of the element of interest; and (6) mass spectrometric analysis.

3.1. Sample selection and extraction

A range of sample selection criteria and methods has been used in preparing samples for measurement of isotope ratios in a mass spectrometer. For studies of secular variations in seawater chemistry and chemostratigraphy, sample selection criteria determine the best-preserved samples in order to extract a near-primary marine isotope signature. These criteria include petrography using plane light, cathodoluminescence, and ultraviolet luminescence, and scanning electron microscopy. The criteria are used to discriminate the original marine from non-marine phases, to identify the least-altered portions of original marine phases, and to detect non-carbonate contaminants (e.g., Montañez et al., 1996, 2000). Separation of the least altered and/or purer portions is accomplished by using mineral separation methods on whole-rock samples (Banner et al., 1988a), or different types of high spatial resolution sampling methods. These include mechanical microsampling drills (Carpenter et al., 1991; Banner and Kaufman, 1994; Mii and Grossman, 1994; Dettman and Lohmann, 1995) and laser ablation methods (Christensen et al., 1995). The tradeoffs between mechanical microsampling and laser ablation methods for Sr isotope analysis, in terms of sample size, spatial resolution, accuracy, precision, and speed of analysis, are discussed in Davidson et al. (1998).

Petrographic criteria are augmented with geochemical criteria, including stable isotope and trace-element analysis (e.g., Veizer, 1983). Such data can be used to independently determine the extent to which original marine phases preserve a marine geochemical signature by using previously determined marine values for a given period of Earth history, or by revealing seasonal geochemical patterns that record depositional processes (e.g., Mii and Grossman, 1994).

3.2. Pretreatment

Pretreatment procedures refer to those used to produce a separation between mineral phases, or to preferentially extract elements from specific sites within mineral phases. These procedures are used after solid or powdered samples have been obtained, and prior to dissolution and ion exchange separation of the element(s) of interest and mass spectrometry. The goal of such procedures on carbonate samples is to (1) physically separate non-carbonate contaminants, especially silicates, or (2) chemically remove Sr from loosely bound exchange sites on surfaces and within the lattice of non-carbonate contaminants, since Sr in these sites is likely to have a different history and isotopic composition than that in the carbonate phase of interest (Banner et al., 1988a;

Montañez et al., 1996; Bailey et al., 2000). Phosphatic materials are also used as records of ancient seawater radiogenic isotope compositions. Pretreatment of conodont samples via sequential acid leaching indicates a progressive removal of diagenetic and/or detrital Sr from the original sample (Martin and Macdougall, 1995; Ruppel et al., 1996). Rigorous sample selection criteria and pretreatment methods in many cases are the only means to obtain a reliable least-altered marine isotopic signature.

3.3. Chemical separation

Prior to measurement of isotope ratios using mass spectrometry, the element of interest must be extracted from the geologic sample and purified in order to minimize mass spectral interferences. The element of interest must be of relatively high purity when introduced into the mass spectrometer because other elements or compounds may (1) have isotopes of similar mass that interfere with the mass spectrum produced by the element of interest, or (2) inhibit or alter the ionization of the element of interest. This elemental separation first requires dissolution of a rock or mineral sample using acids such as nitric or acetic for carbonates and hydrofluoric and nitric acids for silicates. Elemental separation is typically accomplished for radiogenic isotope systems by ion exchange chromatography, wherein elements of interest are separated using acids and resin beads produced from synthetic polymers. The ion exchange process is conducted by adding the dissolved sample to a narrow Teflon or glass column containing resin beads, followed by adding acids of varying strength and/or type selected to partition the elements of interest. For some isotope systems, elemental separation may also be effected by other methods, such as partitioning between two immiscible liquids.

Since samples may be contaminated with extraneous material introduced during the sample collection, preparation, pretreatment, and chemical separation procedures described above, the level of contamination (i.e., blank level) must be monitored. For example, a finite amount of Sr may be introduced to a carbonate sample from airborne dust, saw blades, epoxy, polishing media, ammonium acetate, nitric acid, distilled water, beakers, centrifuge tubes, contact with human hands, etc. Through care in sample handling, purification of reagents, acid cleaning of labware, working in clean rooms, or clean hoods with filtered air under laminar flow, use of Teflon and quartz glass labware, and scaling down the amount of materials used in these procedures, blanks can be maintained at negligible levels ($<5\times10^{-11}$ g) for sample sizes of 5×10^{-8} g of Sr (e.g., Musgrove and Banner, in press). This corresponds to a sample size of 0.5 mg for calcite that contains 100 ppm Sr.

3.4. Measurement of isotope ratios

For radiogenic isotope measurements, the element of interest is introduced into the ion source of a thermal ionization mass spectrometer as a solid salt on a metal filament and ionized by heating the filament. More recently, high-resolution inductively coupled plasma source mass spectrometers (ICP-MS), in which samples in solution form are efficiently ionized in a high-temperature plasma, have also been used for measuring radiogenic isotope ratios (Christensen et al., 1995). These ions are then accelerated via high voltage through a magnetic field, which deflects and separates ions of different mass (and the same charge) into a mass spectrum (e.g., ^{84}Sr, ^{86}Sr, ^{87}Sr, and ^{88}Sr). Lighter mass isotopes are more strongly deflected than heavier isotopes. The relative amounts of the different masses are measured by the current produced when they strike ion detectors (such as Faraday cups or secondary electron multipliers) positioned downstream from the magnetic field. Since the amount of current produced by the different isotopes of an element is a measure of their relative isotopic abundances, measurement of isotope ratios by this method is much more accurate and precise than measurement of absolute isotope abundances.

3.4.1. Interlaboratory comparisons

Research laboratories that conduct Sr isotope studies analyze standard reference materials for interlaboratory comparisons to determine and adjust for biases between mass spectrometers. The most common standards used for this purpose are the National Institute of Standards and Technology Standard Reference Material 987 (SRM987) and modern seawater. Burke et al. (1982) adjusted their sample analyses to a ^{87}Sr/^{86}Sr value of 0.71014 for SRM987. Most recent

Sr isotope studies from other laboratories report a range of $^{87}Sr/^{86}Sr$ values from 0.7102 to 0.7103 for this standard, and comparison of data obtained in these studies and the Burke et al. study must adjust the values measured on samples for the differences in standard values for each laboratory. For example, in order to compare samples measured in laboratory A, which measures a value of 0.71025 on SRM987, to the Burke curve, one must either subtract 0.00011 from the measured values obtained for laboratory A samples, or add an equivalent amount to the Burke curve data. Analytical accuracy and precision for Sr isotope ratios are determined by repeated measurements on standards. External precision (2σ) is typically in the range of ± 0.00001 to ± 0.00003.

3.5. Isotope fractionation

A stable or radiogenic isotope ratio of a given element may change as a result of a variety of natural processes and as a result of the ionization process that occurs during analysis in a mass spectrometer. This change in isotope ratio is referred to as fractionation. All other factors being equal, the extent of fractionation is dependent on the relative differences in mass of the isotopes of interest. Radiogenic systems, which involve relatively heavy isotopes, usually exhibit smaller extents of fractionation than light stable isotope systems because their relative mass differences are small. For example, the mass difference between the isotopes of interest of oxygen (^{16}O and ^{18}O) is approximately 12%, whereas the mass difference between ^{87}Sr and ^{86}Sr is approximately 1%. Hence, oxygen isotopes fractionate to a greater extent during natural geologic processes and during mass spectrometric analysis.

For Sr isotope analysis, the ratio of the stable Sr isotopes, $^{86}Sr/^{88}Sr$, has a value of 0.1194 in nature. This value is adopted by convention and is used in all laboratories to correct for the effects of any fractionation of Sr isotopes that occurs during thermal ionization over the course of analysis in the mass spectrometer. This same correction would apply to any fractionation that occurred in nature prior to analysis, assuming that the natural fractionation process followed the same mass dependence as the instrumental fractionation process. Thus, if fractionation did occur in nature, it would not be observed since its effects are normalized during analysis (Banner and Kaufman, 1994). This means that all minerals precipitated from the same solution, whether inorganic or biogenic, or skeletons of the same or different species or mineralogy, will incorporate the same Sr isotope value. Separating the effects of Sr isotope fractionation that occurs in natural systems vs. mass spectrometers could be accomplished by adding two artificially enriched Sr isotopes to a sample, which would allow for measurement of the extent of instrumental fractionation.

The high degree of Sr isotope homogeneity among Holocene marine shell material of different species and modern seawater (DePaolo and Ingram, 1985; Capo and DePaolo, 1992) indicates that differences that may exist in the nature of instrumental and natural fractionation processes are smaller than the high precision of modern mass spectrometric measurements. In contrast, fractionation of stable isotopes in natural systems is readily discernible and constitutes a principal application of stable isotopes to the study of geologic and biologic processes.

4. Trace-element behavior

The elements that comprise radiogenic isotope systems most commonly occur at trace-element levels in geologic systems. Understanding the trace-element behavior of these elements will therefore provide insight into processes that control radiogenic isotope variations. Rubidium is an alkali element that occurs as the Rb^+ ion in aqueous solution, whereas Sr is an alkaline earth, occurring as the Sr^{2+} ion. As a consequence of the important role that ionic size and charge plays in governing an element's geochemical behavior, Rb and Sr will be incorporated into minerals forming from solution in different amounts. Strontium preferentially substitutes for Ca, and Rb for K, in the crystal lattices of natural minerals (compare ionic radii, Table 2). In carbonate mineral lattices, Sr^{2+} substitutes at Ca^{2+} sites, whereas Rb^+ is comparatively excluded from Ca^{2+} sites. The extent of substitution of trace elements in mineral lattices or on ion exchange sites is quantified by distribution coefficient values, which are determined by studies in experimental and natural systems (e.g., Banner, 1995).

Table 2
Ionic charge and size information for some major and trace elements of interest

Element	Position in periodic table	Common valence in aqueous solution	Ionic radius (Å)
Rubidium	Alkali metal	Rb^{+}	1.52
Potassium	Alkali metal	K^{+}	1.38
Strontium	Alkaline-earth metal	Sr^{2+}	1.18
Calcium	Alkaline-earth metal	Ca^{2+}	1.00
Lanthanum	Lanthanide series	La^{3+}	1.032
Cerium	Lanthanide series	Ce^{3+}, Ce^{4+}	1.01, 0.87
Samarium	Lanthanide series	Sm^{3+}	0.958
Neodymium	Lanthanide series	Nd^{3+}	0.983
Uranium	Actinide series	U^{6+}, UO_2^{2+}	0.73
Thorium	Actinide series	Th^{4+}	0.94
Lead	Group IV metal	Pb^{2+}	1.19
Rhenium	Mn subgroup of transition elements	Re^{7+}	0.53
Osmium	Platinum group element	Os^{4+}	0.63
Lutetium	Lanthanide series	Lu^{3+}	0.93
Hafnium	Group IVB element	Hf^{4+}	0.71

Data from Shannon (1976) for six-fold coordination.

Variations in the radiogenic isotope composition of an element such as Sr serve as a tracer of the source and pathway of dissolved ions in the hydrologic cycle. This is in contrast to variations in the light stable H and O isotopes, which trace the source and pathway of H_2O molecules. Both types of isotope systems provide important complementary information for geochemical studies. Enhanced tracer capabilities are also provided by using both the trace-element behavior and isotope variations in elements such as Sr, Nd, U, and Pb (Banner and Hanson, 1990). Differences among the abundances of the elements of the radiogenic isotope systems of interest yield insight into their geochemical behavior, as developed in succeeding sections (Table 3).

5. Sr isotope evolution of the Earth

The Earth's crust and mantle have distinct ranges of Rb/Sr ratios owing to their distinct mineral assemblages. As was observed for the $^{87}Sr/^{86}Sr$ vs. time diagram (Fig. 4), the slope of Sr isotope evolution lines

Table 3
Concentrations of selected elements in natural waters, the crust, and sedimentary rocks

Element	Rain	River water	Ground-water	Seawater	Upper crust	Shales	Carbonate rocks	Oceanic residence time (years)
Cl	0.1–0.6	8	$1–10^5$	19,350	150	200	150	630×10^6
Na	0.02–0.6	6.1	$1–10^5$	10,760	25,700	13,000	6000	200×10^6
K	0.05–0.09	2	$1–10^3$	399	28,000	27,000	3000	13×10^6
Rb	0.0002	0.0031	0.002	0.12	110	140	4	0.79×10^6
Ca	0.05–0.1	26	$10–10^5$	411	29,450	22,000	380,000	1.3×10^6
Sr	0.0001–0.0002	0.11	0.1–2000	8	316	250	500	5×10^6
Ce	–	6×10^{-5}	–	3.5×10^{-6}	64	80	12	50
Nd	–	1.7×10^{-4}	10^{-6}–10^{-4}	4.2×10^{-6}	26	25	10	400
Sm	–	4.1×10^{-5}	10^{-7}–10^{-5}	0.8×10^{-6}	4.5	7.2	2	400
U	$<1 \times 10^{-6}$	4×10^{-5}	10^{-6}–1	3.1×10^{-3}	2.5	3.2	1	1×10^6
Th	$<2 \times 10^{-5}$	$<1 \times 10^{-4}$	10^{-7}–10^{-5}	6×10^{-8}	10.3	12	0.01	3
Pb	0.0006–0.006	0.003	3×10^{-4}	2×10^{-6}	17	22	5	50
Os	–	$5–25 \times 10^{-9}$	–	1.1×10^{-8}	5×10^{-4}	–	–	10^3–10^5

Concentrations in parts per million. Interocean mixing time is ~1500 years (Broecker and Peng, 1982; Elderfield and Greaves, 1982). Rainwater data are the range for remote and polluted sites in Norway (Reimann and Caritat, 1998). Surface water is world average river water (Reimann and Caritat, 1998), except for Rb, Sr, Sm, and Nd (mean values from global data set of Goldstein and Jacobsen, 1987). Groundwater data are the concentration range for samples that include shallow (dilute) and deep (saline) subsurface, low-temperature waters, from Freeze and Cherry (1979), Banner et al. (1989), Banner and Hanson (1990), Drever (1997), Reimann and Caritat (1998), and Ivanovich and Harmon (1992). Seawater data from Taylor and McLennan (1985), Levasseur et al. (1998), and Burton et al. (1999) for Os. Upper crust data from Reimann and Caritat (1998). Upper crust, shales, and carbonate rock data from Reimann and Caritat (1998), except for Sm and Nd (Banner and Hanson, 1990) and U and Th (Ivanovich and Harmon, 1992). Residence time data from Taylor and McLennan (1985), Nozaki (2001) for lanthanides, and Levasseur et al. (1998) for Os. The Pb abundances in most natural waters are largely due to anthropogenic contamination.

as a function of time will be directly dependent on a sample's or reservoir's Rb/Sr ratio. Therefore, a sample with a high Rb/Sr ratio will evolve to a higher present-day $^{87}Sr/^{86}Sr$ value than a coeval sample with a low Rb/Sr ratio. An analogous view of Fig. 4 is given in Fig. 5 with respect to the evolution of the Earth's crust and mantle. Several features of this diagram are apparent:

(1) The early Earth, represented by the composition of ca. 4.5 b.y. old meteorites, had very low $^{87}Sr/^{86}Sr$ values ($^{87}Sr/^{86}Sr \sim 0.699$).
(2) The Earth's upper mantle, represented by the composition of mantle-derived igneous rocks of varying age, has evolved along a range of relatively shallow trajectories to low present-day $^{87}Sr/^{86}Sr$ values (~ 0.703).
(3) The Earth's crust, which accumulated by differentiation of the Earth's mantle via partial melting and crystal fractionation processes that produce higher Rb/Sr in the resulting magmas, has a wide range of relatively steep trajectories to high present-day values. The heterogeneity of the Earth's crust reflects the wide range of magmatic, sedimentary, and metamorphic evolutionary processes and has produced the wide range of Rb/Sr values. In spite of this heterogeneity, older crustal rocks have, to a first approximation, evolved to higher present-day $^{87}Sr/^{86}Sr$ values than younger crustal rocks.
(4) Phanerozoic seawater $^{87}Sr/^{86}Sr$ has varied between the limits of crustal and mantle values, thereby reflecting the combined inputs from these two sources to the world's oceans. The extent to which seawater $^{87}Sr/^{86}Sr$ reflects variations in the contribution from these and other sources through geologic time will be explored in a later section.

6. Sr isotope tracers of the modern hydrologic cycle

We can examine the modern hydrologic cycle of Sr using the template constructed above of Sr isotope variations in the Earth's crust, mantle, and oceans. This will provide insight into changes in this geochemical cycle in the past, which will in turn have application to studies of ancient ocean chemistry, chemostratigraphy, environmental change, and diagenesis.

6.1. Weathering

Weathering reactions represent the means by which Sr is added to the hydrologic cycle and delivered to the oceans. We consider here the major controls on the weathering and transport of Ca since Sr follows Ca in its low-temperature aqueous geochemistry and substitution in mineral structures (Table 2). Carbonate, silicate, and evaporite minerals may weather by dissolving directly into solution or by weathering reactions that produce residual phases (e.g., clays from igneous or metamorphic silicates, low-Mg calcite from aragonite) plus ions in solution. Ion exchange reactions between natural waters and exchange sites in clay minerals will also introduce new Sr into solution. The following reactions involve the release of Ca^{2+} (and, therefore, Sr^{2+}) aqueous ions (aq) into solution from the breakdown of some principal rock-forming minerals:

dissolution of aragonite:

$$CaCO_3 + CO_2 + H_2O = Ca^{2+} + 2HCO_3^-(aq); \quad (6)$$

dissolution of diopside:

$$CaMgSi_2O_6 + 4CO_2 + 6H_2O = Ca^{2+}(aq) + Mg^{2+}(aq) + 2H_4SiO_4(aq) + 4HCO_3^-(aq); \quad (7)$$

conversion of anorthite to kaolinite:

$$CaAl_2Si_2O_8 + 2CO_2 + 3H_2O = Al_2Si_2O_5(OH)_4 + Ca^{2+}(aq) + 2HCO_3^-(aq). \quad (8)$$

These reactions illustrate the driving force of carbonic acid, produced from the combination of carbon dioxide and water, in weathering minerals. A direct correlation between Sr and Ca concentrations and pH in the global river data set of Goldstein and Jacobsen (1987) reflects the influence of these and similar reactions in the chemical budget of large watersheds. The trace-element behavior of Sr must be considered when determining the effects of formation of secondary phases on the Sr isotopic evolution of the water that mediates a given reaction. On the scale of an aquifer or watershed, Sr isotopes have been used to illustrate that the relative importance and rates of these and other reactions will vary as a function of rock type, climate,

soil type and thickness, vegetation type, porosity–permeability relationships, and anthropogenic influences (Graustein and Armstrong, 1983; Capo et al., 1998; Blum et al., 2002; Cooke et al., in press; Jackson et al., 2002; Musgrove and Banner, in press). Applications of strontium isotopes to ecosystems have also revealed the sources and extent of cycling of cations (English et al., 2001; Kennedy et al., 2002).

6.2. Rain

Since Sr is not a volatile element, it predominantly remains in the ocean during evaporation. As a result, rainwater has very low Sr concentrations (Table 3). One would expect rainfall Sr concentrations to decrease from the coast toward the interior of a landmass as the effects of sea spray decrease and the number of rainout cycles increases. A larger database exists for Ca concentrations in rainwater, which may yield insight into the controls on Sr in rainwater. Rainwater Ca contents generally decrease toward continental interiors, with regionally higher concentrations attributable to wind-blown calcareous soil dust or anthropogenic particulate emissions from industrial sources (Berner and Berner, 1996).

6.3. Surface water

In comparison with variations in major ions such as Na, Ca, and Mg in surface waters, Sr isotope compo-

Table 4
Sr and Nd isotope and major ion data for selected rivers

River	Location	$^{87}Sr/^{86}Sr$	Sr (ppb)	$\varepsilon_{Nd}(0)$	Nd (ppt)	Na	Ca	Mg
North America								
Mississippi	Jacobsen, MN	0.7153	74	−19.4	46	3.7	30	10
Mississippi	Chester, IL	0.7095	264	−8.5	24	21	61	20
Missouri	Washington, MO	0.7100	352	−7.7	23	27	60	17
Colorado	Hoover Dam, NV	0.7108	1161	−8.0	6.0	110	79	29
Fraser	Fitzwilliam, BC	0.7514	39	−24*	–	–	–	–
Fraser	Alexandra Bridge, BC	0.7127	85	−7.5*	–	–	–	–
Merced	Yosemite, CA	0.7077	17	−5.3	22	0.9	1.4	0.2
Canadian rivers	Weighted mean of 39	0.7111	84	–	–	–	18	–
South America								
Amazon	Obidos	0.7109	28	–	–	–	–	–
Greenland								
Isua-F	Isua, W. Greenland	0.9430	3.2	−43	274	0.52	1.50	0.61
Nigsik	Qorqut, W. Greenland	0.8264	4.3	−44	478	0.75	0.69	0.23
Australia								
Avon	Toodyay, WA	0.7326	2940	–	34	3400	208	446
India								
Ganges		0.7257	139	–	–	–	–	–
Brahmaputra		0.7210	82	–	–	–	–	–
Japan								
Mogami	Sakata	0.7071	40	0.1	–	12	8.1	2.5
Philippines								
Cagayan	Aparri	0.7062	172	6.7	–	9.1	25	5.2

Concentrations in parts per million except where noted otherwise (ppb = parts per billion; ppt = parts per trillion). Data from Wadleigh et al. (1985; mean for Canadian rivers); Goldstein and Jacobsen (1987); Palmer and Edmond (1989); Cameron and Hattori (1997, Fraser River). Isotope values are for dissolved material, except where noted by * for suspended material. $\varepsilon_{Nd}(T)=[(^{143}Nd/^{144}Nd_{\text{sample at time T}})/(^{143}Nd/^{144}Nd_{\text{CHUR at time T}})-1]\times 10^4$, where CHUR is a chondritic uniform reservoir, which represents a bulk earth Nd isotope composition. $\varepsilon_{Nd}(0)$ is the present-day $\varepsilon_{Nd}(T)$ value.

sitions reflect a first-order control by the geology (i.e., rock type and age) of the regions that they drain (Wadleigh et al., 1985; Goldstein and Jacobsen, 1987; Palmer and Edmond, 1992). This is well illustrated by the following features of the data given in Table 4 and in Fig. 5:

(1) Strontium isotope values for some major rivers draining the southern part of North America have Sr isotope values of 0.710, which is consistent with a combination of Proterozoic and Paleozoic crustal and sedimentary sources of Sr. A larger data set for Canadian rivers have a higher mean Sr isotopic composition ($^{87}Sr/^{86}Sr \sim 0.711$) likely due to the influence of the older crust of the Precambrian shield (Wadleigh et al., 1985). The Merced river in California, on the other hand, is the lowest of the North American rivers analyzed by Goldstein and Jacobsen (1987), reflecting the fact that the Merced drains the relatively young Sierra Nevada. Strontium isotope trends along individual rivers in North America indicate the diminished influence of older, interior cratonic rocks with increased distance toward the coast (e.g., Mississippi, Fraser rivers).
(2) Rivers draining Early Proterozoic and Archean crust, such as West Greenland and parts of Western Australia, have very high $^{87}Sr/^{86}Sr$ values. The Isua river drains terrain in West Greenland that is comprised in part of 3.8 Ga crust, and has $^{87}Sr/^{86}Sr$ values in excess of 0.8! Relatively high values are found in rivers that drain the Himalayas, consistent with a drainage area that includes unroofed metamorphic rocks with elevated $^{87}Sr/^{86}Sr$ values (Edmond, 1992).
(3) Very low $^{87}Sr/^{86}Sr$ values of 0.704–0.708 are found in rivers draining circum-Pacific volcanic arc terrains such as Japan and the Philippines, consistent with a young, mantle-derived source of Sr for the weathering substrate.

Thus, Sr isotopes provide us with a diagnostic signal of the source of dissolved and suspended constituents in rivers that we could not get through studies of major- or trace-element variations. As noted in the Weathering section above, one can apply Sr isotopes in smaller-scale watersheds to examine the effects of ecosystem dynamics (e.g., changes in soil and vegetation) on surface water geochemistry.

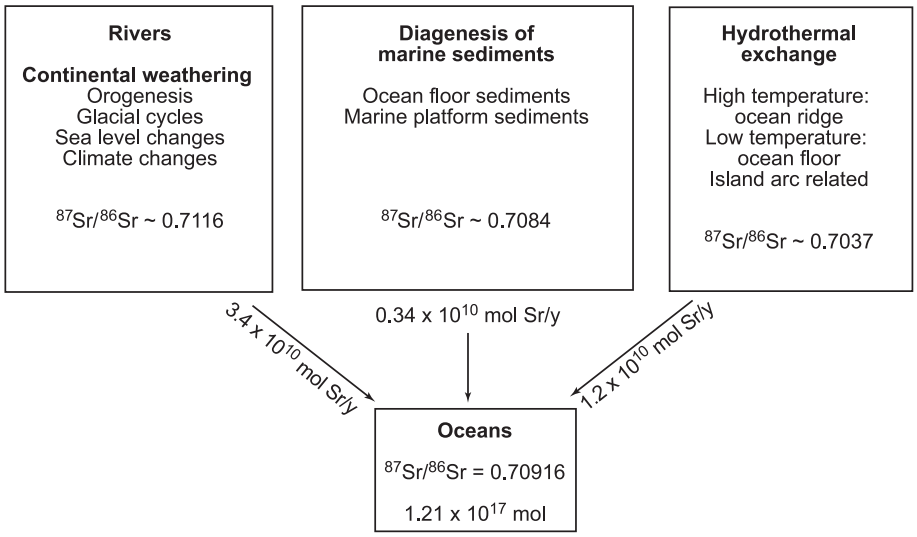

Fig. 6. The modern geochemical cycle of Sr shown in terms of the fluxes (in units of moles of Sr per year) and isotopic composition of the inputs to the oceans (after Holland, 1984; Palmer and Edmond, 1989; and Davis et al., 2003). Changes in the $^{87}Sr/^{86}Sr$ value of the oceans through time are used to infer changes in the Earth surface processes that control these fluxes. The potential power of this approach is limited by uncertainties in quantifying the fluxes and isotopic composition of different contributions to the cycle, as discussed in the text.

6.4. Groundwater

Strontium isotope variations in groundwater are similar to those in surface waters in that Sr isotopes in groundwater reflect the age and rock type of the aquifer. The effects can be more pronounced for groundwater as a consequence of higher temperature, pressure, and ionic strength of deeper groundwater, and the longer transit time and higher mineral-surface to water-volume ratio for groundwater relative to surface water. In conjunction with other chemical and physical methods, Sr isotope variations in groundwater have been used to trace flow paths and specific mineral-solution reactions in soils and aquifer rocks (e.g., Stueber et al., 1983; Chaudhuri et al., 1987; McNutt et al., 1990; Banner et al., 1994).

Based on the perspective of the above discussion, modern surface water and groundwater $^{87}Sr/^{86}Sr$ values will vary as a function of the following features of the rocks that comprise the aquifer or watershed in question: (1) mineralogy, age, and crustal vs. mantle source for igneous and metamorphic rocks; (2) provenance and maturity for shales and sandstones; (3) age and extent of alteration for marine carbonates, evaporites, and phosphorites; and (4) soil composition. Strontium isotope values may also be influenced by additional factors such as climatic controls on the amount of recharge and flow routes (Banner et al., 1996).

6.5. Oceans, budgets, and residence times

Since the oceans are the ultimate receptacle for the continents' surface water and groundwater, the global ocean's Sr isotope composition reflects the relative fluxes of these transport agents of the hydrologic cycle, as well as fluxes from the alteration of oceanic basalts and sediments. A flux is the amount of material (such as the number of atoms of an element, the volume of water, etc.) transported into or out of a reservoir per unit time. Characterizing the amount of Sr and its isotopic composition in the various fluxes of Sr to the oceans is used to construct the oceanic budget of Sr, which yields insight into the relative importance of the different components of this geochemical cycle. The budget represents the mass transfer of materials between reservoirs, as illustrated in Fig. 6. In addition to applying such budgets to assess the state of balance of the modern global cycle of Sr (Davis et al., 2003), one can also use them to infer changes in the fluxes to the oceans over time, as will be discussed in later sections.

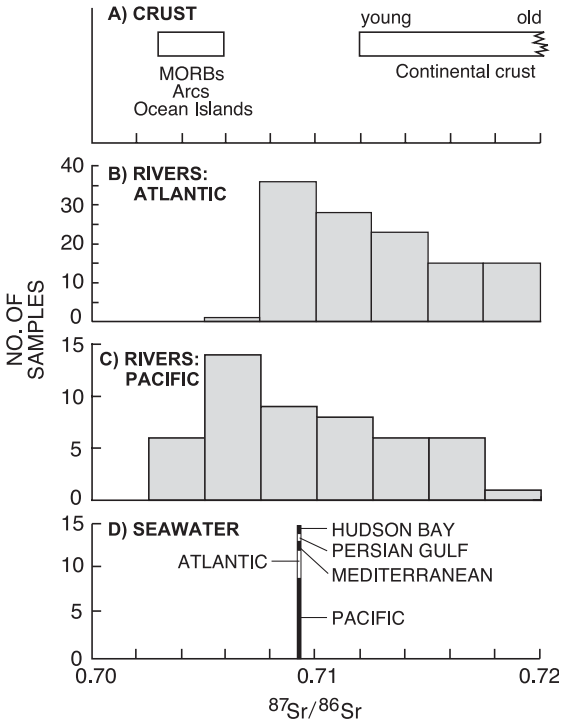

Fig. 7. Comparison of Sr isotopic variability in (A) continental and oceanic crust (MORB = midocean ridge basalts; Arcs = island arc basalts); (B, C) rivers draining to the Atlantic and Pacific Oceans; (D) modern oceans and seas, based on analyses of Holocene marine shells (DePaolo and Ingram, 1985). Analytical uncertainty for Sr isotope analyses is smaller than the width of histogram bar in (D). The values for Holocene shells from geographically and environmentally distinct ocean basins are not analytically distinguishable with present instrumentation. The high degree of Sr isotope homogeneity has been confirmed by analysis of modern seawater samples from different ocean basins (Capo and DePaolo, 1992). River water data are from Goldstein and Jacobsen (1987), Wadleigh et al. (1985), Palmer and Edmond (1989, 1992), Albarède and Michard (1987), Richter et al. (1992), Ingram and Sloan (1992), and Cameron and Hattori (1997). Selecting only the most downstream sample for a given drainage basin yields similar histograms. The Atlantic river dataset has 78 additional samples with $^{87}Sr/^{86}Sr$ values between 0.72 and 0.95, the Pacific dataset has six additional samples with values between 0.72 and 0.76 (four of which are for the Fraser River from Cameron and Hattori, 1997). Data shown are neither weighted for discharge nor are they inclusive of the majority of rivers draining to each ocean. The uncertainties associated with determining the weighted-mean isotopic composition of global or ocean-wide riverine flux are discussed in the text (Section 7.5.3).

In contrast to the wide range of Sr isotopic compositions in the various influxes to the oceans, the oceans themselves display a very high degree of homogeneity in their Sr isotopic composition (Fig. 7). Small variations are found in estuaries where continental inputs occur (Ingram and DePaolo, 1993). The Sr isotope homogeneity of the oceans is a consequence of the long residence time of Sr in the oceans (5×10^6 years) relative to the interocean mixing time (1.5×10^3 years, Table 3). The residence time is defined as the amount of material in a reservoir divided by the rate of addition or removal from that reservoir. The oceanic residence time of Sr of 5 million years represents the amount of time on average that an atom of Sr, once present in the ocean, spends in the ocean. The residence time of Sr may have varied in the past in response to, for example, an increase in the rate of addition due to exposure and weathering of Sr-rich aragonitic carbonate platforms during a sea level fall (e.g., Stoll and Schrag, 1998). This effect is estimated to result in a residence time in the order of 2 million years, which is still several orders of magnitude larger than the modern interocean mixing time. The interocean mixing time was likely longer during periods of Earth history when thermohaline convection of the oceans was much more sluggish than today (Broecker, 1997, 1999). The oceanic Sr isotope record (e.g., Figs. 1 and 8) shows responses to changes in the various influxes on both shorter and longer time scales than the present-day residence time.

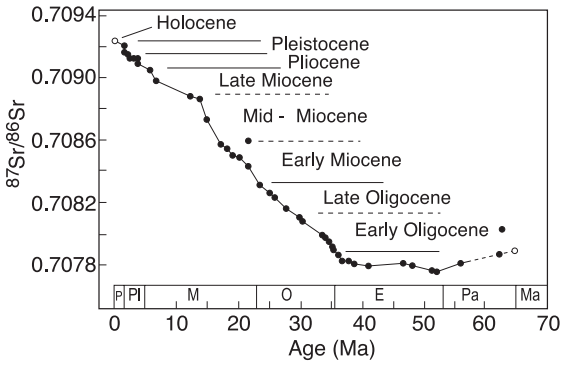

Fig. 8. The Cenozoic segment of the seawater Sr curve, based on analyses of carbonate ooze and chalk from DSDP sites in the Atlantic and Pacific oceans, as well as fossil molluscs and foraminifera from Oligocene and Eocene strata of the US Gulf Coast (DePaolo and Ingram, 1985). Results plotted relative to $^{87}Sr/^{86}Sr$ value of 0.71031 for SRM 987.

7. Applications to the sedimentary record

7.1. Applicability of radiogenic isotopes to chemostratigraphy

Two main features of the geochemical behavior of several radiogenic isotope systems have a special applicability to chemostratigraphy:

(1) The long oceanic residence time of elements such as Sr and U, relative to the oceanic mixing time, accounts for the high degree of homogeneity in world's oceans today (Fig. 7). Such geochemical homogeneity was likely similar during most of Earth history for the world's oceans, although it should be kept in mind that both the residence time of Sr and the mixing time of oceans have certainly varied in the past, particularly during times of stratified oceans (Wilkinson and Algeo, 1989; McArthur, 1994; Broecker, 1997). Strontium isotopic heterogeneities produced in strongly stratified oceans have not been identified to date. The applicability of the isotope composition of short residence time elements such as Nd is discussed in a later section.
(2) The effects of isotope fractionation are negligible for most radiogenic isotope systems.

These two features can be used to establish a rigorous criterion for evaluating the extent to which a marine Sr isotope signal is preserved in ancient marine authigenic sediments. This is because a long oceanic residence time and negligible fractionation will produce identical values in all samples of authigenic marine precipitates that formed at a given time from the same solution (see Isotope fractionation section above). Thus, these features lend credence to first-order trends in the cosmopolitan data set of Burke et al. (1982), whereas it might otherwise be argued that all ancient marine sediments are altered by diagenesis, and that an original marine signal is therefore not retrievable. If this were the case, then these first-order 10–100 Ma trends (Fig. 1) would require that diagenesis has acted hydrologically and chemically in an identical fashion around the world to produce the same values in the altered rocks. This is too great of a coincidence to be tenable. This leads to the criterion that contemporaneous samples are re-

quired to have identical Sr isotope signatures if they are to be considered a faithful record of a marine signal, independent of temperature, metabolic processes, facies, location within or between ocean basins, etc. (Banner and Kaufman, 1994). Note that this criterion is a requirement for samples to be considered well preserved, but not proof that they are well preserved. In addition, this criterion must be applied with caution in marginal marine environments due to the potential influence of freshwater inputs (Bryant et al., 1995; Cochran et al., 2003). This approach has also been used in evaluating the preservation of the U isotope systematics in marine precipitates, as will be discussed in a later section.

In addition to these two features, radiogenic isotope systems such as Rb–Sr (and Sm–Nd and Re–Os) have predictable evolution pathways in different crustal and mantle reservoirs as a function of age and lithology (e.g., Fig. 5). This has direct implications for interpreting the processes that cause secular variations in the oceans and for assessing the effects of post-depositional alteration.

7.2. Uncertainties in applications to ancient sequences

There are three main sources of uncertainty in the application of radiogenic isotopes to ancient marine authigenic precipitates: (1) diagenetic alteration; (2) contributions from detrital components in impure samples; and (3) errors in age assignments. This section considers the first two sources of uncertainty, and errors in age assignments are discussed in Sections 7.6.2 and 12.

Without a means to assess the purity and extent of diagenetic alteration of ancient marine sedimentary rocks, there would be no basis for establishing secular isotope curves or chemostratigraphy. Continuing efforts to advance criteria to assess these factors provide the foundation for these studies. Determining the effect of non-carbonate phases on the Sr isotope composition measured for marine carbonate rocks has been addressed by petrographic analysis, physical separation methods, chemical leaching, and analysis of silicate-diagnostic trace-element contents such as Rb, K, Si, Al, and Fe (Popp et al., 1986; Banner et al., 1988a; Jones et al., 1995; Montañez et al., 1996, 2000; Bailey et al., 2000). Carbonates and phosphates have been the principal phases used for seawater Sr isotope studies, in part because the relative exclusion of Rb from these minerals' crystal structures theoretically makes for negligible growth of ^{87}Sr after deposition from seawater. In practice, however, even very small amounts of silicates in a nearly pure carbonate or phosphate sample can have a significant effect on the measured $^{87}Sr/^{86}Sr$ value, and these effects must be assessed (e.g., Banner, 1995).

A number of criteria have been established for unraveling the effects of diagenesis on altering original marine Sr isotope signatures. These include petrography, stratigraphic tests, trace-element measurements, and other isotopic measurements (e.g., Veizer et al., 1983, 1999; Koepnick et al., 1985; Popp et al., 1986; Carpenter et al., 1991; Banner and Kaufman, 1994; Denison et al., 1994a; Jones et al., 1994a,b; Montañez et al., 1996; Ruppel et al., 1996). Several components have been proposed as candidates for recording ancient seawater chemistry. These include brachiopods, because of their stable low-Mg calcite mineralogy; marine cements, because of their retention of primary fabrics and chemical composition; conodonts, because of their high Sr contents and the utility of their thermal alteration index in assessing diagenetic effects; and corals, because of their seasonal growth banding. Strontium isotopic variations within different parts of single conodont elements and between different types of conodont of the same age illustrate some of the complexities introduced by diagenetic alteration (Trotter et al., 1998; Ebneth et al., 2001). It is clear that some criteria and all components are not universal in their applicability or occurrence in the rock record, and that each must be tested and developed on a case by case basis to determine which works best (Montañez et al., 1996). It is also clear that these issues become more critical with increasing geologic age and with increasing need for higher-resolution secular curves of any age.

Quantitative modeling of diagenetic processes (e.g., Banner and Hanson, 1990) can outline limits on the degree to which diagenesis has chemically altered a given sample and the nature of the alteration processes, including dissolution, recrystallization, and cementation. Such modeling is thus useful for extrapolating back to original marine values and for excluding samples from analysis. In many field and petrographic studies, it may be impossible to obtain pristine, unaltered samples for chemical analysis, in

which case modeling may provide information on which samples are least altered. Studies of the nature of the fluid-rock interaction process may help determine whether (1) diagenesis results predominantly in the loss of original Sr atoms from the carbonate mineral structure, which would result in the preservation of a marine Sr isotope signal; or (2) if diagenesis introduces new, non-marine Sr atoms into the carbonate mineral structure (Banner, 1995). These uncertainties regarding sample purity and diagenesis are treated in more detail in Banner (1995).

7.3. The oceanic Sr isotope record

Once pioneering efforts demonstrated the potential of using Sr isotope variations in seawater (e.g., Peterman et al., 1970; Dasch and Biscaye, 1971; Veizer and Compston, 1974; Burke et al., 1982; see review by McArthur, 1994), significant refinements of the curve covering the Phanerozoic were conducted using improved sample selection, sample preparation, and mass spectrometric techniques. The first major refinements were accomplished for the Cenozoic era (Fig. 8) from mostly DSDP-based studies (DePaolo and Ingram, 1985; Koepnick et al., 1985; Palmer and Elderfield, 1985b; DePaolo, 1986; Hess et al., 1986; Hodell et al., 1989). These results and subsequent efforts in Cenozoic and Mesozoic sections (Figs. 9–11) show the considerable utility and potential for chemical stratigraphy (Fig. 12).

The increase in the size of the error envelope with increasing age in the Burke curve (Fig. 1) is a consequence of the longer diagenetic history and deeper burial to which these older rocks have been typically subjected, the larger effect from ingrowth of

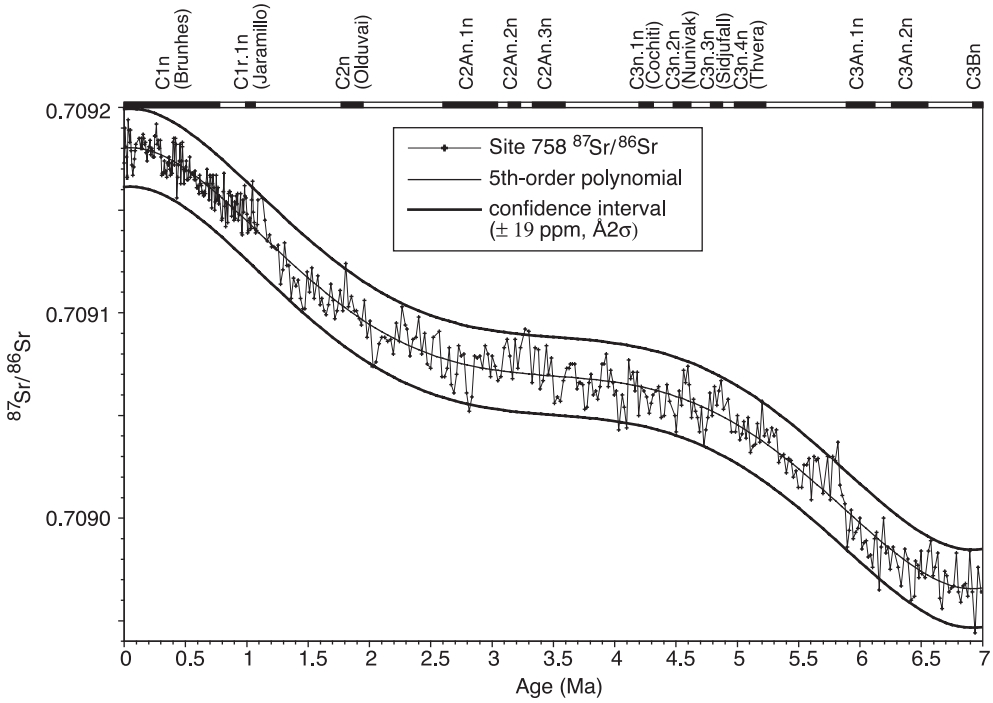

Fig. 9. The Neogene segment of the seawater Sr curve (Farrell et al., 1995). Magnetic chrons shown along the time axis. Diamonds are individual or combined replicate analyses of foraminifera from ODP Site 758. Central curve is a polynomial fit to the data; upper and lower curves comprise a confidence interval based on uncertainty of fit of polynomial. This uncertainty is similar to the external reproducibility of Sr isotope analyses. Continuity and state of sample preservation of Site 758 samples offer a high-resolution curve for the past 6.5 m.y., and are in agreement with Sr isotope curves from several Neogene sections from other ODP and DSDP sites (Richter and DePaolo, 1988; Capo and DePaolo, 1990; Hodell et al., 1989, 1990; Beets, 1991). Results are plotted relative to $^{87}Sr/^{86}Sr$ value of 0.710235 for SRM 987.

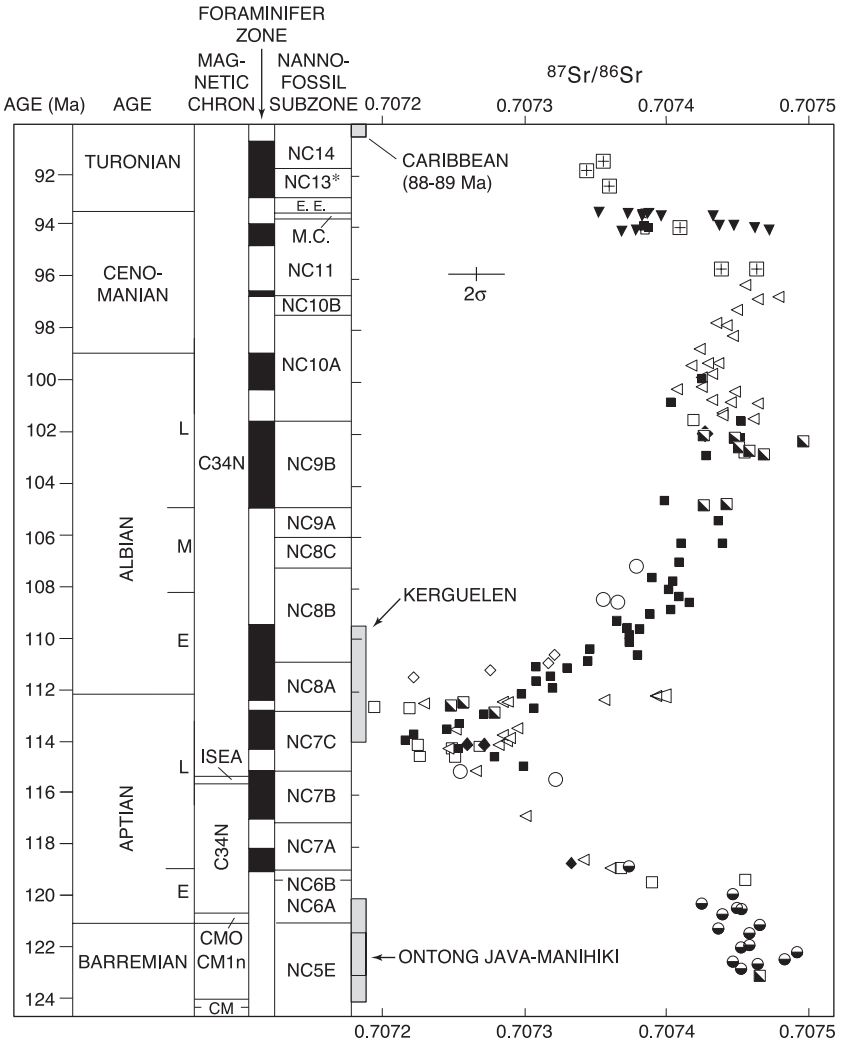

Fig. 10. The Middle Cretaceous segment of the seawater Sr curve, based on analyses of foraminifera from nine DSDP and ODP sites, indicated by the different symbols (Bralower et al., 1997). Age controls are based on nannofossil and foraminifera biostratigraphy and magnetostratigraphy (E.E. = *E. eximius*; M.C. = *M. chiast*). Data have been screened using criteria discussed in text. Results for these deep-sea sections are in close agreement with previous studies of land-based marine sections, when biostratigraphic data and time scales are consistently applied. Shaded bars show age ranges for mid-plate volcanic episodes. $^{87}Sr/^{86}Sr = 0.71025$ for SRM 987. Time scale after Gradstein et al. (1994). Analytical uncertainty for an individual analysis is shown as $\pm 2\sigma_{external}$ in this and following figures.

radiogenic ^{87}Sr in non-carbonate components in older rocks, and the larger absolute errors in age assignments in older parts of the geologic record. Selection of relatively unaltered material in Paleozoic and Precambrian sedimentary rocks is a significant challenge. Studies of carefully selected Paleozoic sections, however, have refined the record (Figs. 13 and 14; Popp et al., 1986; Brookins, 1988; Gao and Land, 1991; Douthit et al., 1993; Banner and Kaufman, 1994, Cummins and Elderfield, 1994; Denison et al., 1994b; Bruckschen et al., 1995; Denison and Koepnick, 1995; Martin and Macdougall, 1995; Diener et al., 1996; Montañez et al., 1996; Ruppel et al., 1996, 1998).

Precambrian seawater Sr data are sparse relative to the large amount of geologic time covered by this

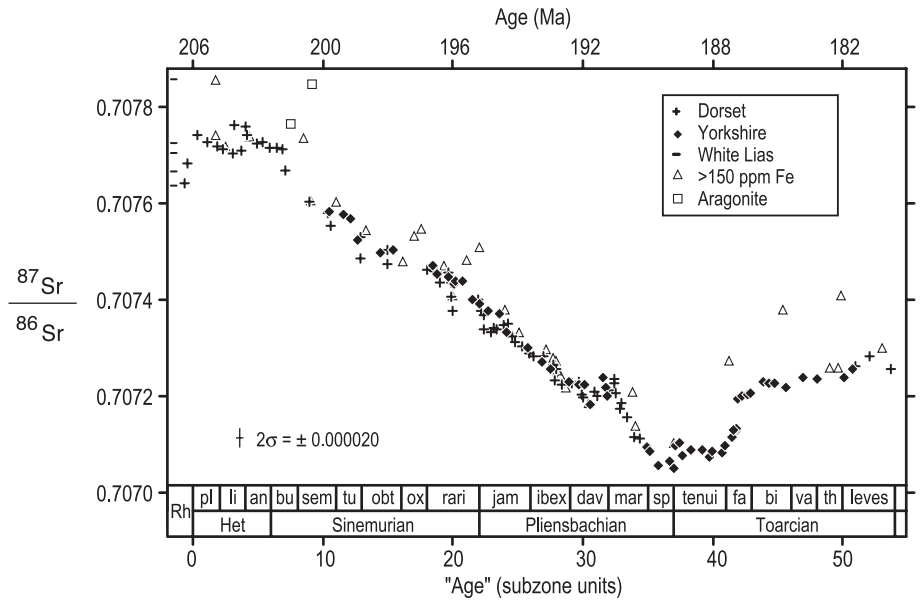

Fig. 11. The Early Jurassic segment of the seawater Sr curve based on analyses of well-preserved oysters and belemnites from land-based marine sections (Jones et al., 1994b). Different sections are denoted by symbols, as are aragonitic samples and samples with greater than 150 ppm Fe. Comparison with ammonite biostratigraphic zonation given along the *x*-axis shows that the Sr isotope chemostratigraphy yields a temporal resolution equivalent to one or two biozones. $^{87}Sr/^{86}Sr = 0.71025$ for SRM 987. Time scale after Harland et al. (1990).

interval (Veizer and Compston, 1976; Veizer et al., 1983; Asmerom et al., 1991; Derry et al., 1992; Kaufman et al., 1993; Melezhik et al., 2001). We should expect significant refinements of the Precambrian portion of the oceanic Sr record in the future, given: (1) the key insight that seawater Sr may provide into crustal evolution as discussed above; (2) the importance of the Archean and Proterozoic periods in the evolution of the continental crust, the oceans, and the atmosphere (e.g., Taylor and McLennan, 1985; Kaufman et al., 1997); (3) advancements in stratigraphic, petrologic, and biogeochemical studies of marine carbonates of this age (Grotzinger, 1994; Hoffman et al., 1998; Walter et al., 2000); and (4) the limited biota of these time periods, which leave chemostratigraphic applications as the major means to correlate strata.

7.4. Implications of the oceanic Sr isotope record for the history of Earth system processes

The oceanic Sr isotope record can be considered along with our previous investigation of the use of Sr isotope tracers of the modern hydrologic cycle to evaluate processes that can account for the temporal Sr isotope variations during different periods of Earth history. Potential applications include improving our understanding of the linked processes that can account for the secular variations, which may ultimately provide insight into the driving mechanisms that create the sedimentary packages of sequence stratigraphy. This section considers the processes that can effect temporal changes in the Sr isotopic composition of seawater and describes a quantitative approach to modeling these changes. The processes that may influence the Sr isotopic composition of seawater include hydrothermal circulation at midocean ridges, tectonic uplift, shifts in the configuration of the continents, climate and sea level change, diagenesis of ocean floor sediments, changes in ocean circulation patterns, and bolide impacts. Our discussion will show that none of these processes alone control the long-term Sr isotope variations in the oceans. This is in contrast to the biogeochemical cycle of other elements. The rate of burial of components such as organic carbon and pyrite, for example, has a dominant role on the long-term geochemical cycles of C and S (Kump, 1989).

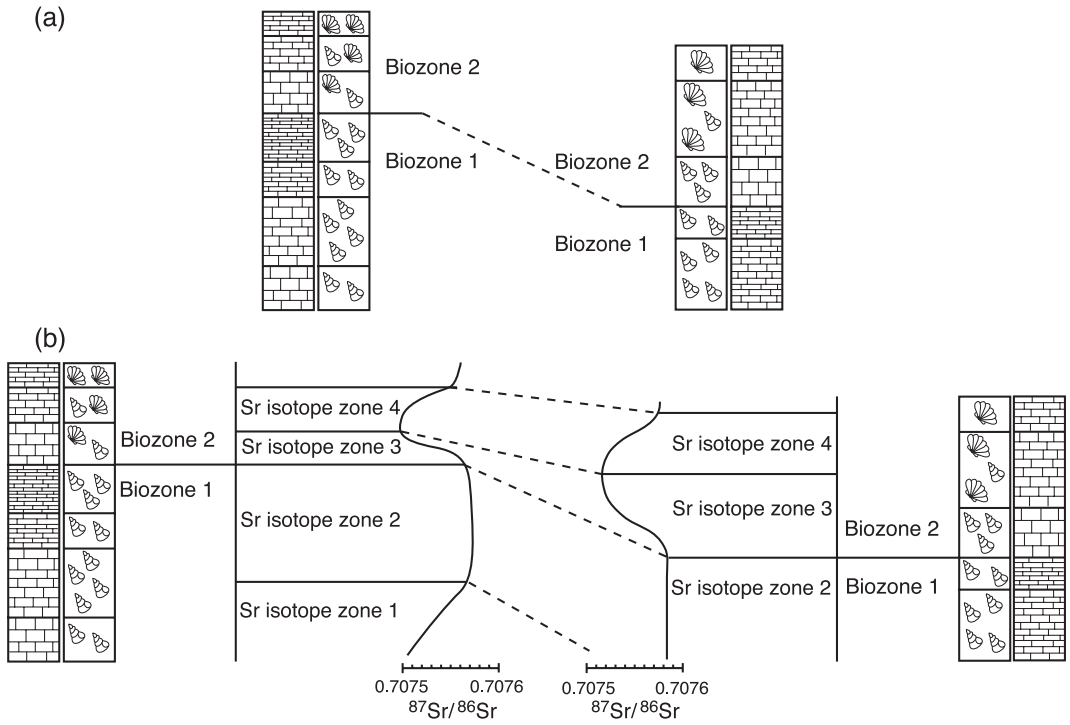

Fig. 12. Comparison of the principles of chemostratigraphic and biostratigraphic correlation and the potential for chemostratigraphy to improve the resolution of stratigraphic correlations. (a) Depicts a typical biostratigraphic boundary. (b) Illustrates the possible improvement in resolution through the section with the application of chemostratigraphy. After Pursell (1997).

7.4.1. Mid-ocean ridge hydrothermal activity driven by changes in seafloor spreading rates

Temporal increases in seafloor spreading will increase submarine hydrothermal activity and the flux of Sr with low $^{87}Sr/^{86}Sr$ from the Earth's mantle to the oceans. These changes are effective on the relatively long-term first and second orders of oceanic Sr isotope variation (1–500 m.y. cycles). The prolonged period of low $^{87}Sr/^{86}Sr$ and prominent minima during the Jurassic and Cretaceous periods (Figs. 1, 10 and 11) is consistent with the major increases in seafloor spreading and ocean crust building known to have occurred during this time (Jones et al., 1994a; Jenkyns et al., 1995; Bralower et al., 1997). Rapid spreading leads to high sea level, which lowers continental weathering rates. Thus, there are multiple processes associated with increased seafloor spreading that would lead to low $^{87}Sr/^{86}Sr$ in the oceans (Bralower et al., 1997; Jones and Jenkyns, 2001). Increased spreading rates also lead to more outgassing of CO_2 into the ocean–atmosphere system, the effects of which are discussed below.

7.4.2. Orogenic processes and paleogeographic configurations

Another driving mechanism affecting the marine Sr isotope record is orogenesis, and its multiple effects of increasing physical and chemical weathering rates of crustal rocks with high $^{87}Sr/^{86}Sr$, altering climatic patterns due to orographic effects, and the metamorphism and unroofing of relatively old crust with very high $^{87}Sr/^{86}Sr$. The role and timing of uplift of the Himalayas on the Cenozoic marine Sr record and, conversely, the application of the marine Sr record to constrain the timing and rate of Himalayan orogenesis, have been intensively studied (Raymo et al., 1988; Raymo and Ruddiman, 1992; Edmond, 1992; Richter et al., 1992; Raymo, 1994; Derry and France-Lanord, 1996). Other Phanerozoic and Precambrian orogenic events have also been investigated in this regard

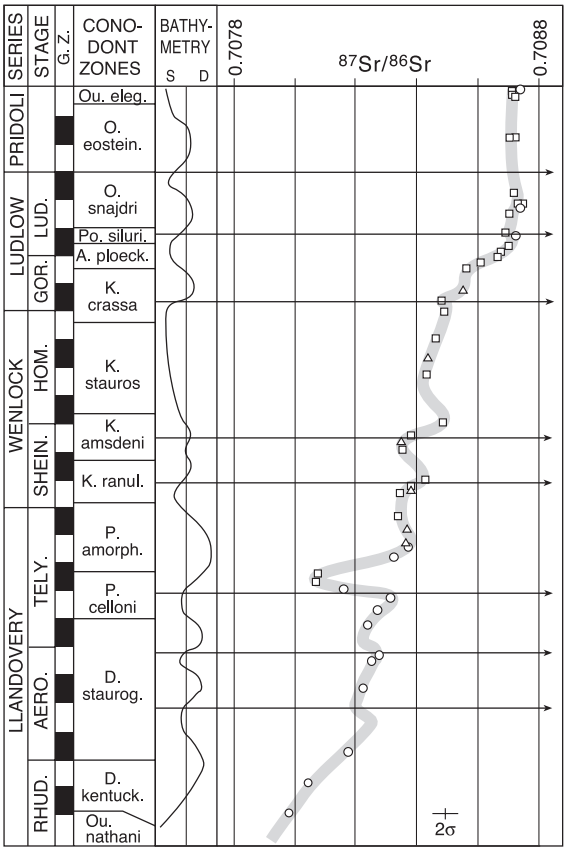

Fig. 13. The Silurian segment of the seawater Sr curve based on analyses of petrographically screened and chemically pre-treated conodonts from Europe and North America (Ruppel et al., 1998). Sea level history and biostratigraphic zonation for conodonts and graptolites (black and white bars in G.Z. column) are shown for comparison. Plot is scaled by assigning equal duration to each graptolite zone (G.Z.). Correlations to conodont zonation and sea level curve from Johnson (1996). Arrows denote sequence boundaries. Shaded band that denotes seawater Sr isotope curve approximates the analytical reproducibility. For bathymetry, S = shallow and D = deep. Sample locations: squares, Oklahoma; triangles, Tennessee; circles, other localities. Higher-frequency fluctuations in seawater $^{87}Sr/^{86}Sr$ have a duration of approximately one conodont zone, and many correspond with sequence boundaries. Recent estimates of 23–26 Ma for the duration of the Silurian (Johnson, 1996) correspond to an average duration of approximately 2 Ma per conodont zone. $^{87}Sr/^{86}Sr = 0.710255$ for SRM 987.

(Raymo, 1991; Asmerom et al., 1991; Derry et al., 1994; Montañez et al., 2000). Variations in the origin and age of exposed crust as a function of time will change the Sr isotopic composition of riverine Sr delivered to the oceans. These changes are tied to the orogenic processes discussed above.

7.4.3. Climate change

Climatic variations, particularly glacial cycles, have a profound influence on rates of physical and chemical weathering on the continents. During periods of frequent fluctuations between glacial and interglacial periods, enhanced weathering results from the creation of freshly exposed mineral surfaces, steep-walled valleys, isostatic rebound, and fluctuations in rainfall. The driving mechanisms of glacial cycles and their potential effects on marine $^{87}Sr/^{86}Sr$, including atmospheric CO_2 fluctuations and changes in Earth's orbital parameters, occur on a large range of time scales. These proposed time scales include 10–100 m.y. (Raymo, 1991), 1–5 m.y. (Hodell et al., 1990), 20,000–100,000 years (Blum and Erel, 1995), and 10–200 years (Brantley et al., 1998), although variations in the Sr isotope composition of the oceans have been resolved only on time scales exceeding 100,000 years. Climate fluctuations during non-glacial periods, such as changing rainfall rates, may also affect the $^{87}Sr/^{86}Sr$ value of riverine and groundwater fluxes to the oceans (e.g., Banner et al., 1996).

7.4.4. Ocean floor sediment diagenesis

Diffusion of Sr released during diagenesis through ocean floor sediment pore waters is a ubiquitous part of the oceanic Sr balance that may vary over time as a function of the areal extent, rate of deposition, and type of ocean floor sediment (Baker et al., 1982; Gieskes, 1983; Richter et al., 1992). As ocean floor sediments have a similar Sr isotopic composition to the overlying water column, this flux of diagenetic Sr will generally have a dampening effect on the rates of change of seawater Sr over time. The fact that Phanerozoic seawater has never attained the high $^{87}Sr/^{86}Sr$ values of continental crust or the low values of oceanic crust likely reflects the fact that fluxes from rivers, the mantle, and seafloor sediment diagenesis have always been in the mix supplying Sr to the oceans. Indeed, the importance of these three major fluxes is reflected in the fact that Phanerozoic seawater has not monotonically increased through time as a result of steady decay of ^{87}Rb in the Earth's crust, as proposed in the first hypothesis regarding secular seawater Sr isotope evolution (Wickman, 1948).

7.4.5. Sea level change

Drops in sea level will expose crust and coastal sediments of different Sr isotope composition than the oceans, and subject them to more chemically aggressive meteoric fluids. Typically, a sea level fall will expose cratonic interiors and continental margin siliciclastics and carbonates, with a net $^{87}Sr/^{86}Sr$ value greater than contemporaneous seawater. An increase in weathering of these sources will deliver Sr with relatively high $^{87}Sr/^{86}Sr$ to the oceans. High-frequency (1–5 m.y.), inverse correlations between sea level and marine $^{87}Sr/^{86}Sr$ values that are observed in Mesozoic and Paleozoic sections are consistent with this model (Figs. 13 and 14; Pursell and Banner, 1997). The long-term, first-order trends in the Phanerzoic seawater Sr curve (Fig. 1) are consistent with the falling-sea-level increasing-$^{87}Sr/^{86}Sr$ model only during the past 100 m.y. (see Fig. 6.6 in Hallam, 1992). As discussed below, a number of other factors, including tectonic activity and climate change, must also be considered in accounting for this part of the Phanerozoic record.

If recently deposited marine carbonate platform sediments composed of aragonite are exposed during a sea level drop, then significant amounts of Sr may be delivered to the oceans through the conversion of high-Sr aragonite to low-Sr calcite by meteoric waters. This would have an even greater dampening effect on the rate of change of seawater $^{87}Sr/^{86}Sr$ compared with the effects of ocean floor sediment diagenesis (Schlanger, 1988; Stoll and Schrag, 1998). In some cases, sea level declines may expose older carbonate platforms with significantly different Sr isotope compositions than contemporaneous seawater. This would, in contrast, enhance the rate of change of seawater $^{87}Sr/^{86}Sr$.

7.4.6. Switching between modes of ocean circulation

Changes in the ocean's thermohaline circulation from well-mixed to stratified may drive and be driven by changes in climate (Wilde and Berry, 1984; Knoll et al., 1996). These shifts may be resolvable in well-preserved ancient sequences by examining temporal Sr isotope and lithologic shifts in shallow water sediments. While such global-scale reorganization of ancient oceans has been proposed on the basis of rapid Sr, C, and O isotope shifts close to the Permian–Triassic boundary (Gruszczynski et al., 1992), more rigorous analysis is required to test this hypothesis. Rapid switches in the mode of oceanic circulation, such as those more clearly reflected on shorter time scales in the Quaternary deep sea and ice core records, were likely common in some ancient time periods (Broecker, 1997).

7.4.7. Geologically instantaneous events

The effects of bolide impacts on the global climate, such as shock heating of atmospheric nitrogen leading to a dramatic increase in acid rain (HNO_3) and continental weathering, have been proposed to account for short-term rises in seawater $^{87}Sr/^{86}Sr$, such as that across the Cretaceous–Tertiary boundary (Macdougall, 1988; Martin and Macdougall, 1991). The stratigraphic uncertainties involved in constructing such an isotope boundary sequence from a global vs. local dataset have led to studies focused on individual localities. These studies have revealed $^{87}Sr/^{86}Sr$ excursions across the $K–T$ boundary at some localities and no excursions at other localities (Nelson et al., 1991; McArthur et al., 1998; MacLeod, 2001). Uncertainties associated with diagenetic effects, stratigraphic assignments, and reworking of fossils are proposed to account for some of these differences (MacLeod, 2001). Resolution of these issues will aid in understanding the paleoenvironmental impacts of such impact events.

7.4.8. The linked processes of seafloor spreading, orogenesis, climate change and sea level, and potential effects on the marine Sr isotope record

It can be seen that the several processes discussed above each affect the oceans' Sr isotope signal in different ways and that they are themselves linked processes in the Earth system. An understanding of these linkages, while incomplete at present, will help determine the relative effects of these processes. Increased mantle volcanism will directly input Sr with low $^{87}Sr/^{86}Sr$ into the oceans, yet the indirect effects of increased volcanism on continental weathering likely lead to the input of Sr with high $^{87}Sr/^{86}Sr$ into the oceans. This is because as CO_2 in the atmosphere and ocean rise in response to increased plate tectonic activity and associated volcanism, global temperatures rise. Higher rates of chemical weathering reactions and an accelerated hydrologic cycle would be two consequences of higher temperatures. More weather-

ing from the continents would deliver Sr from the continents with high $^{87}Sr/^{86}Sr$ relative to mantle fluxes (Fig. 6) to the oceans. Eventually, increased weathering rates would draw down atmospheric CO_2 and lead to cooling (which would lower weathering rates) and potentially glaciation, which would increase

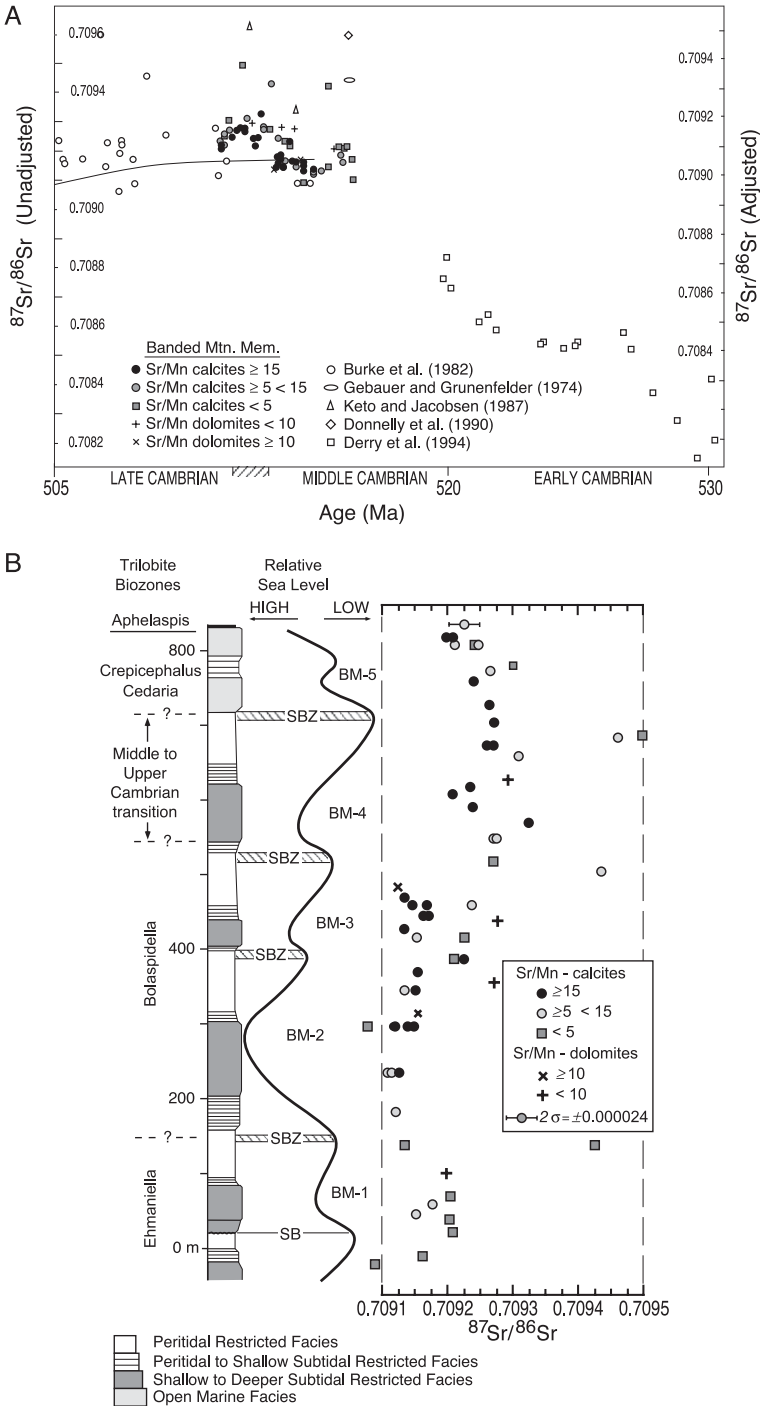

the Sr isotopic composition released during weathering as described above. The competing effects of these linked Earth processes on the isotopic composition of the oceans are addressed by quantitative modeling of the oceanic response, as considered in the next section.

Note from this discussion that there is not a single driving force that controls the long-term Sr isotope variations in the oceans. This is due to the complex interactions of a number of ongoing and periodic Earth system processes that influence the biogeochemical cycle of Sr. In favorable cases, the relative influences of these processes may be discerned.

Based on the analytically resolvable oscillations in the marine Sr isotope record (e.g., Figs. 1, 8–11, 13 and 14)), the oceanic reservoir's response time varies between 0.5 and 200 m.y. This range of response times can be used to constrain the input processes to this reservoir (e.g., Lasaga and Berner, 1998). Quantitative mass balance modeling of a given segment of the marine Sr record can be used to assess the geologic feasibility of the magnitude and rates of the various driving forces behind a particular Sr influx.

7.5. Modeling secular changes in the radiogenic isotope composition of the oceans to constrain Earth system processes

The use of mass balance calculations to model changes in ocean $^{87}Sr/^{86}Sr$ represented by the seawater Sr curve follows the treatment given in, among others, Capo and DePaolo (1990). The rate of change of $^{87}Sr/^{86}Sr$ in seawater, R', is given as

$$R' = N_o^{-1}\Sigma J_i(R_i - R), \quad (9)$$

where J_i = the flux of Sr from source i, in units of 10^{10} mol Sr per year; $R_i = {}^{87}Sr/^{86}Sr$ in source i; N_o = no. of moles of Sr in the oceans (assumed constant at 1.21×10^{17} mol); $R = {}^{87}Sr/^{86}Sr$ in seawater $= R_{in} - (N_o/\Sigma J_i)R'$; R_{in} = mean $^{87}Sr/^{86}Sr$ added at a given time $= \Sigma(J_iR_i)/\Sigma J_i$.

Flux values for the different sources, J_i, are given in Fig. 6. These equations can be used to model a linear segment or series of linear segments of the seawater curve. The assumption of a constant amount of Sr in the oceans is equivalent to assuming a "steady state" ocean with respect to Sr, whereby the input and output amounts are balanced. While this assumption likely holds to a first approximation, there is a range in the Sr contents of marine precipitates over time that indicates some periods of departure from this ideal case (e.g., Carpenter et al., 1991; Stoll and Schrag, 1998). We consider the application of the modeling approach described here to two time periods in the Cenozoic.

7.5.1. The Plio-Pleistocene record

Capo and DePaolo (1990) examined the possible causes of two 0.8 m.y. cycles in seawater $^{87}Sr/^{86}Sr$ observed in the Late Pliocene and Pleistocene record. Quantitative modeling of this portion of the curve shows that if the controlling factor on the seawater $^{87}Sr/^{86}Sr$ record was hydrothermal exchange at mid-ocean ridge spreading centers (Fig. 6), then this flux would have to vary by rates of up to 100% over 10^5 years. Marine magnetic anomalies indicate that the driver of the hydrothermal exchange flux, the rate of seafloor spreading, did not change significantly during the Pleistocene. This suggests that it is unlikely that the isotopic cycles arose from variations in the amount of hydrothermal exchange flux to the oceans. Modeling results also show the difficulty in matching rapid enough or large enough $^{87}Sr/^{86}Sr$ changes in the oceanic record with changes in the rate of seafloor diagenesis. This is because seafloor diagenesis has a relatively low flux and an isotopic composition very similar to contemporaneous seawater. Remaining for consideration are temporal changes in either the flux of Sr or the isotopic composition of Sr delivered by rivers. The latter was considered unlikely because it

Fig. 14. (A) Early to Middle Cambrian segment of the seawater Sr curve from Montañez et al. (1996), based on microsampled and pretreated marine components from Indian Ridge section of Great Basin of Nevada, compared with results from other studies. Values for samples with varying trace-element ratios and mineralogy illustrate the more consistent results achieved using calcites with high Sr/Mn ratios. "Unadjusted" y-axis scale is relative to Burke et al. (1982) $^{87}Sr/^{86}Sr$ value of 0.71014 for NBS Standard 987, adjusted scale is for $^{87}Sr/^{86}Sr$ value of 0.710248. Shaded interval on x-axis represents the Middle to Upper Cambrian transition. (B) Details of the Middle Cambrian segment of the seawater Sr curve from the Great Basin, compared with trilobite biostratigraphy and with sea level history that is based on lithostratigraphy and facies analysis. $^{87}Sr/^{86}Sr = 0.710248$ for SRM 987. Time scale after Harland et al. (1990).

would require that the average $^{87}Sr/^{86}Sr$ value of rocks exposed to weathering change during a short time period (Capo and DePaolo, 1990), although this could occur in some scenarios (e.g., Blum and Erel, 1995; Montañez et al., 1996, 2000). It was therefore concluded that the main process controlling the Plio-Pleistocene Sr isotopic record was variation in the total flux of riverine Sr due to changes in weathering rates driven by glacial–interglacial oscillations (Capo and DePaolo, 1990).

7.5.2. The Neogene record

The rapid rise of seawater $^{87}Sr/^{86}Sr$ that occurred during most of Tertiary time (Figs. 1 and 8) is a feature of the secular Sr isotope curve that has spurred intensive study into the relationships between orogenesis, weathering, and seawater chemistry. Similar to the Plio-Pleistocene studies described above, modeling has been used to quantitatively assess these relationships. The increase in the rate of rise of seawater $^{87}Sr/^{86}Sr$ that occurred in the Late Eocene and Early Miocene corresponds with the timing of uplift of the Tibetan Plateau. This correspondence has led to detailed assessments of the role of the timing and rate of uplift of the Himalayas, as this has implications for variations in the global climate, weathering rates, and the carbon cycle during this time period. The timing and rates of uplift have been addressed by modeling the response of oceanic $^{87}Sr/^{86}Sr$ in the Neogene to the effects of uplift on the flux and isotopic composition of Sr in rivers that drain the Himalayas (Raymo et al., 1988; Raymo and Ruddiman, 1992; Edmond, 1992; Richter et al., 1992; Richter and Turekian, 1993; Raymo, 1994; Derry and France-Lanord, 1996; McCauley and DePaolo, 1997).

7.5.3. Limitations on cause-and-effect studies of seawater Sr isotope variations

The use of a global average for riverine $^{87}Sr/^{86}Sr$ influx (see Fig. 6) in quantitative models is limited by the fact that the bulk of the total global riverine discharge cannot be described by a consideration of only the world's major rivers. As noted by Lasaga and Berner (1998), even using the world's largest 200 rivers only accounts for 60% of the total global discharge. Hence, there are significant uncertainties in determining both the global average riverine $^{87}Sr/^{86}Sr$ signal, as well as the response of this global average to changes in climate and other factors. An additional complexity in determining the response of riverine Sr isotope compositions to environmental changes derives the significant differences in weathering rates of different minerals in the bedrock that characterize a given watershed (e.g., Blum et al., 1994; Blum and Erel, 1995). These factors make it difficult to discern the effects of one or a group of rivers on the oceanic Sr record, which in turn make it difficult to constrain the role of other fluxes to the oceans (Fig. 6) for a given interval of geologic time.

There are other fluxes to the modern ocean that are even less well defined than the riverine flux. For example, the flux of water to the oceans from coastal groundwater discharge may often be significantly underestimated. Using the natural radiotracer ^{226}Ra, it was found that such groundwater discharge may be as large as 40% of the amount of riverine flux (Moore, 1996), compared to the negligible 0.01–10% previously estimated (Church, 1996). Given the higher Sr concentrations of groundwater relative to river water (Table 3), this could make groundwater in some instances an equivalent player in the geochemical cycle of Sr to the oceans. Another example is the hydrothermal flux of Sr to the oceans, which includes components from high temperature ocean ridge systems, low temperature off axis ocean crust, and island arc related spreading environments (Fig. 6). Detailed flux estimates for these components indicate that hydrothermal inputs to the oceans are less than a third of the magnitude of the flux required to balance the riverine and diagenesis fluxes, in contrast to the balanced inputs portrayed in Fig. 6 (Davis et al., 2003).

The interplay between tectonic uplift and the resulting increase in weathering, drawdown of atmospheric CO_2, and climatic cooling is of considerable interest in assessing feedbacks in the global carbon cycle and climate system. Many models of these systems require that as weathering of silicates draws down atmospheric CO_2, the resultant cooling will slow weathering rates and thus keep CO_2 levels from reaching extremely low or high levels that would threaten life on Earth (Walker et al., 1981; Broecker and Sanyal, 1998). The Tertiary record at first glance appears to be inconsistent with this model because the increased weathering that is indicated by the steep rise in seawater $^{87}Sr/^{86}Sr$ is matched by global cooling that

is indicated from the marine oxygen isotope record. It has been proposed that these inconsistencies can be resolved in models involving a change in organic carbon burial rates (Raymo, 1994) or a lack of a temperature control on weathering rates (Edmond and Huh, 1997). These models, however, do not account for the feedbacks needed to keep CO_2 in check (Broecker and Sanyal, 1998). Therefore, although the Himalayan orogeny may indeed have driven the seawater $^{87}Sr/^{86}Sr$ rise during the Tertiary, it was not necessarily representative of global weathering patterns (Kump and Arthur, 1997; Broecker and Sanyal, 1998). Finally, coupled variations in seawater $^{87}Sr/^{86}Sr$ and glacial cycles in the Eocene and Oligocene (similar to those discussed above for the Plio-Pleistocene) also raise the question as to whether the seawater Sr isotope record reflects weathering directly driven by climate change, or whether it reflects weathering driven by tectonic uplift that also drove climate change (Zachos et al., 1999).

This discussion underscores both the utility and the uncertainties involved in using the seawater $^{87}Sr/^{86}Sr$ record to constrain Earth system processes. The use of the Sr cycle to constrain models for the global carbon cycle is also applicable to other geologic time periods (e.g., Derry et al., 1994).

7.6. Strontium isotope chemostratigraphy

The establishment of strontium isotope correlation is best accomplished in sequences that have been tied to radiometrically dated and biostratigraphically calibrated intervals (DePaolo, 1987; McArthur, 1994). Correlations of stratigraphic sections using Sr isotopes have the highest resolution for periods of time for which the seawater curve changes rapidly in one direction. As the analytical resolution of seawater isotope curves is refined, there is a corresponding improvement in chemostratigraphic applicability. The potential use of Sr-isotope seawater curves for attaining comparable or higher resolution than that provided by biostratigraphy is illustrated in Fig. 12. Recent high-resolution studies are discussed below, and some of these refined curves are presented.

7.6.1. Cenozoic

An improved Neogene $^{87}Sr/^{86}Sr$ curve has been developed using detailed analyses of hand-picked and ultrasonically cleaned planktonic foraminifera from Ocean Drilling Program (ODP) Site 758 in the Indian Ocean (Farrell et al., 1995). This curve from a single site refines previous results from this time interval as a result of the continuous section and well-calibrated chronostratigraphy, with an average sampling interval of 15,000 years (Fig. 9). Diagenetic alteration was considered negligible based on the young age and shallow burial depth of the section studied, the optically pristine state of the foraminifera, and the similar oxygen and strontium isotope records between this and other locations of the same age that have different burial histories (Farrell et al., 1995).

7.6.2. Age estimates and their uncertainties

Given a measured $^{87}Sr/^{86}Sr$ value for a Neogene sample, an age estimate can be made graphically from comparison with the Site 758 data. An age can also be calculated from a polynomial regression fit through the same data (Fig. 9). Such curve fitting methods can smooth real structure in secular curves. This limitation has led to the more recent use of nonparametric regression models for obtaining best-fit curves and look-up tables for easy conversion from $^{87}Sr/^{86}Sr$ to numerical age (Howarth and McArthur, 1997; McArthur et al., 2001). Age-estimate errors that are common to all methods arise from: (1) the analytical uncertainty on the $^{87}Sr/^{86}Sr$ measurement and age assignments used to construct the curve, and analytical uncertainty on the $^{87}Sr/^{86}Sr$ measurement of the unknown sample; (2) the slope of the curve; and (3) the extent to which the original marine Sr isotope composition is preserved in both the control and unknown samples. The Sr isotope stratigraphic resolution of the Neogene section shown in Fig. 9 is ± 0.6 m.y. in the lower Pleistocene and upper Miocene, where the curve is steep, and ± 2.03 m.y. in the Middle Pliocene, where the curve is relatively flat.

7.6.3. Mesozoic

Using new and compiled data for Middle Cretaceous deep-sea sediments, Bralower et al. (1997) present an advanced Cretaceous seawater Sr curve that for some intervals has comparable age resolution to foraminifera and nannofossil biostratigraphy (Fig. 10). This curve was constructed using new analyses of planktonic and benthic foraminifera and inoceramid bivalves from 12 DSDP and ODP sites, screened by

scanning electron microscope observations and trace-element analyses. It was found that using the contemporaneous sample criteria described earlier was the most sensitive test for diagenetic alteration. Comparisons of the deep-sea data to Sr isotope curves from land-based marine sections in Europe and North America (Koepnick et al., 1985; Ingram et al., 1994; Jones et al., 1994a,b; McArthur et al., 1994; Jenkyns et al., 1995) revealed numerous disparities, some of which are due to diagenetic alteration and analytical methodology, but many of which can be accounted for by different age-estimation methods. Applying a uniform age-estimation method to all of the samples produced a significantly more consistent global Sr isotope record for the Middle Cretaceous. This refined Cretaceous Sr curve was found to provide enhanced stratigraphic resolution compared with benthic foraminiferal biostratigraphy for analysis of drowned Cretaceous carbonate platforms underlying Pacific guyots (Wilson et al., 1998). This analysis revealed that the platforms were drowned sequentially over 60 m.y. during transport by Pacific plate motion through a narrow paleolatitudinal zone of $\sim 0-10^{\circ}$S, rather than during a single sea-level event (Wilson et al., 1998).

A refined Jurassic seawater Sr curve, based on chemically screened oysters and belemnites, yields an age resolution equivalent to one or two ammonite biozones (i.e., ± 0.5 to 1 m.y.), as illustrated in Fig. 11. The low-Mg calcite shells of these samples were chosen for their relative diagenetic stability, and the section was chosen for its classic, well-constrained biostratigraphy. The contemporaneous sample criteria showed that most samples containing >150 ppm Fe had diagenetically elevated $^{87}Sr/^{86}Sr$ values, whereas O and C isotopes were insensitive indicators of samples with diagenetically altered Sr isotope signals.

The lack of a well preserved seafloor sediment record for Triassic and older time periods dictates detailed investigations of shallow-water platforms. Pursell and Banner (1997) applied petrographic and trace-element criteria to microsample portions of cyclic shallow-water carbonates on an isolated platform of Lower Triassic age. Study of this platform offers stratigraphic continuity over 500 m of section, minimal siliciclastic input, and a well-understood diagenetic history. Silica and iron concentrations provide useful criteria for sample selection in this study. Parts of the curve constructed from this study have improved resolution relative to algal biostratigraphy.

7.6.4. Paleozoic

Paleozoic case studies in which Sr isotope stratigraphy offers resolution comparable to biostratigraphy include the Sr isotope data of Ruppel et al. (1996, 1998) on Silurian conodonts (Fig. 13). This study demonstrated that selecting individual conodont elements with low conodont alteration indices (CAI < 2) and leaching these elements in acetic acid yielded a more coherent seawater curve. The long-term trend of increasing $^{87}Sr/^{86}Sr$ and falling sea level through the Silurian (Fig. 13) is consistent with the mechanistic link drawn between these parameters in the section above on the implications of the ocean Sr isotope record for the history of Earth system processes. This link between seawater $^{87}Sr/^{86}Sr$ and sea level also appears to be recorded at higher frequencies, approximately 2 million years in duration (i.e., third-order depositional sequences; Fig. 13). Alternatively, the switching between modes of ocean circulation, as has been proposed for the Silurian, is another possible cause of high frequency $^{87}Sr/^{86}Sr$ variations in the Paleozoic (Ruppel et al., 1998). Regardless of the mechanism that drives these changes in seawater chemistry, the chemostratigraphic potential of Sr isotope studies is clear when considering the relatively high resolution of Sr isotope curves compared to the relatively low resolution of conodont biostratigraphic zones for some parts of the Silurian such as the Ludlow series (Fig. 13). While the graptolite zonation is more precise than either the $^{87}Sr/^{86}Sr$ or the conodont zonation for the Silurian, graptolites are not common in Paleozoic carbonate platforms.

Montañez et al. (1996) microsampled marine cements and micritic portions of cyclic shallow-water platform carbonates of Middle Cambrian age. They found that a subset of these samples with high Sr/Mn ratios and calcite mineralogy yielded a more consistent secular curve (Fig. 14). The seawater curve from this study provides age resolution within some trilobite biozones. This curve was constructed based on an analysis of Middle Cambrian sections in the Great Basin of Nevada, USA, and was subsequently confirmed and refined via analysis of the same stratigraphic interval in the Canadian Rocky Mountains of Canada (Montañez et al., 2000). The sections ana-

lyzed provide a continental-scale correlation at high temporal resolution and continuity (100s to 1000s of meters) for the Paleozoic. As with the Silurian segment of the seawater Sr curve, the Middle Cambrian portion shows two frequencies of inverse correspondence between $^{87}Sr/^{86}Sr$ and sea level (Fig. 14). The higher frequency $^{87}Sr/^{86}Sr$ fluctuations are on the temporal scale of third-order depositional sequences. Similar high frequency $^{87}Sr/^{86}Sr$ oscillations have been reported for the Middle Devonian (Diener et al., 1996) and Middle Mississippian (Cummins and Elderfield, 1994).

For many stratigraphic intervals, Sr isotope chemostratigraphy offers little to no improvement on biostratigraphy, but it can serve as a corroborating evidence of biostratigraphic assignments. For other intervals, Sr isotope chemostratigraphy can offer a means to date chemical sediments of marine origin in sections where index fossils are absent, including carbonates, phosphates, evaporites, and Fe–Mn deposits (e.g., Müller and Mueller, 1991). As noted above, correlation using Sr isotopes will be an especially important development for the Precambrian period, where sparse and morphologically simple biota limit application of biostratigraphy.

In addition to the correlation of strata, seawater curves can be used to constrain the timing and origin of diagenetic phases. For example, calcite cements of marine origin from the Eocene strata at Enewetak atoll have $^{87}Sr/^{86}Sr$ values of 0.7085, indicating precipitation from Miocene seawater, some 11 million years after deposition of the host strata (Saller and Koepnick, 1990). This approach requires independent information to indicate an unmodified seawater source of diagenetic constituents. If remobilization of Sr by seawater occurs as it migrates through older host rocks, this will produce apparent Sr isotope ages for the diagenetic phases that will be different from their true age. Dolomite within Holocene sediments in Persian Gulf tidal flats has been ascribed origins ranging from marine to continental brine to mixed waters. Sr isotope values for the dolomites are the same as modern seawater, supporting a marine origin (Müller et al., 1991). Strontium isotopes have the potential to distinguish between marine, meteoric, and mixed water origins for other chemical precipitates such as evaporites (Denison et al., 1998) and for fossils that lack diagnostic environments (Spencer and Patchett, 1997).

8. Samarium–neodymium isotope system

8.1. Nd isotope evolution and low-temperature geochemistry of Sm, Nd, and the rare earth elements (REE)

The decay of the radioactive samarium isotope ^{147}Sm via alpha decay is represented by the reaction:

$$^{147}Sm \rightarrow ^{143}Nd + \alpha \quad (10)$$

Isotopic variations in Nd result from the radiogenic growth of ^{143}Nd in reservoirs with varying Sm/Nd ratios. These isotopic variations are expressed relative to the stable, non-radiogenic isotope ^{144}Nd ($^{143}Nd/^{144}Nd$ ratio). The radiogenic growth of ^{143}Nd is analogous to that of ^{87}Sr, with some important similarities and contrasts. Analogous to Eq. (5) for Sr isotope evolution, the evolution of Nd isotopes is expressed as:

$$^{143}Nd/^{144}Nd = ^{143}Nd/^{144}Nd_o + ^{147}Sm/^{143}Nd(e^{\lambda t} - 1) \quad (11)$$

Neodymium and samarium are rare earth elements (REE), a group of trivalent elements with very similar ionic radii (Table 2). This makes for very similar geochemical behavior within this group. Small changes in ionic radius with increasing atomic number through the rare earth group lead to small and predictable changes in geochemical behavior (Hanson, 1980). As a result of these differences in ionic radii, the parent–daughter fractionation of Sm–Nd during the evolution of the Earth's mantle and crust results in lower Sm/Nd ratios in the crust. Notice that this is opposite to the enrichment of Rb/Sr ratios in the crust relative to the mantle, and therefore produces, over the history of the Earth, relatively high $^{143}Nd/^{144}Nd$ values in the mantle and low values in the continental crust (compare Figs. 5 and 15). A sample's deviation from the value for the bulk earth at a given time is expressed using the epsilon notation ε_{Nd} (defined in Table 4).

The REE have very low solubilities in natural waters. The REE are scavenged by settling particles in the ocean and have a short residence time compared to Sr (Table 3). Compared with Sr, the rare earths are relatively immobile during post-depositional alteration based on studies of diagenetic, metamorphic,

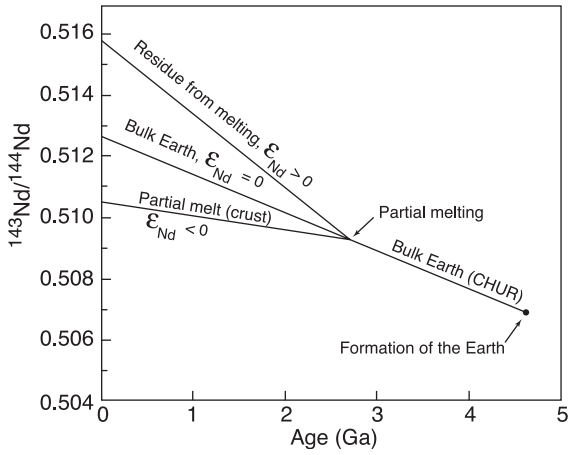

Fig. 15. Nd isotope evolution of bulk Earth, represented by chondritic uniform reservoir (CHUR). Magnitudes of slopes are proportional to the Sm/Nd ratio. Similar to the portrayal of the Rb–Sr system in Figs. 4 and 5 and Eqs. (4) and (5), the Nd isotope evolution of a rock or reservoir is governed by its initial Nd isotope ratio ($^{143}Nd/^{144}Nd)_o$ and its Sm/Nd ratio. In contrast to the Rb–Sr system, mantle sources are enriched in the parent–daughter element ratio, Sm/Nd, relative to continental crust. This produces shallower slopes for crustal vs. mantle evolution lines. ε_{Nd} is a measure of the sample's or reservoir's $^{143}Nd/^{144}Nd$ ratio relative to CHUR (as defined in Table 4). $\varepsilon_{Nd}(T)$ is the ε_{Nd} value at a given time in the past. The evolution lines shown illustrate that the emplacement of a partial melt from the mantle into the crust has an associated Sm–Nd fractionation to lower values (and hence a shallower trajectory leading to a lower present-day ε_{Nd} value). The Sm/Nd ratio in the residual (mantle) material is fractionated to higher values, leading to a higher present-day ε_{Nd} value. After Faure (1986).

and weathering environments (Banner et al., 1988b; Awwiller and Mack, 1989; Borg and Banner, 1996; Holmden et al., 1996; Stille et al., 1996). As a result, Nd isotope signals in ancient chemical precipitates such as carbonates, phosphates, and evaporites are likely to be less altered than Sr isotope signals. This increases the likelihood, relative to Sr, of retention of a primary marine Nd isotope and REE signal in ancient seawater. It also increases the likelihood of retention of a primary depositional provenance signal in ancient siliciclastic rocks.

Rare earth element patterns offer complementary information on the low temperature geochemical behavior of Nd. This is most distinctive in the anomalous low concentration of the rare earth element cerium in oxidizing marine environments (Fig. 16). The tetravalent state of Ce under oxidizing conditions, relative to the other trivalent REE, provides a test for the introduction of REE from a non-marine source during diagenesis.

8.2. Modern rivers

Similar to Sr isotope variations in modern rivers, the isotopic composition of dissolved Nd in rivers gives first-order information on the sources of dissolved rare earth elements. This is illustrated by a consideration of the crustal vs. mantle sources of riverine Nd and Sr in the data given in Table 4. Several features of the river Nd isotope data are similar to the trends observed for Sr isotope variations: (1) mantle Nd isotope signatures (i.e., high $\varepsilon_{Nd}(0)$ values) are observed in rivers draining young volcanic arcs (e.g., $\varepsilon_{Nd}(0) = 0$ to 7 in Japanese and Philippine rivers); (2) typical continental crust Nd isotope signatures are observed in rivers draining continental areas with a range of crustal ages (e.g., $\varepsilon_{Nd}(0) = -19$ to -8 in Mississippi river); and (3) old continental crust Nd isotope signatures are observed in rivers draining old continental areas such as Greenland ($\varepsilon_{Nd}(0)$ values of -44 to -43; Table 4). As was observed for Sr isotope variations in modern rivers, Nd isotope variations offer information on sources of dissolved ions in surface waters that major- and trace-element variations usually cannot provide.

8.3. Oceans

Important contrasts between the geochemical behavior of Nd and Sr that affect the nature of their oceanic records are the much shorter residence time of the rare earth elements, and the concomitant heterogeneous Nd isotope patterns in modern oceans (Table 3, Fig. 17). These contrasts have the advantage of using Nd isotopes in marine sediments as tracers of the provenance of dissolved REE and ocean currents within and between ocean basins. The direction of currents in the deep ocean has been examined using Nd isotope variations in modern seawater (Piepgras et al., 1979; Piepgras and Wasserburg, 1980, 1983; Stordahl and Wasserburg, 1986; Elderfield, 1988) and in ferromanganese nodules and other types of marine sediments that were deposited during the Quaternary (Albarède et al., 1997; Innocent et al., 1997; Ling et al., 1997). For example, seawater Nd

isotope profiles correspond to salinity and dissolved oxygen profiles in the eastern North Atlantic Ocean (Piepgras and Wasserburg, 1983), as all three profiles show the signature of saline, oxygen-poor Mediterranean outflow water centered at 1-km depth.

The sources of REE input into the oceans include rivers, diagenetic fluids discharged from buried seabottom sediments, particulates from the atmosphere and rivers, and hydrothermal fluids. Tracing the sources of the REE in the modern oceans can be strikingly diagnostic, as shown in Fig. 17. Quantifying

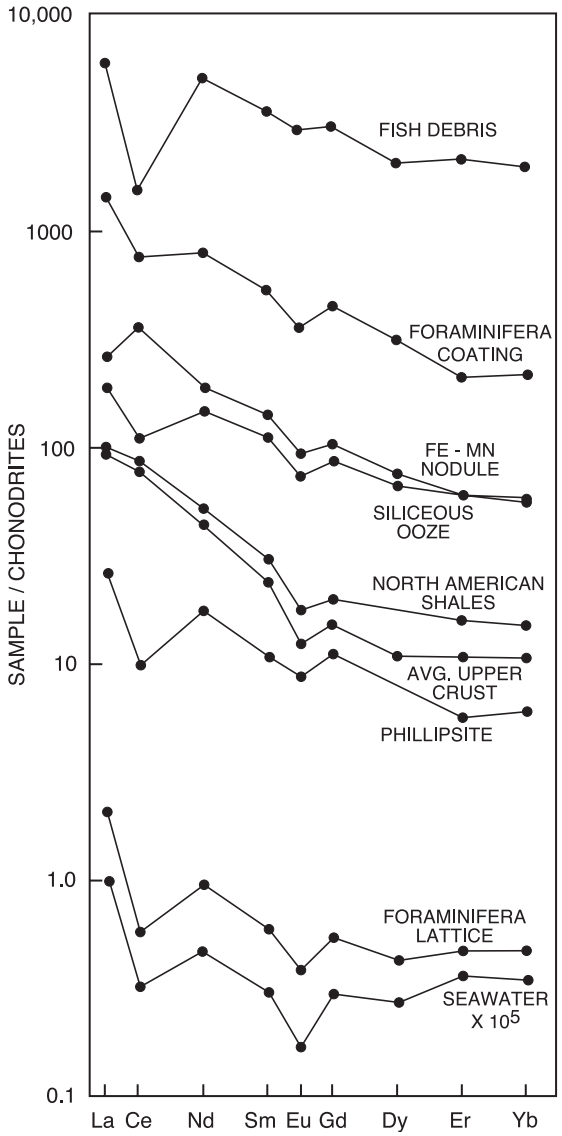

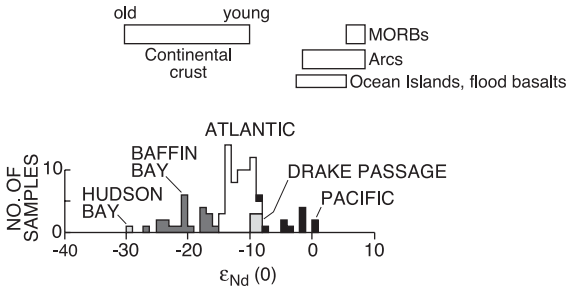

Fig. 17. Nd isotope variations in the modern oceans based on analyses of seawater and ferromanganese nodules. ε_{Nd} notation defined in Table 3. In contrast to Sr isotope results shown in Fig. 7, the short residence time of the rare earth elements relative to the inter-ocean mixing time produces a heterogeneous distribution of Nd isotope values between ocean basins, reflecting the distinct age and lithology of the sources of Nd to the oceans. Some fundamental features of this data set include: (1) the contrasts between the Atlantic and Pacific Oceans, reflecting the high $\varepsilon_{Nd}(0)$ values associated with input of mantle-derived Nd from circum-Pacific volcanism; (2) intermediate values of seawater from the Drake Passage, reflecting mixing between Atlantic and Pacific Ocean water; and (3) the very low $\varepsilon_{Nd}(0)$ values of Baffin Bay seawater, reflecting very old local sources. Compare with Sr isotope distributions in modern oceans shown in Fig. 7. Data from Piepgras et al. (1979), Piepgras and Wasserburg (1980), Piepgras and Jacobsen (1988), Stordahl and Wasserburg (1986), and Capo and DePaolo (1992).

the inputs, however, is not as straightforward as for the geochemical cycle of Sr (Fig. 7). The geochemical cycle of Nd in the oceans is complicated by the

Fig. 16. Rare earth element (REE) variations in components of the sedimentary cycle. Rare earth element concentrations are plotted here as a function of increasing atomic number, and normalized to the concentrations in chondritic meteorites (Hanson, 1980) in order to smooth out natural variations in concentrations between neighboring elements. The similarity of the pattern of REE variations between average upper crust and shales indicates that REE (and, by inference, Nd isotopes) in shales reflect their crustal source. The anomalously high concentration of Ce in Fe–Mn nodules portrays the lower solubility of Ce^{4+} relative to the other trivalent REE in oxidizing aqueous solutions. The resulting preferential sequestering of Ce in oxides and hydroxides and other particulates leaves seawater with anomalously low concentrations of Ce. Authigenic marine minerals, including clays, siliceous oozes, and biogenic calcite and apatite will record this marine REE signature, which serves as a useful indicator of the degree of preservation of Nd isotopic signals in ancient sedimentary rocks. Enrichment of REE in Fe–Mn hydroxide coatings, with similar REE pattern, on foraminifera suggests that REE are enriched in carbonate sediments shortly after deposition (Palmer and Elderfield, 1985a). Note the extremely low concentrations of rare earth elements in seawater. From Banner et al. (1988b).

particle-reactive nature of the REE, uncertainties regarding the reversibility of the exchange between dissolved and particulate REE, the sequestration and subsequent diagenetic remobilization of REE in estuarine sediments, and uncertainties regarding REE speciation in aqueous solution (Wood, 1990; Sholkovitz, 1995; Tachikawa et al., 1999).

8.4. Uncertainties in applications to ancient sequences

Application of the Nd isotope system to secular studies of seawater chemistry faces some disadvantages that result from the contrasts discussed above in geochemical behavior with the Sr isotope system. Most significant is the lack of a single global Nd isotope signal at a given point in geologic time. This precludes the contemporaneous sample test discussed earlier that provided a rigorous criterion for a primary marine Sr isotope signal. There are also much lower REE concentrations in authigenic marine sedimentary rocks compared with Sr (Table 3), so microsampling of pristine components in many cases cannot be conducted at the same resolution. The analytical methods for measuring Nd isotope ratios were developed more recently, and the analytical methods are somewhat more involved compared with methods for Sr isotope analysis, resulting in a somewhat smaller data Nd isotope database for sedimentary rocks. A history of the development of these methods is given in DePaolo (1988). Uncertainties are also associated with our understanding of: (1) the nature of REE substitution in the crystal structure of common sedimentary minerals (Wright et al., 1984; Palmer and Elderfield, 1985a), compared with detailed studies of Sr substitution in carbonates (Pingitore et al., 1992); (2) the mechanism of diagenetic alteration of REE in ancient sedimentary rocks that accounts for the transformation of low-REE carbonates (ppb levels) to carbonates with higher REE contents over time (ppm levels; Banner et al., 1988b); and (3) the apparent variability of diagenetic mobility of the REE in different settings, as discussed in the next section.

8.4.1. Assessing the diagenetic mobility of the REE

REE mobility during diagenesis has been assessed through integrated geochemical (major and trace elements and isotopes) and petrographic studies (cathodoluminescence, backscattered electron imaging, fission tracks, and element mapping). Chemical and mineralogic changes with depth through Gulf Coast, USA, Tertiary shale sequences indicate that changes in provenance and detrital sorting have a relatively narrow range of influence on shale composition. Where REE and Nd isotope variations in these sequences cannot be explained by provenance or sorting processes, it is instead proposed that the REE have been fractionated during mineralogic diagenetic transformations such as those involved in the breakdown of unstable volcanic detritus and the smectite–illite conversion (Awwiller and Mack, 1991; Land et al., 1997). The scale of REE mobility in this setting is at least local, as evidenced by authigenic minerals that are enriched in REE such as apatite (Ohr et al., 1991).

Similar local-scale REE mobility is also found in diagenetic environments that are very different from the deep burial regime of the Gulf Coast. In Mississippian shallow-water carbonate strata in the mid-continent, USA, REE enrichments are observed in diagenetic dolomites that occur in stratigraphic intervals enriched in detrital apatite (Banner et al., 1988b). Through construction of a detailed paragenetic sequence in a black shale from the Ordovician of the Welsh Basin, Lev et al. (1998) evinced the early diagenetic formation of pyrite, apatite, and carbonate, and the later formation of monazite and carbonate. Owing to the REE-enriched nature of apatite and monazite, the chemical reactions that produced this sequence necessitate diagenetic redistribution of the REE on at least the mineral scale. Nd isotope and REE studies of Paleozoic and Proterozoic siliciclastics also indicate diagenetic mobilization of the REE, which suggests caution when interpreting provenance based on REE and Nd isotope studies (Bock et al., 1994; McDaniel et al., 1994). In the surficial environment of soils developed on uplifted Pleistocene reef carbonates, loss of REE during weathering and soil evolution has been documented to occur without significant Sm–Nd fractionation (Borg and Banner, 1996).

Only a small database exists for Nd isotope and REE analyses of diagenetic fluids, including groundwater, surface water, and seawater. This paucity of data is a consequence of the obstacles to analyzing extremely low concentrations of rare earths that are

typical in natural fluids (Tables 3 and 4; Piepgras et al., 1979; Elderfield and Greaves, 1982; Banner et al., 1989; Johannesson et al., 1994).

As will be discussed in the following sections, Nd isotope and REE variations are useful in studies of seawater evolution, provenance, crustal evolution, and stratigraphic correlation. While this utility derives in part from the relatively low mobility of the REE during post-depositional processes, it is clear that REE mobility does occur in a range of diagenetic environments, and that the scale and magnitude of this mobility will need to be assessed on a case by case basis.

8.5. The oceanic Nd isotope record

There have been few attempts at constructing a continuous Nd isotope seawater curve through the Phanerozoic. This is due to a number of factors, including the uncertainties discussed above. Nevertheless, the prospects of using seawater Nd isotope curves for addressing a variety of stratigraphic and sedimentologic problems are excellent, as discussed below. Several of the records of seawater Nd isotope variations that have been constructed are shown in Fig. 18.

As discussed above, Nd isotope studies of modern water samples and Quaternary marine biogenic and chemical sediments have been useful in reconstructing currents in the deep ocean. Nd isotopes have also been found to have high-resolution paleoceanographic reconstruction potential on glacial–interglacial time-

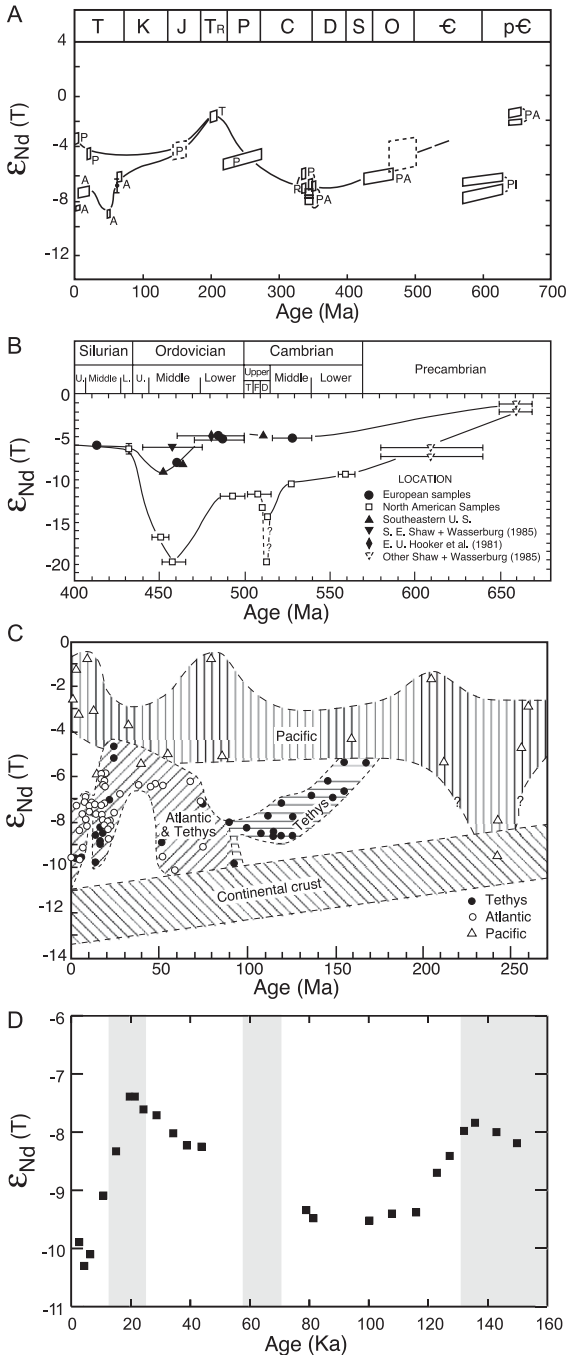

Fig. 18. Secular variations in seawater $\varepsilon_{Nd}(T)$ values. (A) Preliminary Late Precambrian to Phanerozoic seawater Nd isotope variations based on analyses of marine phosphates and metalliferous sediments (Shaw and Wasserburg, 1985). Note the possible delineation of distinct isotopic signatures for Atlantic and Pacific Oceans during the Cenozoic and Mesozoic. (B) Late Precambrian through Silurian seawater Nd isotope variations based on analyses of phosphatic brachiopods and conodonts (Keto and Jacobsen, 1987), marine phosphates (Shaw and Wasserburg, 1985), and metalliferous sediments (Hooker et al., 1981), as compiled by Keto and Jacobsen (1987). Geographic distribution portrays distinct isotopic compositions for Iapetus and Panthalassa Oceans. SE = Southeastern US; EU = Europe. (C) Late Permian through Tertiary seawater Nd isotope variations based on analyses of marine phosphates and carbonates (Stille and Shields, 1997). During the Mesozoic and Cenozoic eras, the Atlantic and Tethys oceans maintained distinct isotopic signatures from that of the Pacific Ocean. (D) Nd isotope variations in the northeast Indian Ocean during the Late Pleistocene based on analyses of planktonic foraminifera from ODP site 758 (Burton and Vance, 2000). The gray bars indicate glacial intervals. Note the strong correspondence between oceanic Nd isotope composition and glacial–interglacial shifts.

scales (Fig. 18D; Abouchami et al., 1997; Reynolds et al., 1999; Burton and Vance, 2000; Frank et al., 2000, 2001). For example, Nd isotope changes in Bay of Bengal foraminifera correspond with global glacial–interglacial shifts over the past 150 k.y., and appear to reflect changes in either local continental input or ocean circulation (Burton and Vance, 2000). The lack of an extensive pre-Cenozoic deep-sea record precludes applications to understanding deep ocean circulation in older strata. A principal application of Nd isotopes to studies of pre-Cenozoic oceans has been the determination of the extent of communication within and between shallow epeiric seas and the open ocean, as discussed below.

8.6. Applications to stratigraphic problems

8.6.1. Paleocean circulation

Neodymium isotope studies have potential for constructing intrabasinal temporal records at a much higher resolution than Sr isotope studies, owing to the short oceanic residence time of Nd (Table 3). Neodymium isotopes may also be used for determining the extent of communication between ancient epeiric seas and the open ocean (Fig. 18; Shaw and Wasserburg, 1985; Palmer and Elderfield, 1985a; Keto and Jacobsen, 1987; Stille et al., 1992, 1996; Holmden et al., 1998). Nd isotopic variations in conodonts and host limestones from Ordovician strata covering a narrow time interval (between two bentonite beds with the same radiometric ages within uncertainty) and a wide geographic region were examined by Holmden et al. (1998). The results indicate that an epeiric sea in eastern Laurentia maintained a regional gradient in Nd (and C) isotopes that reflects restricted circulation between this epeiric sea and the open ocean.

In mixed carbonate–siliciclastic systems, it may be possible to use Nd isotopes and rare earth element distributions to provide chemical signals that distinguish between a continental (as recorded in the siliciclastics) and an open ocean (as recorded in the carbonates) source of rare earth elements. The open ocean signal may be modified by mixing with REE derived from local siliciclastics and produce intrabasinal spatial variations in marine water chemistry. Although yet to be tested, authigenic sediments in such a basin may record the extent of this mixing process.

8.6.2. Provenance applications

A modern example of how Nd isotopes may be used to trace sources of siliciclastics is found in the Fraser River in British Columbia, which flows from an old, stable craton in its source through younger orogens on its way to the Pacific Ocean. Whereas a cratonic Sr signature is carried to coastal zones by the Fraser as part of its dissolved load, Nd is carried to the ocean almost entirely in the suspended load (Cameron and Hattori, 1997). As a consequence, the Nd isotope signature of the riverine flux to the oceans from the Fraser is biased towards Nd isotope values for the orogen comprising the coastward part of Fraser's watershed. This framework will be useful for future studies to distinguish detrital vs. authigenic sources of Sr and Nd in ancient marine sedimentary sequences.

Analysis of siliciclastic sediments in a range of sedimentary basin types also illustrates the use of Nd isotope variations as a provenance indicator for siliciclastic sedimentary rocks (McCulloch and Wasserburg, 1978; Awwiller and Mack, 1989; McLennan, 1989; McLennan et al., 1993; Awwiller, 1994). The utility of this provenance method lies in the apparently low diagenetic mobility of the rare earth elements and in the distinct Sm–Nd characteristics of different crustal source terranes (Fig. 16). The degree of mobility of the REE during weathering and diagenesis, however, appears to vary depending on the system considered, and may need to be evaluated on a case by case basis (see Assessing diagenetic mobility of the REE section above). The provenance method's potential has been demonstrated in young sedimentary basins where the source terranes are well identified and/or where there are independent petrographic indicators of provenance such as percent of lithic volcanic fragments (e.g., Tertiary Hagan and Espanola basin study of Nelson and DePaolo, 1988; modern turbidite study of McLennan et al., 1990).

This approach has important potential for ancient siliciclastic sequences (1) that lack unambiguous petrographic provenance indicators, and (2) where multiple source terranes could have contributed sediment to the basin of interest. In the Early Proterozoic Animikie Basin, which straddles Archean crust of the Superior craton and Early Proterozoic crust of the Wisconsin magmatic terranes, sediment Nd isotope

variations are used to help construct a tectonic evolution for the Superior continental margin. This evolution began as a passive margin in a back arc basin, and ended as a telescoped back arc that closed due to changes in plate convergence (Hemming et al., 1995). On the larger scale of the North American continent, siliciclastic Nd isotope variations reveal changes through time of continental shield, Caledonian–Appalachian, and Cordilleran source regions (Patchett et al., 1999).

8.6.3. Paleoexposure surfaces

Sm–Nd studies in Quaternary soils suggest applications to the nature of sequence boundaries and subaerial exposure surfaces in ancient systems. Soils developed on uplifted coral reef terraces on Barbados, including some as young as 125,000 years old, have a range of Nd concentrations, Sm/Nd ratios, and Nd isotope signatures that reflect atmospheric transport and deposition from several sources (Borg and Banner, 1996). Sm–Nd studies of ancient carbonate sequences have the potential to identify and correlate exposure horizons where the relatively immobile REE accumulate.

8.6.4. Limits and prospects for secular curve construction

Since the Nd system appears to be a useful complement to Sr in terms of oceanic residence time and geochemical behavior, one may wonder why the Nd isotope system (and others to be discussed such as Os and U–Pb) has not been as widely applied to studies of ancient seawater chemistry and chemical stratigraphy. Perhaps the main disadvantage to Nd isotopes discussed above that limits the application of Nd isotopes in this regard is the lack of a single secular seawater curve, such as that for Sr that results from the high degree of homogeneity of $^{87}Sr/^{86}Sr$ in the oceans. In other words, having a priori knowledge that there can be only one right answer to the question "What is the Sr isotope composition of seawater at a given time in Earth history?" has made for a straightforward effort of curve construction. Nevertheless, these same differences in the oceanic geochemistry between Sr and Nd allow the tracing of modern ocean currents (e.g., Piepgras and Wasserburg, 1983), and offer the prospect of reconstructing the paleoceanography of ancient seas.

8.6.5. Stratigraphic correlation and sequence stratigraphy

In the lower Triassic Statfjord Formation oilfields of the North Sea, Nd isotope model ages (defined in the next section) of clastic sediments provide evidence for shifts in sediment provenance between Devonian to Triassic strata from the East Shetland Platform to the southwest, and Lewisian gneisses to the north (Dalland et al., 1995). Statfjord strata lack biostratigraphic indicators and good seismic resolution, so that the Nd isotope data are useful for the correlation of strata from oilfield cores. Dalland et al. (1995) make such correlations of channel sandstones to associated crevasse mudstones in cores over 0.1 km apart, which allows construction of a detailed reservoir zonation, and identification of previously undetected intraformational erosional surfaces and normal faults.

In the Carboniferous to Permian Finnmark platform in the Barents Sea, relatively old Nd-model ages correlate with the lower parts of two successive second-order depositional sequences (Ehrenberg et al., 2000). This indicates that relatively old Caledonian basement was the source of clastic material in the older parts of each sequence, and suggests a tectonic control on the uplift and subsequent peneplenation or burial of this basement during Finnmark deposition.

8.7. Evolution of the sedimentary cycle

A consideration of siliciclastic Nd isotope variations over geologic time is a useful indicator of the extent of recycling of the global sedimentary mass. This in turn provides important clues to the rates of addition of new continental crust during Earth history (McCulloch and Wasserburg, 1978; Allègre and Rousseau, 1984; O'Nions, 1984; McLennan and Taylor, 1991). These studies are based on the assumption that the Sm–Nd isotopic systematics of fine-grained sedimentary rocks reflect their original depositional isotopic signature and that this signature reflects the mean value of the crust from which the sediments are derived. In this way, the Nd isotope composition and Sm/Nd ratio of a fine grained siliciclastic rock can be used to calculate the time in the past when the sample had the same Nd isotopic composition as the mantle. This represents the time that its crustal source was derived from the mantle (e.g., Fig. 15). This time is also referred to as a "Nd model age", or as a "crustal

residence age''. By comparing the stratigraphic age of each sample with its crustal residence age, the extent to which the sedimentary mass reflects recycling vs. new crustal additions can be estimated as a function of time (compare 'no new crust' and 'all new crust' trends in Fig. 19). The results show that during the Archean and Proterozoic, the sedimentary mass was dominated by the erosion of newly formed, mantle-derived crust. Since the Late Proterozoic, by contrast, the sedimentary mass has had a larger recycled component, indicating a decrease in the rate of addition of new crust during this time. This is consistent with modern sediment from the world's large rivers having similar crustal residence ages to post-Archean siliciclastic sediments (Fig. 19). Although the effects of detrital sorting and diagenesis on Nd isotope and Sm/Nd ratios remain as important factors to assess in radiogenic isotope studies of siliciclastics and authigenic sediments (see earlier section on Assessing diagenetic mobility of the REE), the first-order trends in Fig. 19 are unlikely to be changed by these effects.

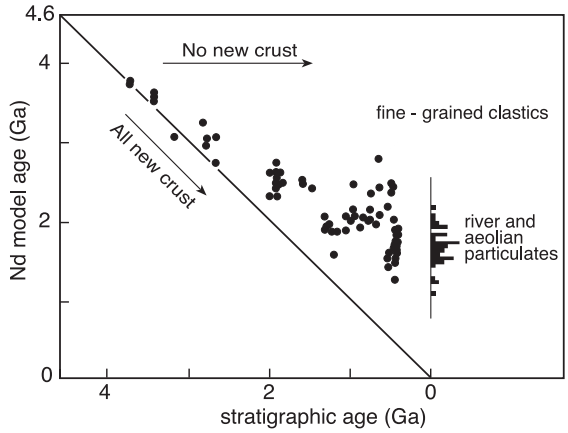

Fig. 19. Relationship between stratigraphic age and Nd model age for fine-grained clastics and modern Aeolian and river particulates (after O'Nions, 1984; Goldstein et al., 1984). Nd model age in this case is equivalent to crustal residence age, and is the age at which a sample had the same Nd isotopic composition as a depleted mantle composition, thus marking the time that the sample was emplaced into the crust. This age is calculated using a sample's present-day Sm/Nd ratio and Nd isotope composition. No new crust trend indicates model pathway that clastics would follow if the sedimentary mass was continuously recycled after formation during Archean time. All new crust trend is that for no recycling of continuously forming crust. Nd isotope variations in fine-grained clastics indicate little to no recycling during the Archean and increasing recycling during the Proterozoic and Phanerozoic. Histogram at zero age shows values for modern Aeolian and river particulates.

Neodymium isotope analysis of Recent turbidite deposits and modern river sediments reveals a clear relationship between crustal residence age and tectonic setting (McLennan et al., 1990; Goldstein and Jacobsen, 1988). The turbidites and river sediment from passive margin settings have older crustal residence ages than do turbidites and river sediment from active tectonic settings. This raises an issue regarding the lack of Phanerozoic and Proterozoic siliciclastic sedimentary rocks with crustal residence ages similar to their stratigraphic age (Fig. 19). In addition to the no-new-crust hypothesis discussed above, it is possible that sediments deposited in the past in active tectonic settings (which, by analogy with the Recent, would have crustal residence ages closer to their stratigraphic age than do those from passive margin settings) have not been preserved or sampled to the same extent as samples from stable tectonic settings. Such a bias against the preservation of sediments from active tectonic settings has significant bearing on models of the evolution of the continental crust (McLennan et al., 1990).

In summary, the Sm–Nd isotope system has considerable potential for studies of ancient sedimentary systems, including improving stratigraphic correlation, paleoceanography, provenance, and the history of the sedimentary mass.

9. Other lanthanide-series radiogenic isotope systems

Within the lanthanide series of elements (REE), the Sm–Nd, La–Ce, and Lu–Hf radiogenic isotope systems have been applied to a variety of sedimentary problems. The range of geochemical behavior and associated fractionation among these parent–daughter isotope pairs leads to their providing complementary information. Whereas Sm and Nd exhibit similar geochemical behavior, the 3+ and 4+ valences of Ce produce fractionation from the other REE as discussed earlier. Lu is the heaviest trivalent lanthanide element, while Hf is a group IVB element with a 4+ valence (Table 2), also leading to dissimilar geochemical behavior relative to Sm–Nd. A variety of analytical

challenges has been made for limited results to date for the La–Ce and Lu–Hf systems.

9.1. Lanthanum–cerium isotope system

The decay of ^{138}La to produce ^{138}Ce produces natural variations in the isotopic composition of Ce, expressed as the ^{138}Ce/^{142}Ce ratio. Similar to the Sm–Nd system discussed above, the La–Ce system involves the radioactive decay of one rare earth element to produce another. In addition, the relatively short residence time of Ce in the oceans (intermediate between Pb and Nd residence times, Table 3) makes for a heterogeneous distribution of Ce isotopes in the oceans, as was seen for Nd and Pb isotopes. Preliminary studies of Ce isotope values in ferromanganese nodules indicate distinct values for nodules from the Pacific, which have more ocean crust type signatures, the Atlantic, which have more continental crust type signatures, and the Drake Passage, which have intermediate values (Amakawa et al., 1996; also compare with Nd isotopes for Atlantic, Pacific, and Drake Passage in Fig. 17). The large range in the parent–daughter La/Ce ratio exhibited by different components of the sedimentary cycle (Fig. 16) produces a large range in ^{138}Ce/^{142}Ce ratios, which could be used for dating and oceanographic tracing (Stille and Shields, 1997). Application of this isotope system has been limited owing to analytical obstacles to measuring the very small amounts of ^{138}Ce that are produced from the minor (0.09% of all La) and slow-decaying ^{138}La.

9.2. Lutetium–hafnium isotope system

The beta decay of ^{176}Lu produces ^{176}Hf, with a half-life of 36 b.y. In contrast to the similar geochemical behavior of the Sm–Nd parent–daughter pair, Hf can be highly fractionated from Lu because Hf substitutes extensively for Zr in zircon. Zircon is highly resistant to weathering and hence Hf is retained relative to the REE during weathering processes, producing large differences in the parent–daughter Lu/Hf ratio in siliciclastic sediments and, by inference, in the Hf isotope composition of material delivered to the oceans. While there is a limited database for Hf variations in the oceans, results for Fe–Mn crusts and other authigenic marine sediments reveal temporal trends that provide unique information relative to other isotopic systems. Analysis of Fe–Mn crusts from the deep central Pacific yields an essentially constant ^{176}Hf/^{177}Hf value since 20 Ma (Lee et al., 1999). As discussed in earlier sections, the large changes that occurred in the global oceanic ^{87}Sr/^{86}Sr record (Fig. 1) over this same time period record processes of enhanced continental weathering and transport to the oceans. While these weathering processes affected Sr in the global ocean, the lack of impact on the Hf record may reflect the increased isolation of the central Pacific from the global ocean (Lee et al., 1999).

The Lu–Hf and Sm–Nd isotope systems display coherent behavior in terrestrial environments. Similar to the relationship between stratigraphic age and Nd isotope crustal residence age for siliciclastic rocks (Fig. 19), Hf isotope crustal residence ages of siliciclastic rocks portray a decrease in the growth rate of the crust through time (Vervoort et al., 1999). In passive margin settings, mud and sand have distinct Lu/Hf and ^{176}Hf/^{177}Hf due to the concentration of Hf-rich zircons with low ^{176}Hf/^{177}Hf in mature sands. In contrast, the juvenile character of sediments from active margins results in only minor differences in Lu/Hf and ^{176}Hf/^{177}Hf (Vervoort et al., 1999). Hf–Nd isotopic data for all terrestrial samples fall along a coherent trend defined by mantle and crustal components. This coherency likely results from mixing in the mantle and homogenization in the crust due to sedimentary processes (Vervoort et al., 1999).

10. Rhenium–osmium isotope system

^{187}Re decays to produce ^{187}Os by beta decay with a long half-life of 42.3 b.y. Large fractionation of Re from Os occurs during mantle and crustal evolution processes, producing large parent–daughter Re/Os ratios in the crust, and therefore large Os isotopic differences (expressed as the ^{187}Os/^{186}Os ratio) between crustal and mantle reservoirs (Walker and Morgan, 1989; Colodner et al., 1993). These differences make for a sensitive detector of the contribution of crustal (^{187}Os/^{186}Os = 10–30) vs. mantle (^{187}Os/^{186}Os ~ 1) sources to the oceans. Modern metalliferous marine sediments are found to have values intermediate between these crustal and mantle

values. Osmium isotope variations in ancient seawater should therefore provide an independent test for inferences regarding continental vs. mantle fluxes to the oceans that are based on the seawater Sr isotope record.

Recent analytical advancements have allowed for the direct measurement of Os isotopic composition of seawater, in which Os occurs at the level of 11 parts per quadrillion (Levasseur et al., 1998). A homogeneous distribution of Os concentrations and isotopic compositions is found in the Indian Ocean, consistent with a residence time that is long relative to the interocean mixing time (Fig. 20; Table 3), whereas a small degree of Os isotopic heterogeneity between ocean basins is inferred from modern metalliferous sediments indicates a shorter oceanic residence time relative to Sr (Burton et al., 1999).

Given the similarities between the Re–Os and Rb–Sr isotope systems, one may expect a similar oceanic record for $^{87}Sr/^{86}Sr$ and $^{187}Os/^{186}Os$. The Tertiary part of the oceanic $^{187}Os/^{186}Os$ record has been constructed in some detail for $^{187}Os/^{186}Os$ (Pegram et al., 1992; Ravizza, 1993; Peucker-Ehrenbrink et al., 1995; Reusch et al., 1998). A large increase in $^{187}Os/^{186}Os$ over the past 65 m.y. recalls the climb in $^{87}Sr/^{86}Sr$ for the same time period (Figs. 1 and 8), indicating that increasing continental weathering over this time period is reflected in both isotopic records. Similar to the studies of Sr isotope record, this rise in Os isotopic composition has been linked to uplift of the Himalayas (e.g., Pegram et al., 1992). Some significant differences exist in the slope of each isotope record, however, and these likely portray differences in the nature of the controls on the Sr and Os isotopic composition of the oceans. These differences include contrasts in the residence times of Sr and Os (Table 3), and the concentration of Re and Os in specific types of rocks exposed to weathering, such as metalliferous phases and organic matter (Ravizza, 1993; Stille and Shields, 1997).

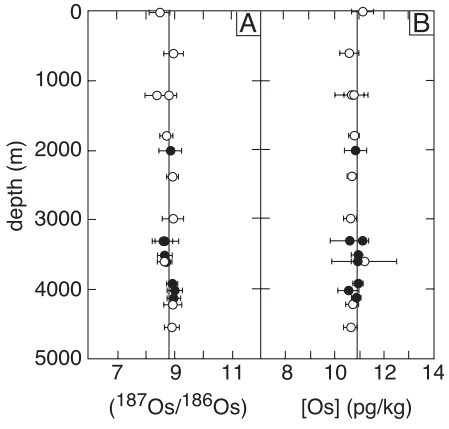

Fig. 20. (A) Osmium isotopic composition, and (B) Os concentrations in modern seawater from varying depths in the Indian Ocean (Levasseur et al., 1998).

Paired Os and Sr isotopic analysis of Himalayan paleosols provides a record of changes in Himalayan rivers (Chesley et al., 2000). This record indicates similar source terranes for Os and Sr during the Neogene, and requires large changes in the flux of both of these elements if Himalayan rivers are responsible for the changes in the Neogene marine Os and Sr record (Chesley et al., 2000). Further difficulties in reconciling the role of Himalayan rivers in the seawater Os isotope record are the low Os flux in modern Himalayan rivers and the dissimilarity between the Os isotopic composition of modern Himalayan rivers ($^{187}Os/^{186}Os = 9.0–22.8$; Sharma et al., 1999) and modern Indian Ocean water ($^{187}Os/^{186}Os = 8.40–8.98$; Levasseur et al., 1998).

A high resolution, Late Pleistocene record of oceanic Os isotope variations broadly corresponds with 10^5 year interglacial–glacial cycles in the marine oxygen isotope record (Fig. 21). This is a higher resolution than has been found for Sr isotopic variations in seawater and is consistent with shorter residence time estimates for Os compared with Sr. In addition, the crustal Os component of the marine Os signal is lowest during Pleistocene glacial maximums, which does not support theories of enhanced weathering during glacial cycles. While such Os isotope systematics suggest considerable potential in high resolution chemostratigraphy and weathering studies, the strong partitioning of Os into sulfide minerals and organic matter has restricted most Os isotope studies, until recently, to enriched metalliferous phases such as those found in meteorites, Fe–Mn nodules, and metalliferous carbonates from the seafloor, ore deposits, and organic-rich sediments (e.g., Ravizza, 1993; Creaser et al., 2002). The potential of the Re–Os system in studies of the sedimentary cycle and crustal and mantle evolution has spurred further analytical advancements, such as those using negative ion ther-

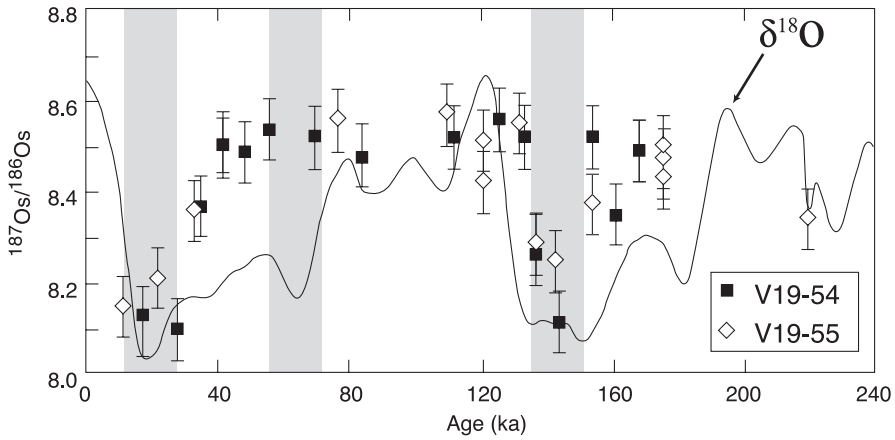

Fig. 21. Os isotopic variations in seawater during the Late Pleistocene based on analyses of bulk sediment from ODP cores V19–54 and V19–55 (Oxburgh, 1998). Solid line is the oxygen isotope record for core V19–55. Low points in the oxygen curve represent glacial intervals and high points represent interglacials. The shaded gray bars are periods of high dust content in Antarctic ice cores and correspond with glacial periods. Note the consistency of records from the two sites, the correspondence of low $^{187}Os/^{186}Os$ values with glacial periods, and the resolution of changes in marine $^{187}Os/^{186}Os$ on time scales of 20,000 years. Owing to the oceanic residence time of Os that exceeds the oceanic mixing time (Table 3), a homogeneous Os isotopic composition can be expected for the world's oceans at a given time (as found in modern oceans, Fig. 20). Owing to the short residence time of Os relative to Sr, higher frequency changes are resolvable in the Os record (compare with Fig. 9). Combined with the Tertiary marine Os isotope record (see text), this has considerable potential for stratigraphic correlation.

mal ionization mass spectrometry and multiple-collector, magnetic sector ICP-MS (e.g., Hemming et al., 1999). Such advancements will allow Re–Os investigations into ancient sedimentary sequences, as the measurements will be applicable to a wider range of rock types and to determining the sites for Re and Os in carbonates, evaporites, phosphates, and other sedimentary rocks with relatively low concentrations of these elements.

11. Uranium–thorium–lead isotope system

The main applications of the U–Th–Pb isotope system in sedimentary geology are for age determinations over a range of time scales, as will be discussed in the section on Geochronology below. Variations in the isotopic composition of the daughter isotopes of lead (Table 1) are also useful oceanographic circulation tracers. Lead occurs in very low concentrations in the oceans, and is thus highly susceptible to anthropogenic contamination from sources such as leaded gasoline. Many paleoceanographic studies have focused on deep-sea ferromanganese nodules and crusts have been the focus of many studies, as they are enriched in lead by natural processes (~ 1000 ppm Pb). Lead isotopic gradients are found within and between the major ocean basins, and can be used to evaluate the extent of mixing between different water masses (Albarède and Goldstein, 1992; Abouchami and Goldstein, 1995; Abouchami et al., 1997; Ling et al., 1997).

Isotopic tracer studies of ferromanganese nodules are hampered by the limited constraints on the time interval over which a given sample grew, and the low spatial resolution at which these slow-growing samples can be analyzed. One approach to achieving higher resolution records of Pb, Nd, and Sr isotope variations of inputs to the oceans is the analysis of the terrigenous component of Quaternary deep-sea sediments (Frank et al., 2001). Other approaches have focused on the application of ^{10}Be to dating the surfaces of ferromanganese nodules and the analysis of Pb isotopic compositions on 150 μm wide areas in the nodules using laser ablation, multiple-collector ICP mass spectrometry (Christensen et al., 1997; Albarède, 1997). Over the last 50 million years, temporal changes in the Pb isotopic composition of seawater (as inferred from measurements on the nodules), occurring over 10–15 million year intervals, closely correspond to changes in the oxygen isotope composition of seawater (Christensen et al., 1997). As the oxygen record represents a

detailed record of glaciation and climate change through the Cenozoic, the correspondence indicates that climate change and weathering must also be driving the Pb isotopic variations on these time scales that are considerably longer than the very short oceanic residence time of Pb (Table 3). Global-scale changes over these time intervals that the Pb record may be preserving include changes in the crustal sources that are being weathered, or changes in the nature of the thermohaline convection of the oceans. As such advancements continue, a temporal record of lead isotope variations in the oceans may be useful in chemostratigraphic applications.

Lead isotope variations in a variety of detrital mineral phases are useful as provenance indicators over a range of geologic time periods. As with other applications of radiogenic isotopes to sedimentary processes, careful petrographic screening and sample pretreatment are needed to avoid analyzing mixtures of original depositional and later diagenetic components (e.g., Hemming et al., 1996). U–Pb isotopic studies on quartz, leached feldspar, and whole rock samples of Late Archean granitoids in northeastern Minnesota yield ages that are consistent with independent geochronologic information, suggesting that the U–Pb system behaved as a closed system since the time of crystallization (Hemming et al., 1994). U–Pb isotope studies on detrital clear quartz in an Early Proterozoic quartzite in northeastern Minnesota yield Late Archean ages, and support an hypothesized Superior Province provenance for the quartzite (Hemming et al., 1994).

In Late Pleistocene deep-sea sediments from the North Atlantic ocean, layers rich in ice-rafted debris called Heinrich layers are proposed to reflect abrupt climate change events that launched great armadas of icebergs into the North Atlantic. Lead isotope analyses of feldspars and the fine sediment fraction in several Heinrich layers are consistent with the clastic component of these layers being derived from ancient continental crust surrounding the Labrador Sea (Gwiazda et al., 1996; Hemming et al., 1998).

12. Geochronology: principles and applicability to dating the sedimentary record

Accurate absolute dating of rocks and minerals is a key factor in enabling advances in the state of the art of many disciplines of sedimentary geology. It serves to ground-truth stratigraphic correlations, and it is a key constraint in understanding nearly all sedimentary processes. A number of biostratigraphic, physical, and chemical records can be constructed that provide relative age information through the use of paragenetic sequences, chemostratigraphy, or precise but floating chronologies derived from seasonally banded sediments or organisms such as trees and corals (e.g., Anderson et al., 1972; Dodge and Brass, 1984). Isotope geochronometers (i.e., radiometric dating methods), however, are required for absolute age determinations. This section describes the basic principles and highlights some exciting developments in the dating of sedimentary processes.

An accurate isotope geochronometer must meet certain criteria, as discussed in Faure (1986), including: (1) the parent and daughter isotopes follow closed-system rather than open-system behavior, meaning that no new material is added and none is removed during a sample's history; (2) accurate values for decay constants are known (Table 1); (3) the initial radiogenic isotope composition (see Eqs. 3–5) of the system is accurately known or estimable; and (4) accurate measurements of the parent and daughter isotopes can be made on samples representative of the rock or mineral to be dated. Radiometric dating using the Rb–Sr, Sm–Nd, U–Pb, Lu–Hf, and Re–Os systems makes use of the isochron method, which requires a significant range in the parent–daughter isotope ratio in order to obtain useful precision on age determinations (Fig. 3). While geochronology has been applied to a wide range of geologic processes, our focus here is on its use in stratigraphic correlation and timing processes of environmental change. Examples of several commonly used radiometric dating methods and applications are discussed here. Details of over 40 radiometric dating methods are given in Geyh and Schleicher (1990).

12.1. Rubidium–strontium

The Rb–Sr system has been used for determining the crystallization age of igneous rocks and the resetting age of metamorphic rocks by the isochron method (Fig. 3). This method has also been applied to detrital sediments in an effort to constrain either the age of the source or the time of diagenetic resetting. Note that

neither of these efforts leads to determination of the time of deposition, which is the time of interest for studies of stratigraphic correlation. The Rb–Sr dating method is not applicable to carbonate mineral suites because carbonates exclude Rb from their crystal structure and hence have a very small range of parent–daughter $^{87}Rb/^{86}Sr$ ratios (Fig. 3). A number of types of sedimentary rocks and minerals have been dated by Rb–Sr, including glauconite and other clays (e.g., Clauer, 1982; Grant et al., 1984; Morton and Long, 1984; Long et al., 1997), chert (Weis and Wasserburg, 1987), and sulfide ore minerals (Brannon et al., 1991). The Rb and Sr in Rb- and Sr-poor minerals such as quartz and sulfides appear to reside in fluid and mineral inclusions (Rossman et al., 1987).

The utility of the Rb–Sr dating method is highly dependent on the extent to which the minerals or rock samples under consideration had homogeneous Sr isotope compositions at the time of formation or resetting, and the extent to which the samples behaved as a closed system since that time. Detrital inheritance and diagenetic resetting are thus primary processes causing inaccuracies in dating sedimentary rocks and minerals. Leaching experiments show that different crystallographic sites in glauconite contain Rb and Sr of depositional vs. diagenetic origin (Morton and Long, 1984). For shales, the finer-grained clay fractions have been found to provide Rb–Sr ages that reflect the time since closure of the Rb–Sr system to diagenesis.

The ultra-fine clay fraction (<0.05 μm) from multiple Mg-rich clay samples in Permian carbonate–evaporite–redbed sequences of the Palo Duro Basin consistently yields the youngest ages on an Rb–Sr isochron diagram (Long et al., 1997). Larger particle size clay samples contain a persistent detrital component, inferred from isochron ages that are older than the stratigraphic age of the samples. The ultra-fine fraction is interpreted to be diagenetic, and Rb–Sr ages for samples from the Tubb, San Andres, Seven Rivers, and Salado–Tansill Formations are each within analytical uncertainty of the stratigraphic ages of these formations. This close agreement indicates that diagenesis was essentially contemporaneous with deposition. Similar applications and uncertainties are associated with Sm–Nd isotope studies of fine-grained argillaceous sedimentary rocks, as will be discussed below.

12.2. Samarium–neodymium

The Sm–Nd system has also been applied using the isochron method to the ages of igneous and metamorphic rocks. The use of Sm–Nd isotope studies in determining the age of the source of detrital sedimentary rocks was explored in the section above on Evolution of the sedimentary cycle. Sm–Nd isotope dating has also been applied to timing the growth of authigenic clay minerals during deposition or diagenesis (Stille and Clauer, 1986). Due to the fine-grained texture and complex nature of clays, detailed mineralogic studies are required to ensure that the samples examined have negligible detrital components. If detrital components are present, then any linear array of samples on an isochron diagram may represent mixing lines instead of isochrons.

Sm–Nd isotope analysis of residue–leachate pairs from Tertiary shales from the Texas Gulf Coast yields younger ages in progressively finer-grained fractions of the same sample (Ohr et al., 1991). These results offer the prospect of Sm–Nd dating of diagenesis of individual shale samples, which removes the uncertainty of initial isotopic heterogeneity associated with multi-sample isochron dating. The relatively wide range in the parent–daughter $^{147}Sm/^{144}Nd$ ratio found in clay minerals makes the isochron method more applicable to argillaceous sedimentary rocks than to carbonate rocks. The apparent low mobility of the REE relative to Rb–Sr in many diagenetic environments makes the Sm–Nd isotopic system more amenable than the Rb–Sr system to geochronologic applications (e.g., Banner et al., 1988b; Ohr et al., 1991).

12.3. Potassium–argon and ^{40}Ar–^{39}Ar

Potassium-40 decays to ^{40}Ca and ^{40}Ar, with a resultant half-life of 1.25 b.y. Radiogenic ^{40}Ca concentrations have very limited variation in nature, and therefore, the K–Ar system has developed more widely as a dating method. As one of the earliest developed geochronometers, K–Ar served as a benchmark to compare ages determined by newer geochronologic methods. The dating of the K-rich clay mineral glauconite was among the first tools used to determine ages of sedimentary rocks. The method has been applied to dating detrital and authigenic grains

for constraining provenance, stratigraphic age, and the timing of diagenesis. The application of the K–Ar system to studies of sedimentary rocks is limited by the uncertainty in assuming that the sample analyzed contained no initial argon, and that the parent ^{40}K and daughter ^{40}Ar (which is a gas) behaved as a closed system. The protracted diagenetic transformations of clay minerals such as glauconite introduce additional complexities (e.g., Grant et al., 1984; Morton and Long, 1984). K–Ar dating of different size fractions of illite from the Permian Rotliegende sandstone of the North Sea indicates that the finer grained fractions grew more recently (or, alternatively, experienced greater diffusive loss), and the timing of diagenetic illite formation corresponds to the timing of major tectonic events in the region (Lee et al., 1989).

The ^{40}Ar–^{39}Ar method uses irradiation of geologic samples in a nuclear reactor, which produces ^{39}Ar (among other isotopes) from ^{39}K. Ages can then be determined from the ^{40}Ar/^{39}Ar ratio without having to measure K concentrations, and allow for the measurement of ages on argon gas released on incremental heating from different sites within a single sample. This method typically produces a spectrum of ages, as the different sites likely have undergone differing degrees of diagenesis and K–Ar mobility. Although this method has its own uncertainties, these advantages and the ability to release argon from individual mineral grains using lasers allow for dating at high spatial resolution, dating weathering and erosion processes, and determining provenance and high-precision rates of sediment accumulation (e.g., Renne et al., 1990, 1991; Vasconcelos et al., 1992; Dong et al., 1997).

12.4. Uranium–lead

The application of U–Pb geochronology to ancient marine carbonates shows considerable promise in timing deposition and exposure (Moorbath et al., 1987; Smith and Farquar, 1989; Hoff et al., 1995; Jones et al., 1995; Winter and Johnson, 1995; Israelson et al., 1996; Rasbury et al., 1997, 1998). The utility of the U–Pb method lies in the fact that ^{238}U, ^{235}U, and ^{232}Th each head a decay series that end with stable radiogenic Pb isotopes (^{206}Pb, ^{207}Pb, and ^{208}Pb, respectively). The extent to which the ages determined from each of these three radiogenic isotope systems are "concordant" (i.e., agree with each other) is a useful test of the closed-system assumption for geochronology, and is therefore a useful indicator of the accuracy of a given age determination, as non-concordancy reflects open-system behavior of the parent and/or daughter isotope.

Uranium–lead analyses of paleosol calcite, selected by careful petrographic screening, from cyclic Late Paleozoic strata indicate that the marine sedimentary record may be dated to a precision of ± 1 m.y. (Fig. 22). Given that previously reported uncertainties on Paleozoic boundaries are typically greater than ± 10 m.y., this represents a major advance. Such age constraints have also been used to determine that Pennsylvanian cyclothems of the Permian and Orogrande Basins of Texas and New Mexico have an average duration of 143 ± 64 k.y. (Rasbury et al., 1998). This duration lies within uncertainty of the 100 k.y. Milankovitch orbital parameter of eccentricity, and provides more precise evidence for the ongoing debate concerning the controls on cyclic sedimentation. The effects of open-system diagenesis on U–Pb ages, which in these cases could have occurred during the 300 million years since subaerial exposure first occurred, must be rigorously evaluated. The potential applications of this method to improving the stratigraphic correlation in marine and terrestrial carbonates and siliciclastics (e.g., Wang et al., 1998; Becker et al., 2001), as well as constraining the amount of time that comprises ancient sequences of sequence stratigraphy, are significant.

Uranium–lead dating of igneous minerals that are intercalated in sedimentary rocks, such as zircons from ash beds, is another important chronostratigraphic tool. This approach has been used to refine the chronology of the Cambrian period and other parts of the Early Paleozoic (Isachsen et al., 1994; Tucker and McKerrow, 1995; Tucker et al., 1998; Bowring and Erwin, 1998). The new Cambrian chronology indicates that the span of time covered by this period is about half of what previous studies had determined. The new chronology also indicates that the major evolutionary trends identified by paleontologists in strata within the Cambrian must have occurred over a much shorter period of time than previously believed. Similarly, the application of U–Pb zircon geochronology to Permo-Triassic strata indicates that the end-Permian mass extinction, in which approximately

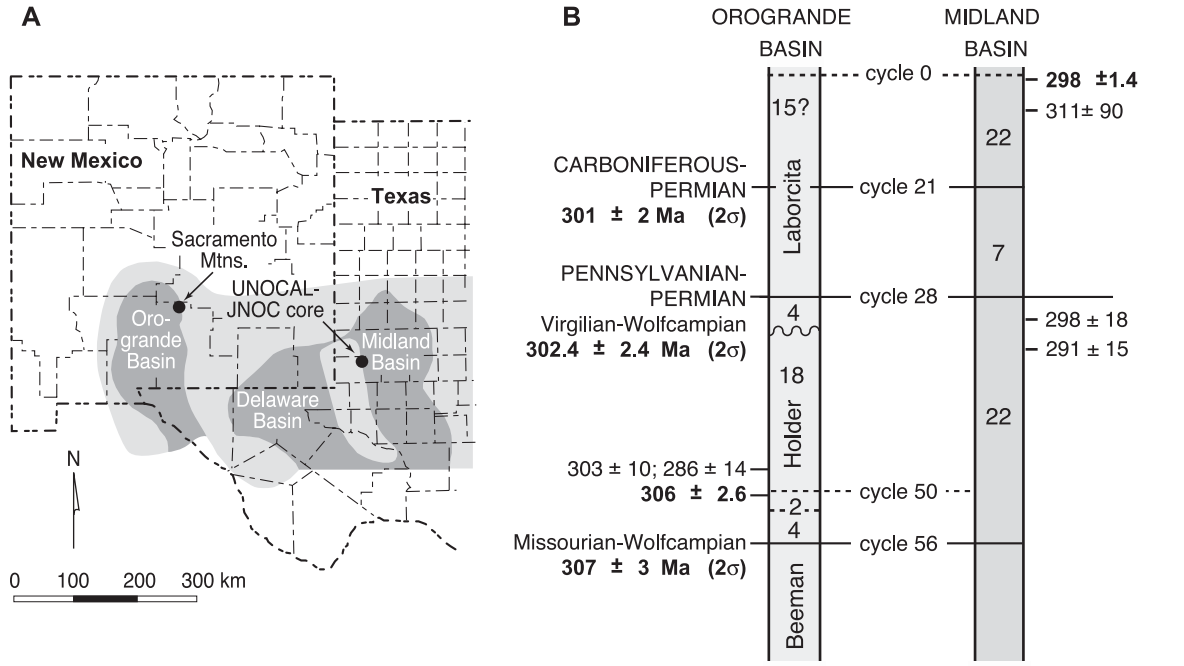

Fig. 22. (A) Late Paleozoic paleogeographic setting of Midland, Delaware, and Orogrande Basins. Dark shaded areas are basins and light shaded areas are topographic highs. After Gournay (1999). Stratigraphic sections shown in (B) are from the Sacramento Mountains, location shown in Orogrande Basin, and the JNOC core, location shown in Midland Basin. The Sacramento Mountain section includes Beeman, Holder, and Laborcita formations. Paleosol calcite from cyclic Pennsylvanian and Permian carbonate strata were sampled for U–Pb geochronology. U–Pb isochron ages and analytical uncertainties are shown next to columns at stratigraphic position of paleosol calcite samples. Numbers on columns indicate the number of stratigraphic cycles between boundaries. Cycles are typically 10 m thick and grade upward from marine and non-marine siliciclastics to marine carbonates that are commonly capped by paleosols. Large uncertainty for some sample ages result from scatter in isochron data. The ages for the Carboniferous–Permian, Pennsylvanian–Permian, and Missouri–Virgilian boundaries are in agreement with estimates from previous studies but are significantly more precise. From Rasbury et al. (1998).

85% of marine species disappeared, occurred over the geologically rapid time interval of less than 1 million years (Bowring et al., 1998).

High-precision lead isotope measurements allow small enrichments in radiogenic Pb isotopes to be determined in relatively young samples (Getty and DePaolo, 1995). This extends the applicability of the U–Pb geochronometer technique to samples as young as 1 Ma.

12.5. Uranium-series disequilibrium

Uranium-series disequilibrium refers to the state of radioactive disequilibrium between a pair of isotopes in the decay chain headed by the parent isotope ^{238}U. A chain of 14 intermediate radioactive daughter isotopes exist in this decay series, which ends in the stable isotope ^{206}Pb. This decay series can be represented as $^{238}U \rightarrow {}^{234}U \rightarrow {}^{230}Th \rightarrow ,\ldots, {}^{206}Pb$. A comprehensive overview of the systematics and applications of U-series isotopes is the subject of Ivanovich and Harmon (1992). A given pair of these isotopes reaches a state of radioactive equilibrium after a period of time equivalent to approximately five half-lives of the daughter. The state of equilibrium can be disrupted as a result of chemical fractionation during geologic processes, such as the growth of an aragonitic coral from seawater. In this case, U is incorporated into the aragonite crystal structure and Th is effectively excluded. This chemical fractionation between U and Th is enhanced by (1) the large differences in solubility between the soluble uranyl ion and the particle-reactive Th, and (2) the ionic size and charge differences between the forms of dissolved U (uranyl carbonate species such as

UO_2CO_3) and Th (Th^{4+}) in surficial seawater and freshwaters (Table 3). ^{230}Th then grows within the coral by radioactive decay from the time since the coral grew its skeleton, and precise measurement of the $^{230}Th/^{238}U$ and $^{234}U/^{238}$ U ratios is used to determine the coral's age. After approximately 400,000 years of radioactive decay and growth, a state of secular equilibrium will be achieved. This means that each ^{230}Th atom produced from the decay of ^{238}U is matched by the decay of another ^{230}Th atom (hence, a state of radioactive equilibrium is achieved). All samples greater than about 400,000 years old will therefore have the same $^{230}Th/^{238}U$ ratio, within analytical uncertainty, and this age is thus the upper limit of the method's utility as a geochronometer (Fig. 23). Some researchers have also made use of the secular disequilibrium between ^{234}U and ^{238}U as a geochronometer, which has an upper limit of 1.2 Ma due to the longer half-life of ^{234}U (Table 1). This method is limited by the significant uncertainties in the initial $^{234}U/^{238}U$ ratio of terrestrial systems.

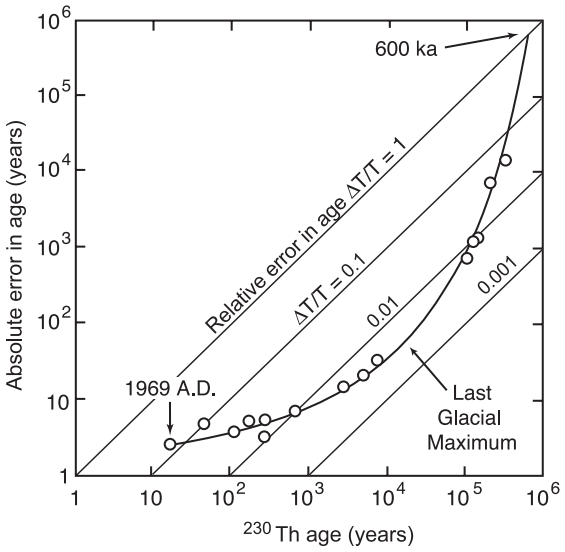

Fig. 23. Absolute and relative errors for ^{230}Th age determinations as a function of sample age (after Edwards, 1988). Error in years is a function of the analytical precision (2σ) on U-series isotope measurements by thermal ionization mass spectrometry (TIMS). $\Delta T/T$ lines indicate theoretical analytical precision on age determination relative to absolute age. Symbols are U-series ages determined on corals by TIMS. Curve connecting these symbols represents the typical analytical uncertainties achievable by TIMS. The errors increase at the high end of the age range as the U-series isotopes in older samples approach the state of secular equilibrium (as discussed in text). Large errors at the low end of age range are due to the increased analytical error inherent in measuring the small concentrations of ^{230}Th contained in these samples. Note the large age range over which errors in age determinations of less than 1% are obtainable.

The uranium series isotope method has experienced a resurgence of use over the past decade due to the development of thermal ionization mass spectrometric techniques, which make more precise measurements on smaller samples than had been previously possible by alpha-counting techniques (Edwards et al., 1987). Measurements of the uranium–protactinium isotope ratio $^{235}U/^{231}Pa$, which is a parent–intermediate-daughter pair in the ^{235}U decay series that is analogous to the $^{238}U/^{230}Th$ pair in the ^{238}U series, have provided an independent check on the accuracy of the $^{230}Th/^{238}U$ age determination on a given sample (Edwards et al., 1997; Musgrove et al., 2001).

Quaternary depositional and diagenetic systems will continue to serve as critical analogs to ancient systems, as Quaternary processes on the sequence and parasequence time scales can be absolutely and precisely dated using high-resolution U-series dating methods. Uranium-series analyses of Quaternary carbonate fossils and cements, from both marine and terrestrial environments, have been used to time changes in sea level, to rigorously test theories of climate change on orbital and shorter time scales, and to calibrate the carbon-14 time scale (Edwards et al., 1987; Bard et al., 1990; Chen et al., 1991; Winograd et al., 1992; Gallup et al., 1994; Guilderson et al., 1994). This technique has also been applied to phosphatic fossils (McDermott et al., 1993). In particular, the precise timing afforded by the mass spectrometric technique has lent an increased rigor to tests of the Milankovitch theory of climate change for the Late Pleistocene via measurements on corals, fine-grained aragonitic slope sediment, and speleothems (e.g., Winograd et al., 1992; Gallup et al., 1994; Stirling et al., 1998; Henderson and Slowey, 2000; Lambeck et al., 2002). Uranium-series analysis of carbonate cements has been used to time diagenesis relative to deposition (Banner et al., 1993).

Geochronologic age determinations require criteria for closed-system behavior from the time of formation of a sample, similar to the criteria discussed earlier for the reconstruction of original marine isotope compositions. For U-series studies, it is possible to establish

a criterion of uniform U isotopic composition for contemporaneous samples (similar to the criterion established for seawater Sr isotope variations) based on the high degree of homogeneity of U isotopes in modern oceans (Fig. 24). This homogeneity, established via high-precision analytical methods, distinguishes U isotope composition as a very sensitive indicator of diagenetic alteration in Quaternary marine carbonates (Bar-Matthews et al., 1993; Gallup et al., 1994). The apparent constancy of seawater U isotope composition during the past 500,000 years (Ludwig et al., 1991; Gallup et al., 1994) also establishes the criterion of a specific U isotopic composition, not simply a uniform U isotopic composition for contemporaneous samples.

12.6. Carbon-14

Carbon-14 is produced in the Earth's upper atmosphere as a result of high-energy cosmic ray neutrons bombarding ^{14}N atoms. Once produced by this "cosmogenic" process, this carbon is converted to CO_2 and is transmitted via precipitation and atmospheric circulation to the Earth's surface. The ^{14}C atoms, which are radioactive, are incorporated into vegetation, animals, rocks, minerals, or water, and then decay back to ^{14}N ($T_{1/2}=5700$ years; Table 1). Assuming closed-system behavior from the time of incorporation, measurement of the proportion of ^{14}C to total C in a given sample yields its age. In contrast to the thermal ionization mass spectrometer techniques described for the other radiogenic isotope systems discussed earlier, ^{14}C analyses have been conventionally performed by means of detecting and counting the radioactive ^{14}C decay events, and more recently by accelerator mass spectrometry for analysis of small samples.

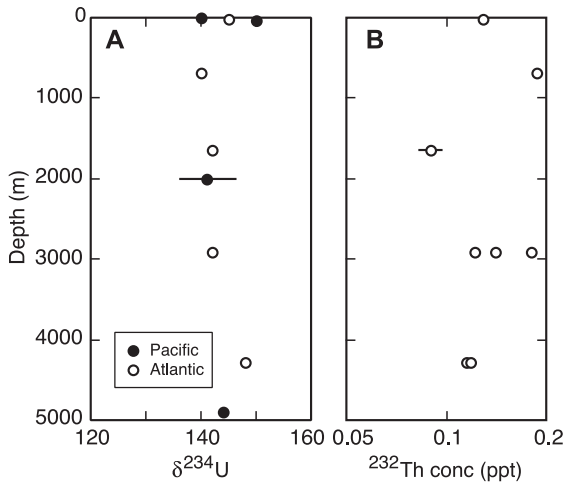

Fig. 24. (A) Isotopic composition of uranium in modern seawater from the Atlantic and Pacific Oceans, and (B) concentration of ^{232}Th in the Atlantic Ocean as a function of depth (Chen et al., 1986). $\delta^{234}U=\{[(^{234}U/^{238}U)\text{sample}/5.472\times10^{-5}]-1\}\times10^{3}$.

The atmospheric production rate of ^{14}C has varied through time, creating uncertainties in age determinations by the ^{14}C method. Independent age information on ^{14}C-dated samples, such as $^{230}Th/^{238}U$ on corals and dendrochronology, has been used to calibrate the ^{14}C time scale (Bard et al., 1990; Edwards et al., 1993; Bard, 1998). This calibration provides information on the rate and magnitude of change of atmospheric ^{14}C production, which have been attributed to changes in the intensity of the Earth's electromagnetic field and to changes in the rates of atmosphere–ocean exchange of CO_2 associated with climatic changes, such as those that occurred during the last deglaciation. These changes have been investigated using ^{14}C paired with an independent chronology on samples as diverse as corals, speleothems, tree rings, and ocean floor sediments (Suess and Linick, 1990; Edwards et al., 1993; Hughen et al., 2000; Beck et al., 2001).

Differences in half-lives and geochemical behavior between the ^{14}C and U–Th systems provide complementary information in Quaternary stratigraphic studies. Carbon-14 methods can be applied to stratigraphic sections that cover the past 40,000 years, whereas the ^{238}U-series method covers the past 400,000 years. Relatively old carbon is introduced into groundwater and surface water by mineral-solution reactions with host rocks. Mixing of this old carbon with atmospherically derived carbon in the same water mass creates uncertainties in the application of the ^{14}C method to dating terrestrial authigenic minerals. Since strong parent–daughter separation occurs between U and Th during growth of calcium carbonate precipitates (see above), many of these types of uncertainties are minimized in applying the ^{238}U-series method to dating terrestrial authigenic minerals such as those found in caves and springs. Carbon-14 is the preferred method for dating

organic deposits and small samples of young marine carbonates. Recent developments in mass spectrometry allow for chromatographic separation and ^{14}C dating of different carbon compounds from the same sample (Eglinton et al., 1997).

12.7. Other atmospherically produced radionuclides

There are several other atmospherically produced isotopes besides ^{14}C and tritium for which analytical methods have been developed more recently and have not been as widely applied as the ^{14}C method (e.g., ^{10}Be). This group of isotopes includes those produced cosmogenically (e.g., ^{10}Be, ^{26}Al, and ^{36}Cl), from gases in the Earth's atmosphere (e.g., ^{210}Pb), and anthropogenically (e.g., ^{137}Cs, produced by atomic bomb tests). Measurements of these isotopes have a wide range of applications to sedimentary processes, ranging from dating exposure surfaces to determining the timing of anthropogenic impact on natural depositional environments.

Some cosmogenic isotopes are predominantly produced within near-surface rocks and sediments by in situ bombardment (e.g., ^{26}Al and ^{36}Cl), while some are produced by bombardment in the atmosphere (e.g., ^{14}C). The utility of cosmogenic isotope systems is comprehensively reviewed by Cerling and Craig (1994), and includes determining the exposure ages of rocks, sediments, and soils, and modeling erosional histories. Particular applications have included dating glacially carved surfaces, desert pavement, and alluvial deposits. Several uncertainties must be addressed in the use of these cosmogenic isotopes, including changes in atmospheric and in situ production rates as a function of time, latitude, altitude, and depth below the surface. The half-lives of these isotopes make them effective dating tools on time scales shorter than the last 10 million years. Applications of cosmogenic isotopes to the ancient sedimentary record therefore rely on the use of recent processes and their rates as analogs for ancient processes and rates. This emerging field will likely see increased applications to stratigraphic and environmental problems in the next decade.

Among the shorter-lived of the atmospherically produced isotopes are ^{7}Be (produced by cosmic ray bombardment of atmospheric nitrogen and oxygen), ^{210}Pb (produced naturally via the decay of ^{222}Rn, a gaseous intermediate daughter in the ^{238}U decay series), and ^{137}Cs (produced as a fission product during nuclear weapons tests in the atmosphere). These nuclides are incorporated into the rain and are deposited with sediments. If the initial concentration of the nuclide of interest can be estimated or measured, then ages within a depositional profile can be determined from measurements of these isotopes. Their relatively short effective dating range makes them useful for studies of ecosystem processes and the timing and rates of anthropogenic impact on natural sedimentary environments such as lakes and shallow marine environments, and the rates of soil erosion and deposition over the past 150 years (e.g., Van Metre et al., 2000; Holmes, 2002). As with longer-lived isotope systems, uncertainties in age determinations arise from post-depositional mobility of the isotopes of interest by pore waters and bioturbation of sediments.

13. Summary and prospects

Radiogenic isotope variations in ancient oceans offer unique insight into crustal evolution, weathering, climate change, and a range of other Earth surface processes. The systematic results obtained from studies of radiogenic isotope variations in ancient marine sedimentary rocks and fossils demonstrate the significant utility of these geochemical tools for stratigraphic correlation and for absolute age determinations of stratigraphic horizons. An example of the systematic nature of ancient ocean geochemistry is the relationship observed between the oceanic residence time of an element, the degree of homogeneity of its isotopic composition in the oceans at a given time, and the time scales of its isotopic variability in paleocean records.

New research efforts will be required to construct high-quality curves that describe the secular variations, and to determine accurate radiometric ages in ancient rocks, that account for the effects of diagenetic alteration and impure samples on original marine isotope signatures. These efforts will include refining petrologic and chemical criteria for assessing the degree of alteration of marine precipitates, such as the advancement of luminescence and electron microscopy techniques. These efforts will also involve

the improvement of the spatial resolution of isotopic analyses through the development of more sensitive mass spectrometers and precise microdrilling and laser ablation systems. It is likely that as the spatial scales and precision of geochemical analyses improve with technological advancements, an isotopic measurement on an ancient marine rock will continue to be only as good as the petrographic and stratigraphic analysis allows. The potential benefits in terms of improved resolution of stratigraphic correlation and timing of various Earth system processes will warrant these efforts.

With such improved resolution, it may be possible to improve our understanding of a number of important concepts in sedimentary geology, including:

- Stratigraphic correlation
- The links between various Earth system processes and the depositional processes by which the fundamental sequences of sequence stratigraphy are constructed
- The functioning of a number of Earth system processes, such as models for the global carbon cycle, weathering of the continents, and temporal changes in the operation of the hydrologic cycle.

Acknowledgements

I thank many people for critical reviews, including Isabel Montañez, Troy Rasbury, Charles Jones, David Awwiller, Tim Denison, Eric James, Dennis Ruez, Lynn Murray, Patrick Mickler, Precious Williams, and Fred McDowell. Several researchers generously shared their data sets, including Steve Ruppel, Charles Jones, John Farrell, and Tim Bralower. The Environmental Science Institute and the Geology Foundation of the University of Texas at Austin and the National Science Foundation (EAR9628535) provided support.

Appendix A. Derivation of equations for expressing radioactive decay and growth

A.1. Derivation of (1) and (2), Section 2.1

For a system with N atoms of the radioactive parent isotope, $-\mathrm{d}N/\mathrm{d}t = \lambda N$, per discussion prior to Eq. (1).

Rearranging gives

$$-\mathrm{d}N/N = \lambda \mathrm{d}t$$

Integrating both sides of the equation gives $-\ln N = \lambda t + C$, where C is the constant of integration; at $t = 0$, $N = N_o$, and $C = -\ln N_o$

Substitution gives

$$\ln N - \ln N_o = -\lambda t$$

$$\ln N/N_o = -\lambda t$$

$$N = N_o e^{-\lambda t} \quad (1)$$

$N_o = N + D^*$, where D^* is the number of radiogenic daughter atoms present after a given amount of time t.

$$D^* = N_o - N = N e^{\lambda t} - N$$

$$D^* = N(e^{\lambda t} - 1) \quad (2)$$

A.2. Derivation of half-life–decay constant relationship

What is t when $N = 0.5\ N_o$?

$$N = N_o e^{-\lambda t}$$

$$0.5 N_o = N_o e^{-\lambda t}$$

$$t = \ln 2/\lambda = 0.693/\lambda$$

$$\text{half-life} = 0.693/\lambda$$

References

Abouchami, W., Goldstein, S., 1995. A lead isotopic study of Circum-Antarctic manganese nodules. Geochim. Cosmochim. Acta 59, 1809–1820.

Abouchami, W., Goldstein, S.L., Galer, S.J.G., Eisenhauer, A., Mangini, A., 1997. Secular changes of lead and neodymium in central Pacific seawater recorded by a Fe–Mn crust. Geochim. Cosmochim. Acta 61, 3957–3974.

Albarède, F., 1997. Isotopic tracers of past ocean circulation: turning lead to gold. Science 277, 908–909.

Albarède, F., Goldstein, S.L., 1992. World map of Nd isotopes in sea floor ferromanganese deposits. Geology 20, 761–763.

Albarède, F., Michard, A., 1987. Evidence for slowly changing $^{87}Sr/^{86}Sr$ in runoff from freshwater limestones of southern France. Chem. Geol. 64, 55–65.

Albarède, F., Goldstein, S.L., Dautel, D., 1997. The neodymium isotopic composition of manganese nodules from the Southern and Indian Oceans, the global oceanic neodymium budget, and

their bearing on deep ocean circulation. Geochim. Cosmochim. Acta 61, 1277–1291.

Allègre, C.J., Rousseau, D., 1984. The growth of the continent through geological time studied by Nd isotope analysis of shales. Earth Planet. Sci. Lett. 67, 19–34.

Amakawa, H., Yoshiyuki, N., Masuda, A., 1996. Precise determination of variations in the 138Ce/142Ce ratios of marine ferromanganese nodules. Chem. Geol. 131, 183–195.

Anderson, R.Y., Dean, W.E., Kirkland, D.W., Snider, H.I., 1972. Permian Castile varved evaporite sequence, west Texas and New Mexico. Geol. Soc. Am. Bull. 83, 59–86.

Asmerom, Y., Jacobsen, S.B., Knoll, A.H., Butterfield, N.J., Swett, K., 1991. Strontium isotopic variations of Neoproterozoic seawater: implications for crustal evolution. Geochim. Cosmochim. Acta 55, 2883–2894.

Awwiller, D.N., 1994. Geochronology and mass transfer in Gulf Coast mudrocks (south–central Texas, USA): Rb–Sr, Sm–Nd and REE systematics. Chem. Geol. 116, 61–84.

Awwiller, D.N., Mack, L.E., 1989. Diagenetic resetting of Sm–Nd isotope systematics in Wilcox Group sandstones and shales, San Marcos Arch, south–central Texas. Gulf Coast Assoc. Geol. Soc. Trans The Association, New Orleans, pp. 321–330.

Awwiller, D.N., Mack, L.E., 1991. Diagenetic modification of Sm–Nd model ages in Tertiary sandstones and shales, Texas Gulf Coast. Geology 19, 311–324.

Bailey, T.R., McArthur, J.M., Prince, H., Thirlwall, M.F., 2000. Dissolution methods for strontium isotope stratigraphy: whole rock analysis. Chem. Geol. 167, 313–319.

Baker, P.A., Gieskes, J.M., Elderfield, H., 1982. Diagenesis of carbonates in deep-sea sediments: evidence from Sr/Ca ratios and interstitial dissolved Sr2+ data. J. Sediment. Petrol. 52, 71–82.

Banner, J.L., 1995. Application of the isotope and trace element geochemistry of strontium to studies of diagenesis in carbonate systems. Sedimentology 42, 805–824.

Banner, J.L., Hanson, G.N., 1990. Calculation of simultaneous isotopic and trace-element variations during water-rock interaction with applications to carbonate diagenesis. Geochim. Cosmochim. Acta 54, 3123–3137.

Banner, J.L., Kaufman, J., 1994. The isotopic record of ocean chemistry and diagenesis preserved in non-luminescent brachiopods from Mississippian carbonate rocks, Illinois and Missouri. Geol. Soc. Am. Bull. 106, 1074–1082.

Banner, J.L., Hanson, G.N., Meyers, W.J., 1988a. Determination of initial Sr-isotopic compositions of dolostones from the Burlington–Keokuk Formation (Mississippian): constraints from cathodoluminescence, glauconite paragenesis, and analytical methods. J. Sediment. Petrol. 58, 673–687.

Banner, J.L., Hanson, G.N., Meyers, W.J., 1988b. Rare earth element and Nd-isotopic variations in regionally-extensive dolostones from the Burlington–Keokuk Formation (Mississippian): implications for REE mobility during carbonate diagenesis. J. Sediment. Petrol. 58, 415–432.

Banner, J.L., Wasserburg, G.J., Dobson, P.F., Carpenter, A.B., Moore, C.H., 1989. Isotopic and trace-element constraints on the origin and evolution of saline groundwaters from central Missouri. Geochim. Cosmochim. Acta 53, 383–398.

Banner, J.L., Edwards, R.L., Kimbell, T.N., Humphrey, J.D., 1993. Geochemistry and geochronology of aragonite cementation in an ancient marine–meteoric mixing zone, Barbados, W.I. Am. Geophys. Union Fall Meeting. Am. Geophys. Union, Washington, DC, p. 328.

Banner, J.L., Musgrove, M., Capo, R., 1994. Tracing ground-water evolution in a limestone aquifer using Sr isotopes: effects of multiple sources of dissolved ions and mineral-solution reactions. Geology 22, 687–690.

Banner, J.L., Musgrove, M., Asmerom, Y., Edwards, R.L., Hoff, J.A., 1996. High-resolution temporal record of Holocene ground-water chemistry: tracing links between climate and hydrology. Geology 24, 1049–1053.

Bard, E., 1998. Geochemical and geophysical implications of the radiocarbon calibration. Geochim. Cosmochim. Acta 62, 2025–2038.

Bard, E., Hamelin, B., Fairbanks, R.G., 1990. U–Th ages obtained by mass spectrometry in corals from Barbados: sea level during the past 130,000 years. Nature 346, 456–458.

Bar-Matthews, M., Wasserburg, G.J., Chen, J.H., 1993. Diagenesis of fossil coral skeletons: correlation between trace elements, textures, and $^{234}U/^{238}U$. Geochim. Cosmochim. Acta 57, 257–276.

Beck, J.W., Richards, D.A., Edwards, R.L., Silverman, B.W., Smart, P.L., Donahue, D.J., Hererra-Osterheld, S., Burr, G.S., Calsoyas, L., Jull, A.J., Biddulph, D., 2001. Extremely large variations of atmospheric ^{14}C concentration during the last glacial period. Science 292, 2453–2458.

Becker, M.L., Cole, J.M., Rasbury, E.T., Pedone, V.A., Montañez, I.P., Hanson, G.N., 2001. Cyclic variations of uranium incorporation in tufa from the Miocene Barstow Formation, Rainbow Basin, Mojave, California. Geology 29, 139–142.

Beets, C.J., 1991. The Late Neogene $^{87}Sr/^{86}Sr$ isotopic record in the western Arabian Sea. Site 722. Proceedings of the Ocean Drilling Program, Scientific Results. The Ocean Drilling Program, College Station, TX, pp. 459–464.

Berner, E.K., Berner, R.A., 1996. . Global Environment: Water, Air and Geochemical Cycles. Prentice Hall, Upper Saddle River, NJ, pp. 80–82.

Blum, J., 1995. Isotope decay data. In: Ahrens, T.J. (Ed.), Global Earth Physics: A Handbook of Physical Constants. American Geophysical Union, Washington, DC, pp. 271–282.

Blum, J., Erel, Y., 1995. A silicate weathering mechanism for elevating marine $^{87}Sr/^{86}Sr$ following global glaciations. Nature 373, 415–418.

Blum, J.D., Erel, Y., Brown, K., 1994. $^{87}Sr/^{86}Sr$ ratios of Sierra Nevada stream waters: implications for relative mineral weathering rates. Geochim. Cosmochim. Acta 57, 5019–5025.

Blum, J.D., Klaue, A., Nezat, C.A., Driscoll, C.T., Johnson, C.E., Siccama, T.G., Eagar, C., Fahey, T.J., Likens, G.E., 2002. Mycorrhizal weathering of apatite as an important calcium source in base-poor forest ecosystems. Nature 417, 729–731.

Bock, B., McLennan, S.M., Hanson, G.N., 1994. Rare earth element redistribution and its effects on the neodymium isotope system in the Austin Glen Member of the Normanskill Formation, New York, USA. Geochim. Cosmochim. Acta 58, 5245–5253.

Borg, L.E., Banner, J.L., 1996. Neodymium and strontium isotopic

constraints on soil sources in Barbados, West Indies. Geochim. Cosmochim. Acta 60, 4193–4206.
Bowring, S.A., Erwin, D.H., 1998. A new look at evolutionary rates in deep time: uniting paleontology and high-precision geochronology. GSA Today 8, 1–8.
Bowring, S.A., Erwin, D.H., Jin, T.G., Martin, M.W., Davidek, K., Wang, W., 1998. U/Pb zircon geochronology and tempo of the end-Permian mass extinction. Science 280, 1039–1045.
Bralower, T.J., Fullagar, P.D., Paull, C.K., Dwyer, G.S., Leckie, R.M., 1997. Mid-Cretaceous strontium-isotope stratigraphy of deep-sea sections. Geol. Soc. Am. Bull. 109, 1421–1442.
Brannon, J.C., Podosek, F.A., Viets, J.G., Leach, D.L., Goldhaber, E.L., Rowan, E.L., 1991. Strontium isotopic constraints on the origin of ore-forming fluids of the Viburnum Trend, southeast Missouri. Geochim. Cosmochim. Acta 55, 1407–1419.
Brantley, S.L., Chesley, J.T., Stillings, L.L., 1998. Isotopic ratios and release rates of strontium measured from weathering feldspars. Geochim. Cosmochim. Acta 62, 1493–1500.
Broecker, W.S., 1997. Thermohaline circulation, the Achilles Heel of our climate system: will man-made CO2 upset the current balance? Science 278, 1582–1588.
Broecker, W.S., 1999. What if the conveyor were to shut down? Reflections on a possible outcome of the great global experiment. GSA Today 9, 1–7.
Broecker, W.S., Peng, T.S., 1982. Tracers in the Sea Eldigio Press, Palisades, NY.
Broecker, W.S., Sanyal, A., 1998. Does atmospheric CO2 police the rate of chemical weathering? Glob. Biogeochem. Cycles 12, 403–408.
Brookins, D.G., 1988. Seawater $^{87}Sr/^{86}Sr$ for the Late Permian Delaware Basin evaporites; New Mexico, USA. Chem. Geol. 69, 209–214.
Brownlow, A.H., 1997. Geochemistry. Prentice-Hall, New Jersey.
Bryant, J.D., Jones, D.S., Mueller, P.A., 1995. Influence of freshwater influx on $^{87}Sr/^{86}Sr$ chronostratigraphy in marginal marine environments and dating of vertebrate and invertebrate faunas. J. Paleontol. 69, 1–6.
Bruckschen, P., Bruhn, J., Veizer, J., Buhl, D., 1995. $^{87}Sr/^{86}Sr$ isotope evolution of Lower Carboniferous seawater: dinantian of western Europe. Sediment. Geol. 100, 63–81.
Burke, W.H., Denison, R.E., Hetherington, E.A., Koepnick, R.B., Nelson, H.F., Otto, J.B., 1982. Variation of seawater $^{87}Sr/^{86}Sr$ throughout Phanerozoic time. Geology 10, 516–519.
Burton, K.W., Vance, D., 2000. Glacial–interglacial variations in the neodymium isotope composition of seawater in the Bay of Bengal recorded by planktonic foraminifera. Earth Planet. Sci. Lett. 176, 425–441.
Burton, K.W., Bourdon, B., Birck, J.-L., Allegre, C.J., Hein, J.R., 1999. Osmium isotope variations in the oceans recorded by Fe Mn crusts. Earth Planet. Sci. Lett. 171, 185–197.
Cameron, E.M., Hattori, K., 1997. Strontium and neodymium isotope ratios in the Fraser River, British Columbia: a riverine transect across the Cordilleran orogen. Chem. Geol. 137, 243–253.
Capo, R.C., DePaolo, D.J., 1990. Seawater strontium isotopic variations from 2.5 million years ago to the present. Science 249, 51–55.
Capo, R.C., DePaolo, D.J., 1992. Homogeneity of Sr isotopes in the oceans. Am. Geophys. Union Fall Meeting. Am. Geophys. Union, Washington, DC, p. 272.
Capo, R.C., Stewart, B.W., Chadwick, O.A., 1998. Strontium isotopes as tracers of ecosystem processes: theory and methods. Geoderma 82, 197–225.
Carpenter, S.J., Lohmann, K.C., Holden, P., Walter, L.M., Huston, T.J., Halliday, A.N., 1991. $\delta^{18}O$ values, $^{87}Sr/^{86}Sr$ and Sr/Mg ratios of Late Devonian abiotic marine calcite: implications for the composition of ancient seawater. Geochim. Cosmochim. Acta 55, 1991–2010.
Cerling, T.E., Craig, H., 1994. Geomorphology and in-situ cosmogenic isotopes. Annu. Rev. Earth Planet. Sci. 22, 273–317.
Chaudhuri, S., Broedel, V., Clauer, N., 1987. Strontium isotopic evolution of oil-field waters from carbonate reservoir rocks in Bindley Field, Central Kansas, USA. Geochim. Cosmochim. Acta 51, 45–53.
Chen, J.H., Edwards, R.L., Wasserburg, G.J., 1986. ^{238}U, ^{234}U and ^{232}Th in seawater. Earth Planet. Sci. Lett. 80, 241–251.
Chen, J.H., Curran, H.A., White, B., Wasserburg, G.J., 1991. Precise chronology of the last interglacial period: $^{234}U-^{230}Th$ data from fossil coral reefs in the Bahamas. Geol. Soc. Am. Bull. 103, 82–97.
Chesley, J.T., Quade, J., Ruiz, J., 2000. The Os and Sr isotopic record of Himalayan paleorivers: Himalayan tectonics and influence on ocean chemistry. Earth Planet. Sci. Lett. 179, 115–124.
Christensen, J.N., Halliday, A.N., Lee, D.C., Hall, C.M., 1995. In situ isotopic analysis by laser ablation. Earth Planet. Sci. Lett. 136, 79–85.
Christensen, J.N., Halliday, A.N., Godfrey, L., Hein, J.R., Rea, D.K., 1997. Climate and ocean dynamics and the lead isotopic records in Pacific ferromanganese crusts. Science 277, 913–918.
Church, T.M., 1996. An underground route for the water cycle. Science 380, 579–580.
Clauer, N., 1982. The Rb–Sr method applied to sediments: certitudes and uncertainties. In: Odin, G.S. (Ed.), Numerical Dating Methods in Stratigraphy. Annual Reviews, Palo Alto, CA, pp. 245–276.
Cochran, J.K., Landman, N.H., Turekian, K.K., Michard, A., Schrag, D.P., 2003. Paleoceanography of the Late Cretaceous (Maastrichtian) Western Interior Seaway of North America: evidence from Sr and O isotopes. Palaeogeog. Palaeoclimatol. Palaeoecol. 191, 45–64.
Colodner, D., Sachs, J., Ravizza, G., Turekian, K., Edmond, J., Boyle, E., 1993. The geochemical cycle of rhenium: a reconnaissance. Earth Planet. Sci. Lett. 117, 205–221.
Cooke, M.J., Stern, L.A., Banner, J.B., Mack, L.E., Stafford, T.W., Toomey, R.S., 2003. Precise timing and rate of massive Late Quaternary soil denudation. Geology (in press).
Creaser, R.A., Sannagrahi, P., Chacko, T., Selby, D., 2002. Further evaluation of the Re–Os geochronometer in organic rich sediments: a test of hydrocarbon maturation effects in the Exshaw Formation, Western Canada Sedimentary Basin, Canada. Geochim. Cosmochim. Acta 66, 3441–3452.
Cummins, D., Elderfield, D., 1994. The strontium isotopic compo-

sition of Brigantian (late Dinantian) seawater. Chem. Geol. 118, 255–270.

Dalland, A., Mearns, E.W., McBride, J.J., 1995. The application of samarium–neodymium (Sm–Nd) Provenance Ages to correlation of biostratigraphically barren strata: a case study of the Statfjord Formation in the Gullfaks Oilfield, Norwegian North Sea. In: Dunay, R.E., Hailwood, E.A. (Eds.), Non-Biostratigraphical Methods of Dating and Correlation. Geological Society, London, pp. 201–222.

Dasch, E.J., Biscaye, P.E., 1971. Isotopic composition of strontium in Cretaceous-to-Recent pelagic foraminifera. Earth Planet. Sci. Lett. 11, 201–204.

Davidson, J.P., Tepley III, F.J., Knesel, K.M. 1998. Isotopic fingerprinting may provide insights into evolution of magmatic systems. EOS, Trans. Am. Geophys. Union, 185–193. Washington DC.

Davis, A.C., Bickle, M.J., Teagle, D.A.H., 2003. Imbalance in the oceanic strontium budget. Earth Planet. Sci. Lett. 211, 173–187.

Denison, R.E., Koepnick, R.B., 1995. Variation in $^{87}Sr/^{86}Sr$ of Permian seawater: an overview. In: Scholle, P.A., Peryt, T.M., Ulmer-Scholle, D.S. (Eds.), The Permian of Northern Pangea-Paleogeography, Paleoclimates, Stratigraphy, vol. I. Springer, Berlin, pp. 124–132.

Denison, R.E., Koepnick, R.B., Fletcher, A., Howell, M.W., Callaway, W.S., 1994a. Criteria for the retention of original $^{87}Sr/^{86}Sr$ in ancient shelf limestones. Chem. Geol., Isot. Geosci. Sect. 112, 131–143.

Denison, R.E., Koepnick, R.B., Burke, W.H., Hetherington, E.A., Fletcher, A., 1994b. Construction of the Mississippian, Pennsylvanian and Permian seawater $^{87}Sr/^{86}Sr$ curve. Chem. Geol. 112, 145–167.

Denison, R.E., Kirkland, D.W., Evans, R., 1998. Using strontium isotopes to determine the age and origin of gypsum and anhydrite beds. J. Geol. 106, 1–17.

DePaolo, D.J., 1986. Detailed record of the Neogene Sr isotopic evolution of seawater from DSDP site 590B. Geology 14, 103–106.

DePaolo, D.J., 1987. Correlating rocks with strontium isotopes. Geotimes 32, 16–17.

DePaolo, D.J., 1988. Neodymium Isotope Geochemistry: An Introduction. Springer, Berlin.

DePaolo, D.J., Ingram, B.L., 1985. High-resolution stratigraphy with strontium isotopes. Science 227, 938–941.

Derry, L.A., France-Lanord, C., 1996. Neogene Himalaya weathering history and river $^{87}Sr/^{86}Sr$: impact on the marine Sr record. Earth Planet. Sci. Lett. 142, 59–74.

Derry, L.A., Kaufman, A.J., Jacobsen, S.B., 1992. Sedimentary cycling and environmental change in the Late Proterozoic: evidence from stable and radiogenic isotopes. Geochim. Cosmochim. Acta 56, 1317–1329.

Derry, L.A., Brasier, M.D., Corfield, R.M., Rozanov, A.Y., Zhuravlev, A.Y., 1994. Sr and C isotopes in Lower Cambrian carbonates from the Siberian craton: a paleoenvironmental record during the ''Cambrian explosion''. Earth Planet. Sci. Lett. 128, 671–681.

Dettman, D.L., Lohmann, K.C., 1995. Approaches to microsampling carbonates for stable isotope and minor element analysis: physical separation of samples on a 20 micrometer scale. J. Sediment. Petrol. A65, 566–569.

Dickin, A.P., 1995. Radiogenic Isotope Geology. Cambridge Univ. Press, Cambridge, UK.

Diener, A., Ebneth, S., Veizer, J., Buhl, D., 1996. Strontium isotope stratigraphy of the Middle Devonian: brachiopods and conodonts. Geochim. Cosmochim. Acta 60, 639–652.

Dodge, R.E., Brass, G.W., 1984. Skeletal extension, density, and calcification of the reef coral, Montastrea annularis: St. Croix, U. S. Virgin Islands. Bull. Mar. Sci. 34, 288–307.

Dong, H., Hall, C.M., Halliday, A.N., Peacor, D.R., 1997. Laser 40Ar–39Ar dating of microgram-size illite samples and implications for thin section dating. Geochim. Cosmochim. Acta 61, 3803–3808.

Douthit, T., Meyers, W.J., Hanson, G.N., 1993. Non-monotonic variation of seawater $^{87}Sr/^{86}Sr$ across the Ivorian–Chadian boundary (Mississippian, Osagean): evidence from marine cements within the Irish Waulsortian Limestone. J. Sediment. Petrol. 63, 539–549.

Drever, J.I., 1997. The Geochemistry of Natural Waters Prentice-Hall, New York.

Ebneth, S., Shields, G.A., Veizer, J., Miller, J.F., Shergold, J.H., 2001. High-resolution strontium isotope stratigraphy across the Cambrian–Ordovician transition. Geochim. Cosmochim. Acta 65, 2273–2292.

Edmond, J.M., 1992. Himalayan tectonics, weathering processes, and the strontium isotope record in marine limestones. Science 258, 5088.

Edmond, J.M., Huh, Y., 1997. Chemical weathering yields from basement and orogenic terrains in hot and cold climates. In: Ruddiman, W.R. (Ed.), Tectonic Uplift and Climate Change. Plenum, New York, pp. 329–351.

Edwards, R.L., 1988. High precision thorium-230 ages of corals and the timing of sea level fluctuations in the Late Quaternary. PhD thesis, California Inst. Technol., Pasadena, CA.

Edwards, R.L., Chen, J.H., Ku, T.L., Wasserburg, G.J., 1987. Precise timing of the last interglacial period from mass spectrometric determination of thorium-230 in corals. Science 236, 1547–1553.

Edwards, R.L., Beck, J.W., Burr, G.S., Donahue, D.J., Chappell, A.L., Bloom, A.L., Druffel, E.R.M., Taylor, F.W., 1993. A large drop in atmospheric 14C/12C and reduced melting in the Younger Dryas, documented with ^{230}Th ages of corals. Science 260, 962–968.

Edwards, R.L., Cheng, H., Murrell, M.T., Goldstein, S.J., 1997. Protactium-231 dating of carbonates by thermal ionization mass spectrometry: implications for quaternary climate change. Science 276, 782–786.

Eglinton, T.I., Benitez-Nelson, B.C., Pearson, A., McNichol, A.P., Bauer, J.E., Druffel, E.R.M., 1997. Variability in radiocarbon ages of individual organic compounds from marine sediments. Science 277, 796–799.

Ehrenberg, S.N., Svana, T.A., Paterson, B.A., Mearns, E.W., 2000. Neodymium isotope profiling of carbonate platform strata: correlation between siliciclastic provenance signature and sequence stratigraphy. Sediment. Geol. 131, 87–95.

Elderfield, H., 1988. The oceanic chemistry of the rare-earth elements. Philos. Trans. R. Soc. London A325, 105–126.
Elderfield, H., Greaves, M.J., 1982. The rare earth elements in seawater. Nature 296, 214–219.
English, N.B., Bertancourt, J.L., Dean, J.S., Quade, J., 2001. Strontium isotopes reveal distant sources of architectural timber in Chaco Canyon, New Mexico. Proc. Natl. Acad. Sci. 98, 11891–11896.
Farrell, J.W., Clemens, S.C., Gromet, L.P., 1995. Improved chronostratigraphic reference curve of Late Neogene seawater $^{87}Sr/^{86}Sr$. Geology 23, 403–406.
Faure, G., 1986. Principles of Isotope Geology. Wiley, New York.
Frank, M., Whiteley, N., Kasten, S., James, R., Hein, J.R., O'Nions, R.K., 2000. Evidence for stronger thermohaline circulation prior to northern hemisphere glaciation from Nd and Pb isotopes in ferromanganese crusts. V. M. Goldschmidt Conference. J. Conf. Abstr. 5 (2), 409.
Frank, M., Davies, G.R., Claude-Ivanoj, C., Hofmann, A.W., 2001. Radiogenic isotopes: new tools help reconstruct paleocean circulation and erosional input. EOS Trans. Am. Geophys. Union. 82, 66–71.
Freeze, R.A., Cherry, J.A., 1979. Groundwater. Prentice-Hall, New York.
Gallup, C.D., Edwards, R.L., Johnson, R.G., 1994. The timing of high sea levels over the past 200,000 years. Science 263, 796–800.
Gao, G., Land, L.S., 1991. Geochemistry of Cambro-Ordovician Arbuckle limestone, Oklahoma: implications for diagenetic $\delta^{18}O$ alteration and secular $\delta^{13}C$ and $^{87}Sr/^{86}Sr$ variation. Geochim. Cosmochim. Acta 55, 2911–2920.
Getty, S.R., DePaolo, D.J., 1995. Quaternary geochronology using the U–Th–Pb method. Geochim. Cosmochim. Acta 59, 3267–3272.
Geyh, M.A., Schleicher, H., 1990. Absolute Age Determination. Springer, Berlin.
Gieskes, J.M., 1983. The chemistry of interstitial waters of deep sea sediments: interpretation of deep sea drilling data. In: Riley, J.P., Chester, R. (Eds.), Chemical Oceanography. Academic Press, New York, pp. 222–271.
Goldstein, S.J., Jacobsen, S.B., 1987. The Nd and Sr isotopic systematics of river-water dissolved material: implications for the sources of Nd and Sr in seawater. Chem. Geol., Isot. Geosci. Sect. 66, 245–272.
Goldstein, S.J., Jacobsen, S.B., 1988. The Nd and Sr isotopic systematics of river-water suspended material: implications for crustal evolution. Earth Planet. Sci. Lett. 87, 249–265.
Goldstein, S.L., O'Nions, R.K., Hamilton, P.J., 1984. A Sm–Nd isotopic study of atmospheric dusts and particulates from major river systems. Earth Planet. Sci. Lett. 70, 22.
Gournay, J.P., 1999. Phylloid algal bioherms and ooid grainstones: characterization of reservoir facies utilizing subsurface data from the Aneth platform and outcrop data along the San Juan River, Paradox Basin, southeastern Utah. PhD Dissertation, Univ. Texas, Austin.
Gradstein, F.M., Agterberg, F.P., Ogg, J.G., Hardenbol, J., van Veen, P., Thierry, J., Huang, Z., 1994. A Mesozoic time scale. J. Geophys. Res. 99, 24051–24074.
Grant, N.K., Laskowski, T.E., Foland, K.A., 1984. Rb–Sr and K–Ar ages of Paleozoic glauconites from Ohio–Indiana and Missouri, USA. Isot. Geosci. 2, 217–239.
Graustein, W.C., Armstrong, R.L., 1983. The use of $^{87}Sr/^{86}Sr$ to measure atmospheric transport into forested watersheds. Science 219, 289–292.
Grotzinger, J.P., 1994. Trends in Precambrian carbonate sediments and their implication for understanding evolution. In: Bengtson, S. (Ed.), Early Life on Earth. Columbia Univ. Press, New York, pp. 245–258.
Gruszczynski, M., Hoffman, A., Malkowski, K., Veizer, J., 1992. Seawater strontium isotopic perturbation at the Permian–Triassic boundary, West Spitsbergen, and its implications for the interpretation of strontium isotopic data. Geology 20, 779–782.
Guilderson, T.P., Fairbanks, R.G., Rubenstone, J.L., 1994. Tropical temperature variations since 20,000 years ago: modulating interhemispheric climate change. Science 263, 663–665.
Gwiazda, R.H., Hemming, S.R., Broecker, W.S., 1996. Tracking the sources of icebergs with lead isotopes: the provenance of ice-rafted debris in Heinrich layer 2. Paleoceanography 11, 77–93.
Hallam, A., 1992. Phanerozoic Sea Level Changes. Columbia Univ. Press, New York.
Hanson, G.N., 1980. Rare earth elements in petrogenetic studies of igneous systems. Annu. Rev. Earth Planet. Sci. 8, 371–406.
Harland, W.B., Cox, A.B., Armstrong, R.L., Craig, L.E., Smith, D.G., Smith, D.G., 1990. A Geologic Time Scale Cambridge Univ. Press, Cambridge, UK.
Hemming, S.R., McLennan, S.M., Hanson, G.N., 1994. Lead isotopes as provenance tools for quartz: examples from plutons and quartzite, northeastern Minnesota, USA. Geochim. Cosmochim. Acta 58, 4455–4464.
Hemming, S.R., McLennan, S.M., Hanson, G.N., 1995. Geochemical and Nd/Pb isotopic evidence for the provenance of the Early Proterozoic Virginia Formation, Minnesota. Implications for the tectonic setting of the Animikie Basin. J. Geol. 103, 147–168.
Hemming, S.R., McDaniel, D.K., McLennan, S.M., Hanson, G.N., 1996. Pb isotope constraints on the provenance and diagenesis of detrital feldspars from the Sudbury Basin, Canada. Earth Planet. Sci. Lett. 142, 501–512.
Hemming, S.R., Broecker, W.S., Sharp, W.D., Bond, G.C., Gwiazda, R.H., McManus, J.F., Klas, M., Hajdas, I., 1998. Provenance of Heinrich layers in core V28–82, northeastern Atlantic: 40Ar/39Ar ages of ice-rafted hornblende, Pb isotopes in feldspar grains, and Nd–Sr–Pb isotopes in the fine sediment fraction. Earth Planet. Sci. Lett. 164, 317–333.
Hemming, N.G., Goldstein, S.L., Fairbanks, R.G., 1999. Osmium isotopic analysis by dynamic multiple collector inductively coupled plasma mass spectrometry using iridium-191 signal normalization. Ninth Annual V.M. Goldschmidt Conference. LPI Contribution, vol. 971. Lunar and Planetary Institute, Houston. Abstract #7314, (CD-ROM).
Henderson, G.M., Slowey, N.C., 2000. Evidence from U–Th dating against Northern Hemisphere forcing of the penultimate deglaciation. Nature 404, 61–66.
Hess, J., Bender, M., Schilling, J.G., 1986. $^{87}Sr/^{86}Sr$ evolution from cretaceous to present. Science 231, 979–984.
Hodell, D.A., Mueller, P.A., McKenzie, J.A., Mead, G.A., 1989.

Strontium isotope stratigraphy and geochemistry of the Late Neogene ocean. Earth Planet. Sci. Lett. 92, 165–178.
Hodell, D.A., Mead, G.A., Mueller, P.A., 1990. Variation in the strontium isotopic composition of seawater (8 Ma to present): implications for chemical weathering rates and dissolved fluxes to the oceans. Chem. Geol. 80, 291–307.
Hoff, J.A., Jameson, J., Hanson, G.N., 1995. Application of Pb isotopes to the absolute timing of regional exposure events in carbonate rocks: an example from U-rich dolostones from the Wahoo Formation (Pennsylvanian), Prudhoe Bay, Alaska. J. Sediment. Res., Sect A. 65, 225–233.
Hoffman, P.F., Kaufman, A.J., Halverson, G.P., 1998. Comings and goings of global glaciations on a Neoproterozoic tropical platform in Namibia. GSA Today 8, 1–9.
Holland, H.D., 1984. The Chemical Evolution of the Atmosphere and Oceans. Princeton Univ. Press, Princeton, NJ.
Holmden, C., Creaser, R.A., Muehlenbachs, K., Bergstrom, S.M., Leslie, S.A., 1996. Isotopic and elemental systematics of Sr and Nd in 454 Ma biogenic apatites: implications for paleoseawater studies. Earth Planet. Sci. Lett. 142, 425–437.
Holmden, C., Creaser, R.A., Muehlenbachs, K., Leslie, S.A., Bergstrom, S.M., 1998. Isotopic evidence for geochemical decoupling between ancient epeiric seas and bordering oceans: implications for secular curves. Geology 26, 567–570.
Holmes, C.W., 2002. Geochronology of terrestrial sediments: South Florida. USGS Factsheet, http://sofia.usgs.gov/publications/fs/sed_geochron/print.html.
Hooker, P.J., Hamilton, P.J., O'Nions, R.K., 1981. An estimate of the Nd isotopic composition of Iapetus seawater from ca. 490Ma metalliferous sediments. Earth Planet. Sci. Lett. 56, 180–188.
Howarth, R.J., McArthur, J.M., 1997. Statistics for strontium isotope stratigraphy: a robust LOWESS fit to the marine Sr-isotope curve for 0 to 206 Ma, with look-up table for derivation of numeric age. J. Geol. 105, 441–456.
Hughen, K.A., Southon, J.R., Lehman, S., Overpeck, J., 2000. Synchronous radiocarbon and climate shifts during the last deglaciation. Science 290, 1951–1954.
Ingram, B.L., Sloan, D., 1992. Strontium isotopic composition of estuarine sediments as paleosalinity–paleoclimate indicator. Science 255, 68–72.
Ingram, B.L., DePaolo, D.J., 1993. A 4300 year strontium isotope record of estuarine paleosalinity in San Francisco Bay, California. Earth Planet Sci. Lett. 119, 103–119.
Ingram, B.L., Coccioni, R., Montonari, A., Richter, F.M., 1994. Strontium isotopic composition of Mid-Cretaceous seawater. Science 264, 546–550.
Innocent, C., Fagel, N., Stevenson, R.K., Hillaire-Marcel, C., 1997. Sm–Nd signature of modern and Late Quaternary sediments from the northwest North Atlantic: implications for deep current changes since the Last Glacial Maximum. Earth Planet. Sci. Lett. 146, 607–625.
Isachsen, C.E., Bowring, S.A., Landing, E., Samson, S.D., 1994. New constraint on the division of Cambrian time. Geology 22, 496–498.
Israelson, C., Halliday, A.N., Buchardt, B., 1996. U–Pb dating of calcite concretions from Cambrian black shales and the Phanerozoic time scale. Earth Planet. Sci. Lett. 141, 153–159.
Ivanovich, M., Harmon, R.S. (Eds.), 1992. Uranium Series Disequilibrium: Applications to Environmental Problems. Clarendon Press, Oxford.
Jackson, R.B., Banner, J.L., Jobbagy, E.G., Pockman, W.T., Wall, D.H., 2002. Ecosystem carbon loss with woody plant invasion of grasslands. Nature 418, 623–626.
Jenkyns, H.C., Paull, C.D., Cummins, D.E., Fullagar, P.D., 1995. Strotium-isotope stratigraphy of Lower Cretaceous atoll carbonates in the mid-Pacific Mountains. Proceedings of the Ocean Drilling Program, Scientific Results. The Program, College Station, TX, pp. 89–97.
Johannesson, K.H., Lyon, W.B., Fee, J.H., Gaudette, H.E., McArthur, J.M., 1994. Geochemical processes affecting the acidic groundwaters of Lake Gilmore, Yilgarn Block, Western Australia: a preliminary study using neodymium, samarium, and dysprosium. J. Hydrol. 154, 271–289.
Johnson, M.E., 1996. Stable cratonic sequences and a standard for Silurian eustasy. In: Witzke, B.J., Ludvigson, G.A., Day, J.E. (Eds.), Paleozoic Sequence Stratigraphy: Views from the North American Craton. Geological Society of America, Boulder, CO, pp. 203–211.
Jones, C.E., Jenkyns, H.C., 2001. Seawater strontium isotopes, oceanic anoxic events, and sea-floor hydrothermal activity in the Jurassic and Cretaceous. Am. J. Sci. 301, 112–149.
Jones, C.E., Jenkyns, H.C., Coe, A.L., Hesselbo, S.P., 1994a. Strontium isotopic variations in Jurassic and Cretaceous seawater. Geochim. Cosmochim. Acta 58, 3061–3074.
Jones, C.E., Jenkyns, H.C., Hesselbo, S.P., 1994b. Strontium isotopes in Early Jurassic seawater. Geochim. Cosmochim. Acta 58, 1285–1301.
Jones, C.E., Halliday, A.B., Lohmann, K.C., 1995. The impact of diagenesis on high-precision U–Pb dating of ancient carbonates: an example from the Late Permian of New Mexico. Earth Planet. Sci. Lett. 134, 409–423.
Kaufman, A.J., Jacobsen, S.B., Knoll, A.H., 1993. The Vendian record of Sr and C isotopic variations in seawater: implications for tectonics and paleoclimate. Earth Planet. Sci. Lett. 120, 409–430.
Kaufman, A.J., Knoll, A.H., Narbonne, G.M., 1997. Isotopes, ice ages, and terminal Proterozoic earth history. Proc. Natl. Acad. Sci. 94, 6600–6605.
Kennedy, M.J., Hedin, L.O., Derry, L.A., 2002. Decoupling of unpolluted temperate forests from rock nutrient sources revealed by natural $^{87}Sr/^{86}Sr$ and 84Sr tracer addition. Proc. Natl. Acad. Sci. 99, 9639–9644.
Keto, L.S., Jacobsen, S.B., 1987. Nd and Sr isotopic variations of Early Paleozoic oceans. Earth Planet. Sci. Lett. 84, 27–41.
Knoll, A.H., Bambach, R.K., Canfield, D.E., Grotzinger, J.P., 1996. Comparative Earth history and Late Permian mass extinction. Science 273, 452–457.
Koepnick, R.B., Burke, W.H., Denison, R.E., Hetherington, E.A., Nelson, H.F., Otto, J.B., Waite, L.E., 1985. Construction of the seawater $^{87}Sr/^{86}Sr$ curve for the Cenozoic and Cretaceous: supporting data. Chem. Geol. 58, 55–81.
Kump, L., 1989. Alternative modeling approaches. Am. J. Sci. 289, 390.
Kump, L.R., Arthur, M.A., 1997. Global chemical erosion during

the Cenozoic: weatherability balances the budgets. In: Ruddiman, W.F. (Ed.), Tectonic Uplift and Climate Change. Plenum, New York, pp. 400–424.

Lambeck, K., Esat, T.M., Potter, E.-K., 2002. Links between climate and sea levels for the past three million years. Nature 419, 199–206.

Land, L.S., Mack, L.E., Milliken, K.L., Lynch, F.L., 1997. Burial diagenesis of argillaceous sediment, south Texas Gulf of Mexico sedimentary basin: a reexamination. Geol. Soc. Am. Bull. 109, 2–15.

Lasaga, A.C., Berner, R.A., 1998. Fundamental aspects of quantitative models for geochemical cycles. Chem. Geol. 145, 161–175.

Lee, M., Aronson, J.L., Savin, S.M., 1989. Timing and conditions of Permian Rotliegende Sandstone Diagenesis, Southern North Sea: K/Ar and oxygen isotopic data. AAPG Bull. 73, 195–215.

Lee, D.-C., Halliday, A.N., Hein, J.R., Burton, K.W., Christensen, J.N., Gunther, D., 1999. Hafnium isotope stratigraphy of ferromanganese crusts. Science 285, 1052–1054.

Lev, S.M., McLennan, S.M., Meyers, W.J., Hanson, G.N., 1998. A petrographic approach for evaluating trace-element mobility in a black shale. J. Sediment. Res. 68, 970–980.

Levasseur, S., Birck, J.-L., Allègre, C.J., 1998. Direct measurement of femtomoles of osmium and the $^{187}Os/^{186}Os$ ratio in seawater. Science 282, 272–274.

Ling, H.F., Burton, K.W., O'Nions, R.K., Kamber, B.S., von Blanckenburg, F., Gibb, A.J., Hein, J.R., 1997. Evolution of Nd and Pb isotopes in Central Pacific seawater from ferromanganese crusts. Earth Planet. Sci. Lett. 146, 1–12.

Long, L.E., Erwin, M.E., Fisher, R.S., 1997. Rb–Sr ages of diagenesis of Mg-rich clay in Permian sediments, Palo Duro Basin, Texas panhandle, United States. J. Sediment. Res., Sect. A. 67, 225–234.

Ludwig, K.R., Szabo, B.J., Moore, J.G., Simmons, K.R., 1991. Crustal subsidence rate off Hawaii determined from $^{234}U/^{238}U$ ages of drowned coral reefs. Geology 19, 171–174.

Macdougall, J.D., 1988. Seawater strontium isotopes, acid rain, and the Cretaceous–Tertiary boundary. Science 239, 485–487.

MacLeod, K.G., 2001. Evidence for a small ($\sim$ 0.000030) but resolvable increase in seawater $^{87}Sr/^{86}Sr$ ratios across the Cretaceous–Tertiary boundary. Geology 29, 303–306.

Martin, E.E., Macdougall, J.D., 1991. Seawater Sr isotopes at the Cretaceous/Tertiary Boundary. Earth Planet. Sci. Lett. 104, 166–180.

Martin, E.E., Macdougall, J.D., 1995. Sr and Nd isotopes at the Permian/Triassic boundary: a record of climate change. Chem. Geol. 125, 73–99.

McArthur, J.M., 1994. Recent trends in strontium isotope stratigraphy. Terra Nova 6, 331–358.

McArthur, J.M., Kennedy, W.J., Chen, M., Thirlwall, M.F., Gale, A.S., 1994. Strontium isotope stratigraphy for Late Cretaceous time: direct numerical calibration of the Sr isotopic curve based on the U. S. Western Interior. Palaeogeog. Palaeoclim. Palaeoecol. 108, 95–119.

McArthur, J.M., Thirlwall, M.F., Engkilde, M., Zinmeister, W.J., Howarth, R.J., 1998. Strontium isotope profiles across the *K–T* boundary in Denmark and Antarctica. Earth Planet. Sci. Lett. 160, 179–192.

McArthur, J.M., Howarth, R.J., Bailey, T.R., 2001. Strontium isotope stratigraphy: LOWESS Version 3: best fit to the marine Sr-isotope curve for 0–509 Ma and accompanying look-up table for deriving numerical age. J. Geol. 109, 155–170.

McCauley, S.E., DePaolo, D.J., 1997. The marine $^{87}Sr/^{86}Sr$ and $\delta^{18}O$ records, Himalayan alkalinity fluxes, and Cenozoic climate models. In: Ruddiman, W.F. (Ed.), Tectonic Uplift and Climate Change. Plenum, New York, pp. 427–467.

McCulloch, M.T., Wasserburg, G.J., 1978. Sm–Nd and Rb–Sr chronology of continental crust formation. Science 200, 1003–1011.

McDaniel, D.K., Hemming, S.R., McLennan, S.M., Hanson, G.N., 1994. Resetting of neodymium isotopes and redistribution of REEs during sedimentary processes: the Early Proterozoic Chelmsford Formation, Sudbury Basin, Ontario, Canada. Geochim. Cosmochim. Acta 58, 931–941.

McDermott, F., Grün, R., Stringer, C.B., Hawkesworth, C.J., 1993. Mass-spectrometric U-series dates for Israeli Neanderthal/early modern hominid sites. Nature 363, 252–255.

McLennan, S.M., 1989. Rare earth elements in sedimentary rocks: influence of provenance and sedimentary processes. In: Lipin, B.R., McKay, G.A. (Eds.), Geochemistry and Mineralogy of Rare Earth Elements: MSA Reviews in Mineralogy, vol. 21, pp. 169–200.

McLennan, S.M., Taylor, S.R., 1991. Sedimentary rocks and crustal evolution: tectonic setting and secular trends. J. Geol. 99, 1–21.

McLennan, S.M., Taylor, S.R., McCulloch, M.T., Maynard, J.B., 1990. Geochemical and Nd–Sr isotopic composition of deep-sea turbidites: crustal evolution and plate tectonic associations. Geochim. Cosmochim. Acta 54, 2015–2050.

McLennan, S.M., Hemming, S., McDaniel, D.K., Hanson, G.N., 1993. Geochemical approaches to sedimentation, provenance, and tectonics. In: Johnsson, M.J., Basu, A. (Eds.), Processes Controlling the Composition of Clastic Sediments. GSA Spec. Paper, vol. 284, pp. 21–39. Boulder, Colorado.

McNutt, R.H., Frape, S.K., Fritz, P., Jones, M.G., MacDonald, I.M., 1990. The $^{87}Sr/^{86}Sr$ values of Canadian Shield brines and fracture minerals with applications to groundwater mixing, fracture history, and geochronology. Geochim. Cosmochim. Acta 54, 205–215.

Melezhik, V.A., Gorokhov, I.M., Kuznetsov, A.B., Fallick, A.E., 2001. Chemostratigraphy of Neoproterozoic carbonates: implications for 'blind dating'. Terra Nova 13, 1–11.

Mii, H.-S., Grossman, E.L., 1994. Late Pennsylvanian seasonality reflected in the ^{18}O and elemental composition of a brachiopod shell. Geology 22, 661–664.

Montañez, I.P., Banner, J.L., Osleger, D.A., Borg, L.E., Bosserman, P.J., 1996. Integrated Sr isotope stratigraphy and relative sea-level history in Middle to Upper Cambrian platform carbonates: Implications for the evolution of Cambrian seawater $^{87}Sr/^{86}Sr$. Geology 24, 917–920.

Montañez, I.P., Osleger, D.A., Banner, J.L., Mack, L.E., Musgrove, M., 2000. Evolution of the Sr and C isotope composition of Cambrian oceans. GSA Today 10 (5), 1–5.

Moorbath, S., Taylor, P.N., Orpen, J.L., Teloar, P., Wilson, J.F., 1987. First direct radiometric dating of Archean stromatolitic limestone. Nature 326, 865–867.

Moore, W., 1996. Large groundwater inputs to coastal waters revealed by 226Ra enrichments. Nature 380, 612–614.

Morton, J.P., Long, L.E., 1984. Rb–Sr of glauconite recrystallization: dating times of regional emergence above sea level. J. Sediment. Petrol. 54, 495–506.

Müller, D.W., Mueller, P.A., 1991. Origin and age of the Mediterranean Messinian evaporites: implications from Sr isotopes. Earth Planet. Sci. Lett. 107, 1–12.

Müller, D.W., McKenzie, J.A., Mueller, P.A., 1991. Abu Dhabi Sabkha, Persian Gulf, revisited: application of strontium isotopes to test an early dolomitization model. Geology 18, 618–621.

Musgrove, M., Banner, J.L., 2003. Controls on the spatial and temporal variability of vadose dripwater geochemistry: Edwards aquifer, central Texas. Geochim. Cosmochim. Acta (in press).

Musgrove, M., Banner, J.L., Mack, L.E., Combs, D.M., James, E.W., Cheng, H., Edwards, R.L., 2001. Geochronology of Late Pleistocene to Holocene speleothems from central Texas: implications for regional paleoclimate. Geol. Soc. Am. Bull. 113, 1532–1543.

Nelson, B.K., DePaolo, D.J., 1988. Application of Sm–Nd and Rb–Sr isotope systematics to studies of provenance and basin analysis. J. Sediment. Petrol. 58, 348–357.

Nelson, B.K., MacLeod, G.K., Ward, P.D., 1991. Rapid change in strontium isotopic composition of sea water before the Cretaceous/Tertiary boundary. Nature 351, 644–647.

Nozaki, Y., 2001. Rare earth elements and their isotopes in the ocean. In: Steele, J.H., Turekian, K.K., Thorpe, S.A. (Eds.), Encyclopedia of Ocean Sciences, vol. 4. Academic Press, London, pp. 2354–2366.

Ohr, M., Halliday, A.N., Peacor, D.R., 1991. Sr and Nd isotopic evidence for punctuated clay diagenesis, Texas Gulf Coast. Earth Planet. Sci. Lett. 105, 110–126.

O'Nions, R.K., 1984. Isotopic abundances relevant to the identification of magma sources. Philos. Trans. R. Soc. Lond. Ser. A 310, 591–603.

Oxburgh, R., 1998. Variations in the osmium isotopic composition of sea water over the past 200,000 years. Earth Planet. Sci. Lett. 159, 183–191.

Palmer, M.R., Edmond, J.M., 1989. The strontium isotope budget of the modern ocean. Earth Planet. Sci. Lett. 92, 11–26.

Palmer, M.R., Edmond, J.M., 1992. Controls over the strontium isotope composition of river water. Geochim. Cosmochim. Acta 56, 2099–2111.

Palmer, M.R., Elderfield, H., 1985a. Variations in Nd isotopic composition of foraminifera from the Atlantic Ocean sediments. Earth Planet. Sci. Lett. 73, 299–305.

Palmer, M.R., Elderfield, H., 1985b. Sr isotope composition of seawater over the past 75 Myr. Nature 314, 526–528.

Papanastassiou, D.A., Wasserburg, G.J., 1969. Initial strontium isotopic abundances and the resolution of small time differences in the formation of planetary objects. Earth Planet. Sci. Lett. 5, 361–376.

Patchett, J.P., Ross, G.M., Gleason, J.D., 1999. Continental drainage in North America during the Phanerozoic from Nd isotopes. Science 283, 671–673.

Pegram, W.J., Krishnaswami, S., Ravizza, G.E., Turekian, K.K., 1992. The record of sea water $^{187}Os/^{186}Os$ variation through the Cenozoic. Earth Planet. Sci. Lett. 113, 569–576.

Peterman, Z.E., Hedge, C.E., Tourtelot, H.A., 1970. Isotopic composition of strontium in seawater throughout Phanerozoic time. Geochim. Cosmochim. Acta 34, 105–120.

Peucker-Ehrenbrink, B., Ravizza, G., Hofmann, A.W., 1995. The marine $^{187}Os/^{186}Os$ record of the past 80 million years. Earth Planet. Sci. Lett. 130, 155–167.

Piepgras, D.J., Jacobsen, S.B., 1988. The isotopic composition of neodymium in the north Pacific. Geochim. Cosmochim. Acta 52, 1373–1381.

Piepgras, D.J., Wasserburg, G.J., 1980. Neodymium isotopic variations in seawater. Earth Planet. Sci. Lett. 50, 128–138.

Piepgras, D.J., Wasserburg, G.J., 1983. Influence of the Mediterranean outflow on the isotope composition of neodymium in waters of the North Atlantic. J. Geophys. Res. 88, 5997–6006.

Piepgras, D.J., Wasserburg, G.J., Dasch, E.J., 1979. The isotopic composition of Nd in different ocean masses. Earth Planet. Sci. Lett. 45, 223–236.

Pingitore, N.E., Lytle, F.W., Davies, B.M., Eastman, M.P., Eller, P.G., Larson, E.M., 1992. Mode of incorporation of Sr^{2+} in calcite: determination by X-ray absorption spectroscopy. Geochim. Cosmochim. Acta 56, 1531–1538.

Popp, B.N., Podosek, F.A., Brannon, J., Anderson, T.F., Pier, J., 1986. $^{87}Sr/^{86}Sr$ ratios in Permo-Carboniferous sea water from the analyses of well-preserved brachiopod shells. Geochim. Cosmochim. Acta 50, 1321–1328.

Pursell, B.P., 1997. A record of changing seawater chemistry and diagenesis derived from $^{87}Sr/^{86}Sr$ variations through the Latemar carbonate platform, dolomites, Northern Italy. MS thesis. Univ. Texas, Austin.

Pursell, B., Banner, J., 1997. A refined Middle Triassic seawater $^{87}Sr/^{86}Sr$ curve based on petrographic and geochemical criteria. GSA Annu. Meeting, Abstr. with Programs, A-42.

Rasbury, E.T., Hanson, G.N., Meyers, W.J., Saller, A.H., 1997. Dating the time of sedimentation using U–Pb ages for paleosol calcite. Geochim. Cosmochim. Acta 61, 1525–1529.

Rasbury, E.T., Hanson, G.N., Meyers, W.J., Goldstein, R., Saller, A.H., 1998. U–Pb dates of paleosols: constraints on Late Paleozoic cycle durations and boundary ages. Geology 26, 403–406.

Ravizza, G., 1993. Variations of the $^{187}Os/^{186}Os$ ratio of seawater over the past 28 million years as inferred from metalliferous carbonates. Earth Planet. Sci. Lett. 118, 335–348.

Raymo, M.E., 1991. Geochemical evidence supporting T. C. Chamberlin's theory of glaciation. Geology 19, 344–347.

Raymo, M.E., 1994. The Himalayas, organic carbon burial, and climate in the Miocene. Paleoceanography 9, 399–404.

Raymo, M.E., Ruddiman, W.F., 1992. Tectonic forcing of Late Cenozoic climate. Nature 359, 117–122.

Raymo, M.E., Ruddiman, W.F., Froelich, R.N., 1988. Influence of Late Cenozoic mountain building on ocean geochemical cycles. Geology 16, 649–653.

Reimann, C., Caritat, P., 1998. Chemical Elements in the Environment. Springer, Berlin.

Renne, P.R., Becker, T.A., Swapp, S.M., 1990. 40Ar/39Ar laser-probe dating of detrital micas from the Montgomery Creek For-

mation, northern California: clues to provenance, tectonics, and weathering processes. Geology 18, 563–566.
Renne, P.R., Fulford, M.M., Busby-Spera, C., 1991. High resolution 40Ar/39Ar chronostratigraphy of the Late Cretaceous El Gallo Formation, Baja California del Norte, Mexico. Geophys. Res. Lett. 18, 459–462.
Reusch, D.N., Ravizza, G., Maasch, K.A., Wright, J.D., 1998. Miocene seawater $^{187}Os/^{186}Os$ ratios inferred from metalliferous carbonates. Earth Planet. Sci. Lett. 160, 163–178.
Reynolds, B.C., Frank, M., O'Nions, R.K., 1999. Nd- and Pb-isotope time series from Atlantic ferromanganese crusts: implications for changes in provenance and paleocirculation over the last 8 Myr. Earth Planet. Sci. Lett. 173, 381–396.
Richter, F.M., DePaolo, D.J., 1988. Diagenesis and Sr isotopic evolution of seawater using data from DSDP 590B and 575. Earth Planet. Sci. Lett. 90, 382–394.
Richter, F.M., Turekian, K.K., 1993. Simple models for the geochemical response of the ocean to climatic and tectonic forcing. Earth Planet. Sci. Lett. 119, 121–131.
Richter, F.M., Rowley, D.B., DePaolo, D.J., 1992. Sr isotope evolution of seawater: the role of tectonics. Earth Planet. Sci. Lett. 109, 11–23.
Rossman, G.R., Weis, D., Wasserburg, G.J., 1987. Rb, Sr, Nd and Sm concentrations in quartz. Geochim. Cosmochim. Acta 51, 2325–2329.
Ruppel, S.C., James, E.W., Barrick, J.E., Nowlan, G.S., Uyeno, T.T., 1996. High-resolution $^{87}Sr/^{86}Sr$ chemostratigraphy of the Silurian: implications for event correlation and strontium flux. Geology 24, 831–834.
Ruppel, S.C., James, E.W., Barrick, J.E., Nowlan, G.S., Uyeno, T.T., 1998. High-resolution Silurian $^{87}Sr/^{86}Sr$ record: evidence of eustatic control of seawater chemistry? In: Landing, E., Johnson, M.E. (Eds.), Silurian Cycles Linkages of Dynamic Stratigraphy with Atmospheric, Oceanic, and Tectonic Changes; James Hall Centennial Volume. New York State Museum Bulletin, vol. 491, pp. 285–295.
Saller, A.H., Koepnick, R.B., 1990. Eocene to Early Miocene growth of Enewetak Atoll: insight from strontium isotopic data. Geol. Soc. Am. Bull. 102, 381–390.
Schlanger, S.O., 1988. Strontium storage and release during deposition and diagenesis of marine carbonates related to sea-level variations. In: Lerman, A., Meybeck, M. (Eds.), Physical and Chemical Weathering in Geochemical Cycles. Kluwer Academic Publishing, Dordrecht, pp. 323–339.
Shannon, R.D., 1976. Revised effective ionic radii and systematic studies of interatomic distances in halides and chalcogenides. Acta Crystallogr. A32, 751–767.
Sharma, M., Wasserburg, G.J., Hofmann, A.W., Chakrapani, G.J., 1999. Himalayan uplift and osmium isotopes in oceans and rivers. Geochim. Cosmochim. Acta 63, 4005–4012.
Shaw, H.F., Wasserburg, G.J., 1985. Sm–Nd in marine carbonates and phosphates: implications for Nd isotopes in seawater and crustal ages. Geochim. Cosmochim. Acta 49, 503–518.
Sholkovitz, E., 1995. The aquatic chemistry of rare earth elements in rivers and estuaries. Aquat. Geochem. 1, 1–34.
Smith, P.E., Farquar, R.M., 1989. Direct dating of Phanerozoic sediments by the $^{238}U-^{206}Pb$ method. Nature 341, 518–521.
Spencer, J.E., Patchett, P.J., 1997. Sr isotope evidence for a lacustrine origin for the upper Miocene to Pliocene Bouse Formation, lower Colorado trough, and implications for timing of Colorado Plateau uplift. Geol. Soc. Am. Bull. 109, 767–778.
Stille, P., Clauer, N., 1986. Sm–Nd isochron-age and provenance of the argillites of the Gunflint Iron Formation in Ontario, Canada. Geochim. Cosmochim. Acta 50, 1141–1146.
Stille, P., Shields, G., 1997. Radiogenic isotope geochemistry of sedimentary and aquatic systems. Lecture Notes in Earth Sciences, vol. 68. Springer, Berlin.
Stille, P., Chaudhuri, S., Kharaka, Y.K., Clauer, N., 1992. Neodymium, strontium, oxygen and hydrogen isotope compositions of waters in present and past oceans: a review. In: Clauer, N., Chaudhuri, S. (Eds.), Isotopic Signatures and Sedimentary Rocks. Springer, Berlin, pp. 389–410.
Stille, P., Steinmann, M., Riggs, S.R., 1996. Nd isotope evidence for the evolution of the paleocurrents in the Atlantic and Tethys Oceans during the past 180 Ma. Earth Planet. Sci. Lett. 144, 9–19.
Stirling, C.H., Esat, T.M., Lambeck, K., McCulloch, M.T., 1998. Timing and duration of the Last Interglacial: evidence for a restricted interval of widespread coral reef growth. Earth Planet. Sci. Lett. 160, 745–762.
Stoll, H.M., Schrag, D.P., 1998. Effect of Quaternary sea level cycles on strontium in seawater. Geochim. Cosmochim. Acta 62, 1107–1118.
Stordahl, M.C., Wasserburg, G.J., 1986. Neodymium isotopic study of Baffin Bay water: sources of REE from very old terranes. Earth Planet. Sci. Lett. 77, 259–272.
Stueber, A.M., Pushkar, P., Hetherington, E.A., 1983. A strontium isotopic study of Smackover brines and associated solids, southern Arkansas. Geochim. Cosmochim. Acta 48, 1637–1649.
Suess, H.E., Linick, T.W., 1990. The ^{14}C record in bristlecone pine wood of the past 8000 years based on the dendrochronology of the late C.W. Ferguson. Philos. Trans. R. Soc. Lond. Ser. A A330, 403–412.
Tachikawa, K., Jeandel, C., Roy-Barman, M., 1999. A new approach to the Nd residence time in the ocean: the role of atmospheric inputs. Earth Planet. Sci. Lett. 170, 433–446.
Taylor, S.R., McLennan, S.M., 1985. The Continental Crust: Its Composition and Evolution. Blackwell, Oxford.
Trotter, J.A., Korsch, M.J., Nicoll, R.S., Whitford, D.J., 1998. Sr isotopic variation in single conodont elements: implications for defining the Sr seawater curve. Boll. Soc. Paleontol. Ital. 37, 504–507.
Tucker, R.D., McKerrow, W.S., 1995. Early Paleozoic chronology: a review in light of new U–Pb zircon ages from Newfoundland and Britain. Can. J. Earth Sci. 32, 368–379.
Tucker, R.D., Bradley, D.C., Ver Straeten, C.A., Harris, A.G., Ebert, J.R., McCutcheon, S.R., 1998. New U–Pb zircon ages and the duration and division of Devonian time. Earth Planet. Sci. Lett. 158, 175–186.
Van Metre, P.C., Mahler, B.J., Furlong, E.T., 2000. Urban sprawl leaves its PAH signature. Environ. Sci. Technol. 34 (19), 4064–4070.
Vasconcelos, P.M., Becker, T.A., Renne, P.R., Brimhall, G.H., 1992. Age and duration of weathering by $^{40}K/^{40}Ar$ and

$^{40}Ar/^{39}Ar$ analysis of potassium–manganese oxides. Science 258, 451–455.
Veizer, J., 1983. Chemical diagenesis of carbonates: theory and application of trace element technique. Soc. Econ. Paleon. Mineral. Short Course. 10, 3.1–3.100.
Veizer, J., Compston, W., 1974. $^{87}Sr/^{86}Sr$ composition of seawater during the Phanerozoic. Geochim. Cosmochim. Acta 56, 431–443.
Veizer, J., Compston, W., 1976. $^{87}Sr/^{86}Sr$ in Precambrian carbonates as an index of crustal evolution. Geochim. Cosmochim. Acta 40, 905–914.
Veizer, J., Compston, W., Clauer, N., Schidlowski, M., 1983. $^{87}Sr/^{86}Sr$ in Late Proterozoic carbonates: evidence for a "mantle" event at ~900 Ma ago. Geochim. Cosmochim. Acta 47, 295–302.
Veizer, J., Ala, D., Azmy, K., Brukschen, P., Buhl, D., Bruhn, F., Carden, G.A.F., Diener, A., Ebneth, S., Godderis, Y., Jasper, T., Korte, C., Pawelleck, F., Podlaha, O., Strauss, H., 1999. $^{87}Sr/^{86}Sr$, $\delta^{13}C$, and $\delta^{18}O$ evolution of Phanerozoic seawater. Chem. Geol. 161, 59–88.
Vervoort, J.D., Patchett, P.J., Blichert-Toft, J., Albarède, F., 1999. Relationships between Lu–Hf and Sm–Nd isotopic systems in the global sedimentary system. Earth Planet. Sci. Lett. 168, 79–99.
Wadleigh, M.A., Veizer, J., Brooks, C., 1985. Strontium and its isotopes in Canadian rivers: fluxes and global implications. Geochim. Cosmochim. Acta 49, 1727–1736.
Walker, R.J., Morgan, J.W., 1989. Rhenium–osmium isotope systematics of carbonaceous chondrites. Science 243, 519–522.
Walker, J.C.G., Hays, P.B., Kasting, J.F., 1981. A negative feedback mechanism for the long-term stabilization of Earth's surface temperature. J. Geophys. Res. 86, 9776–9782.
Walter, M.R., Veevers, J.J., Calver, C.R., Gorjan, P., Hill, A.C., 2000. Dating the 850–544 Ma Neoproterozoic interval by isotopes of strontium, carbon, and sulfur in seawater, and some interpretative models. Precambrian Res. 100, 371–433.
Wang, Z.S., Rasbury, E.T., Hanson, G.N., Meyers, W.J., 1998. Dating the time of sedimentation of clastic sedimentary rocks using U–Pb system of calcretes. Geochim. Cosmochim. Acta 62, 2823–2835.
Weis, D., Wasserburg, G.J., 1987. Rb–Sr and Sm–Nd systematics of cherts and other siliceous deposits. Geochim. Cosmochim. Acta 51, 959–972.
White, W., 1996. EAS 656, Isotope Geochemistry Lecture Notes. Cornell Univ. Dept. Earth Atm. Sci. http://www.geo.cornell.edu/geology/classes/Geo656/656notes.html.
Wickman, F.W., 1948. Isotope ratios: a clue to the age of certain marine sediments. J. Geol. 56, 61–66.
Wilde, P., Berry, W.B.N., 1984. Destabilization of the oceanic density structure and its significance to marine "extinction" events. Palaeogeog. Palaeoclimatol. Palaeoecol. 48, 143–162.
Wilkinson, B.H., Algeo, T.J., 1989. Sedimentary carbonate record of calcium–magnesium cycling. Am. J. Sci. 289, 1158–1194.
Wilson, P.A., Jenkyns, H.C., Elderfield, H., Larson, R.L., 1998. The paradox of drowned carbonate platforms and the origin of Cretaceous Pacific guyots. Nature 392, 889–894.
Winograd, I.J., Coplen, T.B., Landwehr, J.M., Riggs, A.C., Ludwig, K.R., Szabo, B.J., Kolesar, P.T., Revesz, K.M., 1992. Continuous 500,000-year climate record from vein calcite in Devils Hole, Nevada. Science 258, 255–260.
Winter, B.L., Johnson, C.M., 1995. U–Pb dating of a carbonate subaerial exposure event. Earth Planet. Sci. Lett. 131, 177–187.
Wood, S.A., 1990. The aqueous geochemistry of the rare earth elements and yttrium: 1. Review of available low temperature data for inorganic complexes and the inorganic REE speciation of natural waters. Chem. Geol. 82, 159–186.
Wright, J., Seymour, R.S., Shaw, H.F., 1984. REE and Nd isotopes in conodont apatite: variations with geological age and depositional environment. GSA Spec. Pap. 196, 325–340.
Zachos, J.C., Opdyke, B.N., Quinn, T.M., Jones, C.E., Halliday, A.N., 1999. Early Cenozoic glaciation, Antarctic weathering, and seawater $^{87}Sr/^{86}Sr$: is there a link? Chem. Geol. 161, 165–180.

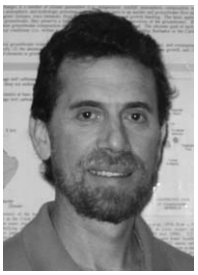

Dr. Jay L. Banner is a Professor in the Department of Geological Sciences and Director of the Environmental Science Institute at the University of Texas at Austin. His research interests include carbonate diagenesis, hydrogeology, climate change, the chemical evolution of groundwater, stream water, and ancient oceans. He uses the principles of isotope geochemistry to study these processes. Dr. Banner received his B.A. in Geology from the University of Pennsylvania, and Master's and PhD in Earth Sciences from the State University of New York at Stony Brook. He was a postdoctoral fellow at the California Institute of Technology and Louisiana State University prior to joining the faculty at the University of Texas in 1990.